

NCAT Report 09-08

PHASE III NCAT TEST TRACK FINDINGS

By

**Richard Willis
David Timm
Randy West
Buzz Powell
Mary Robbins
Adam Taylor
Andre Smit
Nam Tran
Michael Heitzman
Alessandra Bianchini**

December 2009



at AUBURN UNIVERSITY

277 Technology Parkway ■ Auburn, AL 36830

PHASE III NCAT TEST TRACK FINDINGS

By

Richard Willis
David Timm
Randy West
Buzz Powell
Mary Robbins
Adam Taylor
Andre Smit
Nam Tran
Michael Heitzman
Alessandra Bianchini

Sponsored by

Alabama Department of Transportation
Florida Department of Transportation
Georgia Department of Transportation
Indiana Department of Transportation
Mississippi Department of Transportation
Missouri Department of Transportation
North Carolina Department of Transportation
Oklahoma Department of Transportation
South Carolina Department of Transportation
Tennessee Department of Transportation
Texas Department of Transportation,
Federal Highway Administration
Oldcastle Materials Group

December 2009

ACKNOWLEDGEMENTS

This project was sponsored by Alabama Department of Transportation (DOT), Florida DOT, Georgia DOT, Mississippi DOT, Missouri DOT, North Carolina DOT, Oklahoma DOT, Tennessee DOT, Texas DOT, Federal Highway Administration, and the Old Castle Materials Group. The project team appreciates and thanks Alabama DOT, Florida DOT, Georgia DOT, Mississippi DOT, Missouri DOT, North Carolina DOT, Oklahoma DOT, Tennessee DOT, Texas DOT, Federal Highway Administration, and the Oldcastle Materials Group for their sponsorship of this project.

DISCLAIMER

The contents of this report reflect the views of the authors who are responsible for the facts and accuracy of the data presented herein. The contents do not necessarily reflect the official views or policies of Alabama DOT, Florida DOT, Georgia DOT, Mississippi DOT, Missouri DOT, North Carolina DOT, Oklahoma DOT, Tennessee DOT, Texas DOT, Federal Highway Administration, the Oldcastle Materials Group or the National Center for Asphalt Technology, or Auburn University. This report does not constitute a standard, specification, or regulation. Comments contained in this paper related to specific testing equipment and materials should not be considered an endorsement of any commercial product or service; no such endorsement is intended or implied.

TABLE OF CONTENTS

LIST OF ACRONYMS	v
EXECUTIVE SUMMARY	1
CHAPTER 1 - INTRODUCTION.....	4
CHAPTER 2 - OVERVIEW OF THE 2006 TEST TRACK (PHASE III)	6
EXPERIMENTAL DESIGN	7
CONSTRUCTION.....	10
TRAFFIC	12
PERFORMANCE MONITORING	12
CHAPTER 3 - MIXTURE PERFORMANCE COMPARISONS.....	13
VALIDATION OF THE ENERGY RATIO CONCEPT	13
Laboratory Energy Ratio Determination	14
Observed and Mapped Cracks	14
In-Situ Pavement Response	15
Core Observations.....	15
Bond Strength Testing	15
Energy Ratio Conclusions.....	16
LABORATORY AND APT TESTING OF MODERATE AND HIGH RAP CONTENT MIXES	17
Field Performance.....	18
Laboratory Testing.....	19
Summary	21
LOW NOISE PAVEMENT STRUCTURES	22
Low Noise Pavement Design.....	22
<i>Materials</i>	22
<i>Surface Macrotexture Measurements</i>	22
Sound Testing	23
Sound Pressure and Intensity Measurements.....	23
Findings.....	25
<i>Macrotexture</i>	25
<i>Sound Pressure</i>	25
<i>Sound Intensity</i>	26
<i>Sound Absorption</i>	26
Summary	26
TEST TRACK FRICTION.....	27
CONSTRUCTION AND PERFORMANCE OF PERMEABLE SURFACE MIXES	29
Experimental Design.....	29
Placement.....	30
Laboratory Performance	30
Field Performance.....	31
<i>Noise</i>	34
<i>Drainage</i>	38
Conclusions and Recommendations	39

DETERMINATION OF RUT DEPTH CRITERIA FOR LABORATORY PERMANENT DEFORMATION EVALUATION.....	39
Experimental Plan.....	40
Specimen Preparation.....	40
Laboratory Testing.....	41
Test Results and Analysis.....	41
Conclusion.....	46
LOW AIR VOIDS EXPERIMENT.....	46
CHAPTER 4 - STRUCTURAL STUDY.....	50
EXPERIMENTAL OBJECTIVES.....	50
2006 TEST SECTIONS.....	51
Florida DOT: Sections N1 and N2.....	51
Alabama DOT and FHWA: Sections N3 – N7.....	51
Oklahoma DOT: Sections N8 and N9.....	52
FHWA: Supplemental N9.....	52
Missouri: N10.....	53
Alabama DOT: S11.....	53
INSTRUMENTATION.....	54
CHAPTER 5 - MECHANISTIC PAVEMENT ANALYSIS.....	55
TEMPERATURE AND SPEED EFFECTS.....	55
Objectives.....	56
Field Testing.....	56
<i>Test Section</i>	56
<i>Testing Dates and Speeds</i>	56
Field Results and Discussion.....	56
<i>Strain Definition</i>	56
<i>Strain vs. Speed</i>	57
<i>Strain vs. Temperature</i>	58
<i>Combined Effect</i>	58
<i>Application of Regression Models</i>	59
Summary.....	61
FIELD-BASED PERPETUAL PAVEMENT STRAIN THRESHOLDS.....	62
Objective and Scope.....	63
2000 Test Track.....	63
2003 Test Track.....	67
2006 Test Track.....	69
Threshold Development.....	74
Conclusions.....	75
CHAPTER 6 - LABORATORY AND FIELD COMPARISONS.....	77
GRANULAR MATERIALS LABORATORY AND FIELD COMPARISONS.....	77
Unbound Materials Used in the Structural Study.....	77
Laboratory Testing.....	78
Backcalculation Cross-Section Investigation.....	82
Field Characterization of Unbound Materials.....	85
<i>Methodology</i>	85
<i>Model Generation</i>	86

<i>Model Calibration</i>	88
<i>Summary of Field-Calibrated Stress-Sensitivity Models</i>	91
Comparison of Laboratory and Field Results	92
<i>Summary of Findings from Laboratory and Field Modulus Comparisons</i>	94
Recommendations.....	95
E* LABORATORY AND MODEL COMPARISONS	96
Objectives and Scope.....	96
Models to Determine E*	96
Witczak 1-37A E* Predictive Equation.....	97
Witczak 1-40D E* Predictive Equation.....	98
Hirsch E* Predictive Model.....	99
Testing Protocol.....	100
Mixtures Tested	101
Results and Discussion	102
Summary.....	105
LABORATORY FATIGUE THRESHOLDS AND FIELD-MEASURED STRAINS	105
Laboratory Testing.....	106
Laboratory Testing and Field Data Comparisons	106
<i>Phase One – Comparison of Fatigue Threshold to Modeled Strain Levels</i>	107
<i>Phase One - Analysis Results</i>	108
<i>Phase Two – Location of Fatigue Thresholds on Cumulative Distribution Plots</i>	109
<i>Phase Two – Analysis Results</i>	110
<i>Phase Three – Ratio Comparison</i>	112
<i>Phase Three – Analysis Results</i>	113
Fatigue Threshold Summary.....	114
CHAPTER 7 – FINDINGS AND STATE DOT IMPLEMENTATIONS	115
Mechanistic-Empirical Pavement Design.....	115
Alabama	115
Florida.....	115
Georgia.....	116
Indiana.....	117
Mississippi	117
Missouri	119
North Carolina	120
Oklahoma.....	120
South Carolina	121
Tennessee.....	122
Texas.....	123
CHAPTER 8 – 2009 TEST TRACK PLANS.....	124

LIST OF ACRONYMS

AASHTO: American Association of State Highway and Transportation Officials
ALDOT: Alabama Department of Transportation
AMPT: Asphalt Mixture Performance Tester
APA: asphalt pavement analyzer
APT: accelerated pavement testing
ARAN: Automatic Road Analyzer
ASTM: American Society for Testing and Materials
CAM: crack attenuating mix
CDF: cumulative distribution function
CTM: circular texture meter
DFT: dynamic friction tester
DGA: dense-graded asphalt
DSR: dynamic shear rheometer
E*: dynamic modulus
ER: energy ratio
ESAL: equivalent single axle load
ETG: expert task group
FDOT: Florida Department of Transportation
FHWA: Federal Highway Administration
Fn: flow number
FWD: falling weight deflectometer
GDOT: Georgia Department of Transportation
HMA: hot mix asphalt
HWTD: Hamburg wheel-tracking device
HVS: heavy vehicle simulator
IDT: indirect tension
IFI: international friction index
INDOT: Indiana Department of Transportation
IRI: international roughness index
LA: Los Angeles
LWT: loaded wheel tester
M-E: mechanistic-empirical
MDL: maximum density line
MDOT: Mississippi Department of Transportation
MEPDG: mechanistic-empirical pavement design guide
MODOT: Missouri Department of Transportation
MTD: material transfer device
NAPA-REF: National Asphalt Pavement Association – Research and Education Foundation
NCAT: National Center for Asphalt Technology
NCDOT: North Carolina Department of Transportation
NCHRP: National Cooperative Highway Research Program
NMAS: nominal maximum aggregate size
OBSI: on-board sound intensity
ODOT: Oklahoma Department of Transportation
OGFC: open-graded friction course

PEM: porous European Mixture
PATB: permeable asphalt treated base
QC: quality control
RAP: reclaimed asphalt pavement
RBL: rich bottom layer
RMS: root-mean square
RTFO: rolling thin-film oven
SBS: styrene-butadiene-styrene
SCDOT: South Carolina Department of Transportation
SGC: Superpave gyratory compactor
SMA: stone matrix asphalt
SPL: sound pressure level
SPT: Simple Performance Tester
SRTT: standard reference test tire
TDOT: Tennessee Department of Transportation
TXDOT: Texas Department of Transportation
TWPD: three-wheeled polishing device
ULIP: ultra-light inertial profiler
VFA: voids filled with asphalt
VMA: voids in mineral aggregate
WMA: warm mix asphalt

PHASE III NCAT TEST TRACK FINDINGS

Richard Willis, David Timm, Randy West, Buzz Powell, Mary Robbins, Adam Taylor,
Andre Smit, Nam Tran, Michael Heitzman, and Alessandra Bianchini

EXECUTIVE SUMMARY

The original National Center for Asphalt Technology (NCAT) Pavement Test Track was built in 2000 in Opelika, Alabama where it has served as a state-of-the-art, full-scale, closed-loop accelerated loading facility. The construction, operation, and research at the Test Track are funded through a cooperative effort of agency and industry sponsors with individual pavement research objectives. The Test Track was designed to test 46 pavement sections (200 feet in length) with 10 million equivalent single axle loads (ESALs) of traffic over two years. The test sections allow pavement engineers and researchers to study pavement responses and distresses to make pavement design more economical and efficient. The Test Track underwent its first reconstruction phase in the summer of 2003.

After the second phase of testing (i.e., the second 10 million ESALs) had been completed, twenty-two test sections at the Test Track were either milled or removed down to the subgrade to prepare for the third phase of testing at the Test Track. Reconstruction for Phase III occurred in the summer and fall of 2006. Trafficking of the pavement began on November 10, 2006 and ran until December 4, 2008. At this point, the Phase III test sections had received 10 million ESALs of traffic, whereas the remaining Phase II test sections had accumulated 20 million ESALs, and eight test sections remaining from the original construction had accumulated 30 million ESALs.

During the experimental phase of the 2006 Test Track, two distinct large-scale studies were performed that encompassed many smaller sectional analyses: the mixture performance study and the structural study. The mix performance study encompassed sections that were originally built in 2000 and left in place through three cycles of traffic to quantify mixture rutting potential in addition to newly placed mill and inlay sections containing high percentages of reclaimed asphalt pavement (RAP).

A RAP experiment was conducted using mill and inlay sections at the 2006 Track. This study was designed to evaluate the practicality of producing high percentage (25+%) RAP surface mixtures. Six sections containing RAP at either 20 or 45% were compared to a control section of virgin mix. The sections were found to perform favorably in both the laboratory and field in terms of rutting and cracking.

The Florida Department of Transportation (FDOT) has been developing a methodology for predicting top-down cracking potential in a mixture based on an energy ratio (ER). To validate this methodology, two sections were sponsored by FDOT with varying energy ratios. The section with a lower energy ratio (N1) was expected to crack first. While the section with a lower energy ratio did crack first, a forensic investigation was completed to ensure other potential sources were not the cause of this early cracking. The forensic analysis validated the difference in

cracking between the two sections was not caused by differences in mechanistic properties or bond strength.

The Georgia Department of Transportation (GDOT) funded construction and testing in sections N11, N12 and N13 to compare the construction and performance of permeable surface mixes containing two different aggregate sources that were placed with conventional and dual layer paving equipment. While all the sections were constructed well, the section placed by the dual layer paver seemed to be the most effective in terms of drainage and noise reduction.

One of the objectives of the NCAT Pavement Test Track study was to evaluate correlations between laboratory permanent deformation measurements using the Asphalt Pavement Analyzer (APA) and Flow Number (F_n) tests and field rutting performance for a variety of mixtures. APA and F_n tests were conducted on the mixes placed at the Test Track, and they were correlated to rut measurements taken from the field. Based on these correlations, rut depth criteria were determined and proposed for future implementation.

The structural study actually began during Phase II (2003-2005), part of which was continued in the 2006 Test Track. This specific study was designed to aid in the calibration and verification of mechanistic-empirical (M-E) design concepts by embedding instrumentation in the pavement structure to measure mechanistic responses in the pavement under dynamic loading. The 2006 Test Track had eleven test sections as part of this study. Four sections (N3, N4, N6, and N7) were left in-place from Phase II while six test sections (N1, N2, N8, N9, N10, and S11) were reconstructed from the subgrade up. Section N5 received a mill and inlay, to mitigate top-down cracking, so it could endure an extra cycle of trafficking.

Four studies in the structural section were developed to verify or challenge different M-E design principles. The first study compared the load durations of strain measurements at the base of the hot-mix asphalt (HMA) in a 14 inch pavement section to the predicted load durations from the mechanistic-empirical pavement design guide (MEPDG). This study found that the MEPDG over-predicted the load duration of the pavement by about 80%. This could lead to a pavement structure being over-designed.

A second study examined a common laboratory concept, fatigue thresholds, and developed a field-based perpetual pavement strain threshold. This concept was developed by creating cumulative strain distributions for test sections at the Test Track. The test sections that were part of the 2003 and 2006 structural studies were chosen to be a part of this study as well as six sections from the 2000 Test Track which survived for at least 20 million ESALs. This study found that the cumulative strain distributions of test sections that experienced fatigue cracking were different from those sections that performed well. The findings support a field-based strain criterion (a strain distribution) for flexible perpetual pavement design based on data from sections that survived 20 million ESALs without fatigue cracking. These strain distributions were also related to the laboratory measured fatigue endurance limit by the development of a fatigue ratio.

The comparison of laboratory and field characterizations for granular materials was the focus of a third M-E design study. Falling weight deflectometer (FWD) testing was conducted to

characterize the granular materials in the structural sections of the 2006 Test Track, and these backcalculated moduli were compared with popular recommended models. The results of this study showed that either the MEPDG model or the universal model provide the best fit to laboratory resilient modulus data, and the universal model provided the best model fit to backcalculated resilient moduli. Therefore, the multi-variable constitutive models are recommended over the single-variable models.

A final M-E study compared laboratory measured dynamic modulus (E^*) values to predicted E^* values from the three recommended models. At the current state of the MEPDG, Witczak E^* predictive equations, 1-40D and 1-37A, are employed to determine dynamic modulus given volumetric, gradation and binder properties of a mixtures. In applying these models to ten mixtures included in the 2006 Test Track structural study, neither model consistently estimated laboratory dynamic moduli values to a high degree of accuracy. Because both the 1-37A and 1-40D models were found to be unreliable and the 1-40D model largely over-predicts dynamic modulus, it is recommended that the Hirsch E^* model be used. It should be used with caution however, as discrepancies at lower temperatures and/or higher frequencies were found.

One of the greatest benefits the Test Track has to offer its sponsors is the ability to test new pavement design concepts and technologies in a controlled environment. States such as Florida, Alabama, Missouri, Mississippi and Georgia have used research at the Track to develop or change construction practices, alter design specifications, or validate new crack prediction concepts.

The 2009 NCAT Pavement Test Track plans to expand the current structural study by developing a six section "Group experiment." This experiment will be used to validate M-E concepts as well as study the durability and mechanistic properties of Warm-Mix Asphalt (WMA). A second RAP study will be conducted to investigate the affects including high percentages of RAP in base mixtures. Trafficking should begin for Phase IV of the Test Track in the summer of 2009 and conclude in the fall of 2011.

CHAPTER 1 - INTRODUCTION

As new asphalt technologies and design frameworks move from the laboratory and computer modeling toward implementation, there is a need to validate the new materials, processes, and design methods. While some organizations consider full-scale testing on actual in-service roads, completing such research can be limited by the following factors: 1) field performance evaluations often take many years (15-20) to complete, 2) it is often difficult and unsafe to close lanes on in-service roads for inspection and testing, 3) Departments of Transportation are reluctant to leave roads in service until failure occurs, 4) the public can be intolerant to traffic delays due to road closures, and 5) changes in personnel and political climates can compromise long-term experiments (*1*).

Because of these difficulties, accelerated pavement testing (APT) facilities have become more popular. Today, several APT facilities are scattered across the globe developing and testing cutting edge materials and paving techniques to build longer lasting and more cost efficient pavements. One such APT facility, the NCAT Pavement Test Track located in Opelika, Alabama, just finished its ninth year of HMA research under controlled, but live, traffic.

The Test Track was constructed in 2000 as a 1.7 mile closed loop facility. The Test Track was developed as a partnership between Auburn University (who purchased the land) and the Alabama Department of Transportation (ALDOT) who built the original research infrastructure. The cost of site development, construction of the Test Track pavement foundation and buildings, and data infrastructure was funded by ALDOT. This made it possible for other states to conduct cost-effective pavement research without startup cost. The pooled fund research cooperative with 3-year sponsorship commitments that was chosen as the original funding model for Track construction and operations is still in use today.

Construction of the inaugural Track (Figure 1.1) was completed in the summer of 2000 and then subjected to 10 million ESALs of truck traffic through December of 2002. Built as a perpetual pavement, the first cycle of testing was a study of surface mix performance for forty-six 200 foot test sections (Figure 1.2). Many of the test sections were rebuilt in the summer of 2003, this time with a combination of mill/inlay surface mixes and variable thickness structural sections. 10 million ESALs were applied to the new sections and sections which remained in place from the original track accumulated 20 million ESAL loadings. Likewise, the 2006 Track was a combination of varied thickness structural sections and mill/inlay surface mixes. The 2006 NCAT Pavement Test Track represents the third 3-year research cycle.



Figure 1.1. The NCAT Test Track

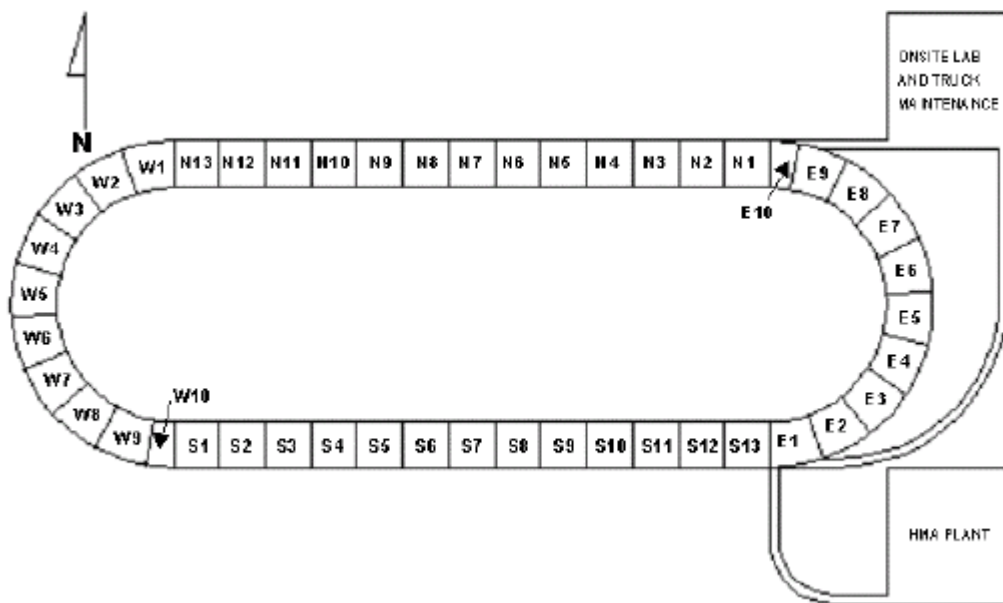


Figure 1.2. Layout of Test Track (L)

CHAPTER 2 - OVERVIEW OF THE 2006 TEST TRACK (PHASE III)

Upon the completion of the 2003 NCAT Pavement Test Track experiment, the sponsoring agencies were consulted in preparation of the 2006 Test Track experiment. While the 2003 Test Track had twenty-two test sections (Figure 2.1) remaining in place from the original 2000 Test Track, only eight of original test sections (shown in white) were chosen to receive a third cycle of 10 million ESALs. Sixteen sections built during the 2003 experiment (shown in yellow) were left in-place, and twenty-two sections (in blue) were either reconstructed or rehabilitated based upon the sponsor's research goals.

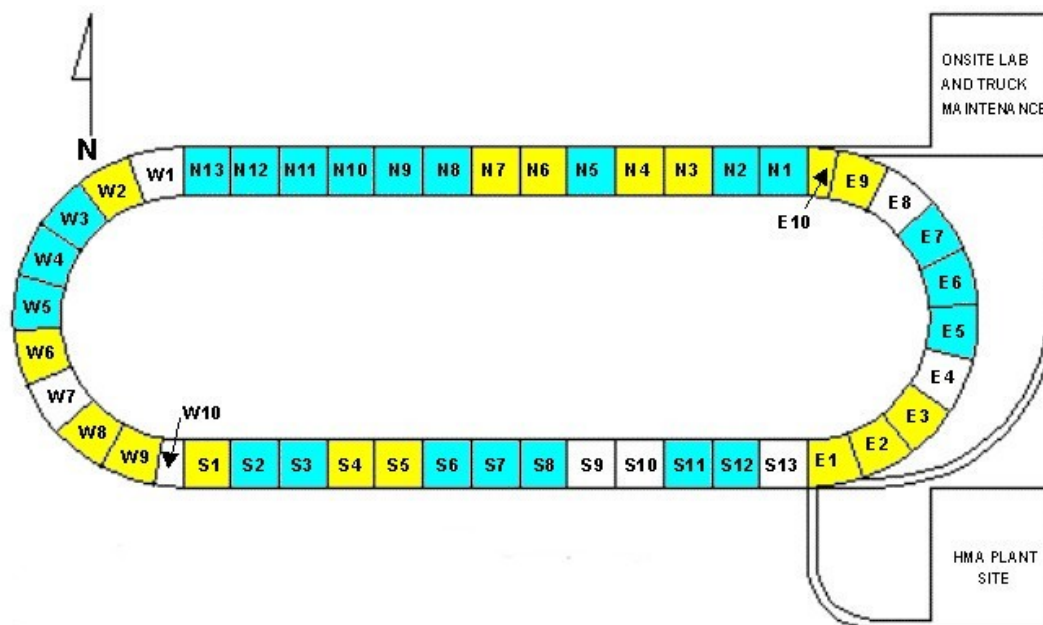


Figure 2.1. 2006 NCAT Test Track

Six sections (N1, N2, N8, N9, N10, and S11) were fully reconstructed from the subgrade up. Pavement materials were excavated to the desired depth from these sections so new subgrade, base and HMA materials could be constructed to each sponsoring organization's requested design thickness. These six sections, along with one mill and fill rehabilitation (N5), comprised the new structural study for the 2006 Test Track. These seven sections, along with four remaining from the 2003 experiment, brought the total of fully instrumented pavement sections at the Test Track to eleven.

The remaining fifteen sections were milled and inlaid. These treatments ranged in milled thickness from 1.25 to 4 inches. These sections were located in the outside (i.e. trafficked) wheelpath. These fifteen sections were designed by state agencies to validate the effects of air voids, RAP percentages, permeable surface treatments, and poor Los Angeles (LA) abrasive aggregate on the field performance of the mix.

The 2006 Test Track was designed to perpetuate many of the same research objectives as the 2003 Test Track. Its main objective was to evaluate the field performance of experimental pavement mixes and structures in the field. The structural test sections were designed to validate

and calibrate new transfer functions for M-E design, develop recommendations for mechanistic-based material characterization, characterize pavement responses in rehabilitated flexible pavement structures, and determine field-based fatigue thresholds for perpetual pavements (2).

EXPERIMENTAL DESIGN

The pooled fund research cooperative that funded the 2006 Test Track was supported by a total of 13 states, the Federal Highway Administration (FHWA), and Oldcastle Materials Group. Experimental design, construction, trucking operations, laboratory performance testing, field performance testing, and forensics were funded by sponsor fees. Completion of all project tasks was the responsibility of NCAT under the direction of the sponsor oversight group. Sponsors could either provide their own mix designs, or mix designs could be developed by NCAT. Individual experiments were designed by each sponsor to best meet their specific needs. NCAT also evaluated Test Track sections as a large pool of data in order to draw conclusions that could be broadly applied to the industry.

ALDOT funded research in sections N3, N4, N6, N7, S11 and joined with other sponsors in the six section RAP experiment. Traffic was extended from the 2003 research cycle on sections N3, N4, N6 and N7 to encompass perpetual pavement design concepts. A new structural buildup was constructed in section S11 as part of the broad focus on general M-E analysis and design. All ALDOT structural sections are supported by the stiff, low plasticity metamorphic quartzite soil indigenous to the Track under 6 inches of dense crushed granite base.

FDOT funded construction and testing in sections N1 and N2. Both sections were constructed with fully instrumented structural buildups that were intended to complement general work in M-E analysis and design. However, the primary objective of the experiment was to validate FDOT's energy ratio method for predicting surface cracking. This research is presented in greater detail in Chapter 3.

GDOT funded construction and testing of sections N11, N12 and N13. The objective of the GDOT study was to compare the construction and performance of permeable surface mixes containing two different aggregate sources that were placed with conventional and dual layer paving equipment. All three sections were placed on perpetual foundations to ensure that distresses would be isolated to the experimental surface mixes. This research is also presented in greater detail in Chapter 3.

The Indiana Department of Transportation (INDOT) funded construction and testing of sections S7 and S8. The objective of the INDOT experiment was to quantify the relationship between air voids measured in quality control (QC) volumetric samples and rutting performance in mixes produced with unmodified binder. Specifically, it was hoped that lower boundary (i.e. air void percentage where removal and replacement would be mandatory) could be identified. Lower levels of air voids were achieved by increasing the asphalt content and adjusting the gradation in accordance with guidance provided by INDOT. Because the mix produced in this study contained the same materials mixed in different proportions, it was decided to double the scope of the experiment by splitting sections S7 and S8 in half.

The Mississippi Department of Transportation (MDOT) funded construction and testing of sections S2 and S3. The original section S2 surface mix (the top 1 ½ inches) from the 2000 Track was milled and stored for use as RAP in the new section S2. The 3/8 inch nominal maximum aggregate size (NMAS) replacement mix was finer than the original ½ inch NMAS 2000 mix (33 percent passing the #16 sieve versus 23), with a lower level of design gyrations (85 versus 100) and higher asphalt content (7.0 versus 4.9). Further, the 2000 mix contained all virgin materials with 8 percent limestone, while the 2006 mix contained 15 percent RAP and no limestone. Both the old and new mixes were produced using styrene butadiene styrene (SBS)-modified PG 76-22. Reconstruction in section S3 consisted of the placement of 1½ inches of 75 gyration 3/8 inch NMAS stone matrix asphalt (SMA) mix containing 70 percent limestone under 1 inch of 50 gyration permeable surface mix containing 100 percent gravel. Mix in both S3 lifts was produced with SBS-modified PG 76-22.

The Missouri Department of Transportation (MODOT) funded construction and testing of a fully instrumented M-E structural section in N10. The buildup consisted of 8 inches of HMA over 4 inches of dense crushed stone base over stiff Track subgrade. Although no direct experimental control is available for this section, the similar buildup of Alabama's S11 does provide for comparability of N10 to the broader M-E experiment of which S11 is a part.

The North Carolina Department of Transportation (NCDOT) funded continued trafficking on sections S9 and S10 and also contributed funding for the RAP experiment. Sections S9 and S10 are two of the original sections from the 2000 construction. S9 is a fine-graded Superpave mix with PG 67-22 binder; S10 is a comparison coarse-graded section.

The Oklahoma Department of Transportation (ODOT) funded construction and testing in sections N8 and N9. Both sections were fully instrumented for M-E analysis; however, the HMA thicknesses were selected to investigate perpetual pavement design.

The South Carolina Department of Transportation (SCDOT) funded traffic continuation in section S1. Originally built for the 2003 research cycle on a perpetual foundation, the 1-3/4 inch thick surface in section S1 was built with a ½ inch NMAS SMA using an aggregate blend with a history of poor LA Abrasion values.

The Tennessee Department of Transportation (TDOT) funded research in sections S4, S5, S6 and E1 on the 2006 Track. Traffic was extended on sections S4, S5 and E1 from 2003. Sections S4 and E1 represented TDOT's very first permeable surface mix and SMA design efforts, respectively. Continuing traffic on the permeable surface for the 2006 research cycle extended the scope of the study to encompass long term drainability performance while the focus of traffic continuation on the SMA surface was durability.

The Texas Department of Transportation (TXDOT) funded construction and testing in section S12. The objective of the TXDOT experiment was to evaluate the effectiveness of a crack attenuating mix (CAM) at preventing reflective cracking on slab concrete pavement. Construction of section S12 presented a challenge, since no concrete pavements have been placed at the Test Track. To meet TXDOT's research needs, the surface of the original section S12 was milled to a depth of 4 inches. This was necessary because the CAM mix was to be

overlaid with a conventional dense surface mix. After milling had been completed, a large diameter masonry saw was used to cut the Track's remaining perpetual foundation in both the longitudinal and transverse direction, effectively creating 15 foot (in the longitudinal direction) by 12 foot (full lane width) free standing slabs. Approximately half of the 200 foot section was cut in this manner, with the other half uncut to serve as a control. Fine sand was carefully poured into the saw cuts to prevent the cracks from "healing," then the mixes selected by TXDOT were placed.

FHWA funded construction and testing in sections N5 and contributed to the RAP experiment. The foundation for section N5 was the 5 inch thickness of structural section remaining after the top 2 inches of 2003's section N5 was milled for rehabilitation.

Oldcastle Materials Group was the only private sector partner to fully support a test section in the 2006 research cycle. They contributed funding for the construction and testing of the RAP experiment.

A summary of research within all 46 experimental sections on the 2006 NCAT Pavement Test Track is provided in Table 2.1. A "+" was added by the binder grade to designate a mix design with binder greater than optimum.

In addition to the primary sponsors, the Track also received supplemental financial support from several different sources. Both Nebraska and Wisconsin provided funds that were used to support general research activities. A portion of the financial endowment from the National Asphalt Pavement Association's Research and Education Foundation (NAPA-REF) that is used to partially fund NCAT's mission was used to indirectly support project activities at the Track. Additionally, Auburn University provided funding that was used to design and deploy the high-speed wireless data acquisition network at the Track. While the data infrastructure upgrade was an important step in protecting the safety of the NCAT research team (enabling them to collect high-speed response data from the safety of the laboratory rather than from the roadside), the enhanced wireless network also created multi-disciplinary opportunities for other Auburn University researchers.

The cost for Track reconstruction and operations is minimized through the generous support of several different equipment manufacturers who donated the use of equipment and technical support. During construction, Astec Industries routinely provided equipment that facilitates plant production as well as mix placement. Compaction and placement equipment has been provided by Bomag Americas, Dynapac, Ingersoll Rand and Roadtec. Construction materials were provided by Boral Material Technologies, the Blaine Companies, Dravo Lime, Hanson Aggregates, Martin Marietta Aggregates, MeadWestvaco, Oldcastle Materials Group and Vulcan Materials. Many other material supply companies donated materials directly to state DOT sponsors. Equipment for mix and pavement quality testing has been provided by CPN International, the Gilson Company, HMA Lab Supply, Instrotek, Transtech Systems and Troxler Electronic Laboratories.

Table 2.1. 2006 Research Cycle (Newly Reconstructed Sections Shown in Bold Type)

Sec Num	Test Sec	Study HMA (in)	Surface Mix Stockpile Materials	Year of Completion	Design Methodology	Specified Binder	Total HMA (in)	Base Material	Sub-Grade	Research Objective(s)
1	E2	4	Calced Bauxite	2003	Superpave	Epoxy	24	Granite	Stiff	HVS PG67 Validation w/ High Friction Surface
2	E3	4	Calced Bauxite	2003	Superpave	Epoxy	24	Granite	Stiff	HVS PG76 Validation w/ High Friction Surface
3	E4	4	Granite	2000	Superpave	PG76-22	24	Granite	Stiff	Performance of Coarse Gradation
4	E5	2	Grn/Lms/Snd (45% RAP)	2006	Superpave	PG67-22	24	Granite	Stiff	RAP Mix Design/Construction/Performance
5	E6	2	Grn/Lms/Snd (45% RAP)	2006	Superpave	PG76-22	24	Granite	Stiff	RAP Mix Design/Construction/Performance
6	E7	2	Grn/Lms/Snd (45% RAP)	2006	Superpave	PG76-22s	24	Granite	Stiff	RAP Mix Design/Construction/Performance w/ Sasobit
7	E8	4	Granite	2000	Superpave	PG67-22	24	Granite	Stiff	Performance of Fine Gradation
8	E9	2	Granite/Limestone/Sand	2005	Superpave	PG67-22	24	Granite	Stiff	Evothem Warm Mix
9	E10	2	Granite/Limestone/Sand	2005	Superpave	PG76-22	24	Granite	Stiff	Evothem Warm Mix w/ Latex
10	N1	7	Granite/Limestone	2006	Superpave	PG67-22	7	Limerock	Stiff	Fracture Energy & M-E Design
11	N2	7	Granite/Limestone	2006	Superpave	PG76-22	7	Limerock	Stiff	Fracture Energy & M-E Design
12	N3	9	Granite/Limestone/Sand	2003	Superpave	PG67-22	9	Granite	Stiff	M-E Design Validation/Calibration
13	N4	9	Granite/Limestone/Sand	2003	Superpave	PG76-22	9	Granite	Stiff	M-E Design Validation/Calibration
14	N5	7	Granite/Limestone/Sand	2006	Superpave	PG67-22	7	Granite	Stiff	M-E Design Validation/Calibration
15	N6	7	Granite/Limestone/Sand	2003	Superpave	PG67-22	7	Granite	Stiff	M-E Design Validation/Calibration
16	N7	7	Georgia Granite	2003	SMA	PG76-22	7	Granite	Stiff	M-E Design Validation/Calibration
17	N8	10	Oklahoma Granite	2006	SMA	PG76-28	10	Stiff Sub	Soft	Perpetual Pavement & M-E Design
18	N9	14	Oklahoma Granite	2006	SMA	PG76-28	14	Stiff Sub	Soft	Perpetual Pavement & M-E Design
19	N10	8	St Louis/Porphyry	2006	Superpave	PG70-22	8	Limestone	Stiff	M-E Design Validation/Calibration
20	N11	2.75	Georgia Granite	2006	OGFC	PG76-22	24	Granite	Stiff	Drainable Mix w/ Cubicle Aggregates
21	N12	2.75	Georgia Granite	2006	OGFC	PG76-22	24	Granite	Stiff	Drainable Mix w/ F&E Aggregates
22	N13	4	Georgia Granite	2006	OGFC	PG76-22	24	Granite	Stiff	Twin Layer Drainable Mix w/ F&E Aggs
23	W1	4	Georgia Granite	2000	SMA	PG76-22	24	Granite	Stiff	Columbus Granite SMA
24	W2	4	Porphyry/Limestone	2000	SMA	PG70-22	24	Granite	Stiff	SMA Aggregate Quality
25	W3	2	Grn/Lms/Snd (20% RAP)	2006	Superpave	PG76-22	24	Granite	Stiff	RAP Mix Design/Construction/Performance
26	W4	2	Grn/Lms/Snd (20% RAP)	2006	Superpave	PG67-22	24	Granite	Stiff	RAP Mix Design/Construction/Performance
27	W5	2	Grn/Lms/Snd (45% RAP)	2006	Superpave	RA500	24	Granite	Stiff	RAP Mix Design/Construction/Performance
28	W6	1	Limestone/Gravel/Sand	2003	Superpave	PG76-22	24	Granite	Stiff	Low Volume Road Preservation
29	W7	4	Nova Scotia Granite	2002	NovaChip	PG76-22	24	Granite	Stiff	Surface Friction Restoration
30	W8	1	North Carolina Granite	2003	NovaChip	PG70-28	24	Granite	Stiff	Low Volume Road Preservation
31	W9	1	North Carolina Granite	2003	Superpave	PG76-22	24	Granite	Stiff	Low Volume Road Preservation
32	W10	4	Gravel/Limestone	2000	Superpave	PG76-22	24	Granite	Stiff	Durability of Coarse Gravel Mix
33	S1	4	South Carolina Granite	2003	SMA	PG76-22	24	Granite	Stiff	High LA Abrasion Loss SMA Aggregates
34	S2	1.5	Gravel/Sand (15% RAP)	2006	Superpave	PG76-22	24	Granite	Stiff	Lower Gyration Mix Performance
35	S3	2.5	Gravel	2006	OGFC	PG76-22	24	Granite	Stiff	100% Gravel OGFC Performance
36	S4	4	Limestone	2003	OGFC	PG76-22	24	Granite	Stiff	100% Limestone OGFC Performance
37	S5	1.5	Gravel/Limestone/Sand	2003	Superpave	PG76-22	24	Granite	Stiff	Lower Gyration Mix Performance
38	S6	1.25	Grv/Lms/Snd (15% RAP)	2006	Superpave	PG76-22	24	Granite	Stiff	Lower Gyration Mix Performance
39	S7A	2	Granite-/Limestone+Sand-	2006	Superpave	PG64-22	24	Granite	Stiff	Effect of Low QC Air Voids on Rutting
40	S7B	2	Granite/Limestone/Sand	2006	Superpave	PG64-22++	24	Granite	Stiff	Effect of Low QC Air Voids on Rutting
41	S8A	2	Granite/Limestone/Sand	2006	Superpave	PG64-22++	24	Granite	Stiff	Effect of Low QC Air Voids on Rutting
42	S8B	2	Granite/Limestone/Sand	2006	Superpave	PG64-22+++	24	Granite	Stiff	Effect of Low QC Air Voids on Rutting
43	S9	3	North Carolina Granite	2000	Superpave	PG67-22	24	Granite	Stiff	Performance of Coarse Gradation
44	S10	3	North Carolina Granite	2000	Superpave	PG67-22	24	Granite	Stiff	Performance of Fine Gradation
45	S11	7	Granite/Limestone/Sand	2006	Superpave	PG76-22	7	Granite	Stiff	M-E Design Validation/Calibration
46	S12	4	Arkansas Granite	2006	Superpave	PG76-22	24	Granite	Stiff	Rich Bottom Layer On Slab Pavement
47	S13	4	Oklahoma Granite	2000	Superpave	PG70-28	24	Granite	Stiff	Performance of Early Superpave Mix
48	E1	4	Tennessee Limestone	2003	SMA	PG76-22	24	Granite	Stiff	100% Limestone SMA Performance

CONSTRUCTION

Previous Test Track experiments were developed, let, and administered by the ALDOT. However, the 2006 Test Track was let and administered under a contract through Auburn University. A competitive bidding process was used to select the contractor that produced all the mixes for the project. Although the contract contained a provision to allow any state-certified contractor to install a portable plant onsite, the work was ultimately awarded to a local contractor with only a 10 minute haul distance who submitted the low bid.

Job mix formulas submitted by research sponsors typically require the use of aggregates that must be hauled from remote locations. Since the NCAT trucking fleet was not being used in the off-traffic reconstruction cycle, it was temporarily reassigned to the open road to long-haul the necessary stockpiles. Because all the materials specified in the GDOT job mix formulas for sections N11, N12 and N13 could be picked up and delivered within a single work day, they were hauled with NCAT research tractors driven by staff drivers pulling leased dump trailers. Stockpiles that required overnight travel were outsourced to local trucking companies. After the necessary aggregate materials were stockpiled on the contractor's yard, trial and placement mix production could begin.

Due to storage limitations on the contractor's yard, it was necessary to stage select truckloads of material at storage locations adjacent to the track before they were needed for mix production.

In these cases, the contractor was required to then short haul material from the Track back to the plant in a manner that facilitated the production schedule. A loader with an operator and a dump truck were assigned to the Track for this purpose. A detailed mapping process was utilized at both the track and the asphalt plant to ensure that stockpile confusion did not lead to bad mix production runs.

Prior to placement on the Track, trial mixes were initially produced so that plant proportioning could be adjusted as necessary and research sponsors could witness the mix being placed. Trucks containing trial mixes were hauled to the Track and sampled as if they were production mixes to facilitate laboratory testing and evaluation. When all test data related to the trial mix were compiled, they were presented to the research sponsors so changes to the plant settings could be incorporated into the subsequent production of mix for placement in test sections.

A special sequence of events was needed at the plant to produce uniform truckloads of mix that exhibited predictable properties. After calibrating the aggregate flow rate for each unique stockpile, sufficient quantities of uncoated aggregates (usually less than a truckload) were initially run through the plant to ensure a uniform gradation. Liquid asphalt was then turned on, with enough material bypassed from the drag chain to ensure that uncoated particles were not placed in the storage silo. The bypass chute was then closed, and the coated material was run into the storage silo until the computer indicated that approximately one truckload had accumulated. This material was discharged into a waiting truck and moved away for disposal on the contractor's yard.

At this point in the process, it was assumed that steady state conditions were attained and that subsequent material run into the silo would be uniform in terms of aggregate gradation or asphalt content. As soon as a truckload of material had again accumulated in the storage silo, it was discharged into a haul truck using standard best loading practices and sent to the Track laboratory for sampling and testing. If the mix was intended for placement on the Track, the process was repeated until a sufficient quantity of material was available to lay the required mat. If the mix was run for trial purposes, or if it was the last truckload necessary to lay the required mat, another truckload of coated material was run into the silo before the flow of liquid asphalt was stopped and the plant was shut down. The cold feed bins were unloaded, and the plant was readied for the next test mix (calibrating aggregate flow rates, resetting plant proportioning, etc).

The contractor was responsible for hauling mixed material back to the Track for placement as either trial mix or production mix. A sufficient work force and equipment resources were staged at the Track to support both operations which were completed sometimes only minutes apart. A sample stand located behind the NCAT laboratory adjacent to the Track was used to obtain representative samples from haul trucks prior to placement of mix on the Track. These mixes were split down to sample sizes that were suitable for standard volumetric analysis, asphalt content testing and gradation analysis. Compiled data were shared with sponsor representatives who were onsite to oversee production and placement activities, and mat placements were not accepted until they met with the sponsor's approval.

The compaction effort was achieved by at least three passes of a steel-wheeled roller. The roller had the capability of vibrating during compaction; however, this technique was not used on

every test section. After the steel-wheeled roller was removed from the pavement mat, the contractor continued compacting the mat with a rubber tire roller until the desired density was achieved.

While many of the construction efforts were inlays into milled sections, the construction of six new structural sections required excavations to the subgrade material for new subgrade, base and HMA materials to be placed. These sections were constructed by creating a ramp at both ends of the section for machinery entry and exit. The ramps allowed material to be excavated to the needed depth below the surface of the pavement. Some excavations were over five feet in depth. Once the excavations were complete, granular materials were placed and compacted before the contractor placed the HMA.

TRAFFIC

Trafficking at the 2006 Test Track was conducted in a similar manner to previous Test Track experiments. Four triple flat-bed trailer trucks and one triple box trailer loaded the pavement from 5:00 AM until approximately 10:40 PM Tuesday through Saturday. Trafficking began on November 10, 2006, and ended December 4, 2008, after approximately 10 million ESALs had been applied to the pavement structures.

Table 2.2 provides the axle weights for each of the five trucks under normal loading conditions. There were occasions when either due to a specialized study or due to mechanical malfunction trailers were removed from their given tractor. This left the tractor pulling either a single flat-bed trailer or a combination of double flat-beds.

Table 2.2. Truck Weights for 2006 Test Track

Truck ID	Steer, lb	Tandem, lb		Single, lb				
	Axle 1	Axle 2	Axle 3	Axle 4	Axle 5	Axle 6	Axle 7	Axle 8
1	10,150	19,200	18,550	21,650	20,300	21,850	20,100	19,966
2	11,000	20,950	20,400	20,950	21,200	21,000	20,900	20,900
3	10,550	20,550	21,050	21,000	21,150	21,150	21,350	20,850
4	10,500	21,050	20,700	21,100	21,050	21,050	20,900	21,050
5	11,200	19,850	20,750	20,350	20,100	21,500	19,500	20,300
Average	10,680	20,320	20,290	20,760	20,760	21,310	20,550	20,613
COV, %	3.9	3.9	4.9	2.2	2.5	1.7	3.6	2.2

PERFORMANCE MONITORING

Every Monday, trucking operations were suspended on the Track so that surface condition studies could be conducted to document performance of all experimental sections. Field performance evaluations focused on the middle 150 feet of each 200-foot test section to eliminate the effects of transitions near section ends.

Rutting, texture, and roughness were measured by using a high speed Automated Road Analyzer (ARAN) van. Cracking was determined by manually inspecting the surface of the test sections. The manually detected cracks are often so fine (low severity) that they cannot be detected with automated systems. Crack maps were generated from these examinations to quantify the extent of cracking and to monitor the progression of cracking.

CHAPTER 3 - MIXTURE PERFORMANCE COMPARISONS

For one-to-one comparisons between mixes, pavement engineers need locations where mixes can be tested side-by-side in the same conditions. While there are some limitations that engineers must be aware of when comparing test sections at the NCAT Test Track, HMA mixes placed during the same research cycle are generally ideal for making mixture performance comparisons given they are in similar locations.

Past Test Track research compared performance characteristics of modified versus unmodified asphalt binders, fine versus coarse graded mixtures, SMA versus Superpave, and the effects of other aggregate properties. In 2006, this objective was expanded by introducing sections that had low air voids, high percentages of RAP, and permeable surface mixes. The main purpose of these sections was to investigate rutting resistance and/or early field durability.

VALIDATION OF THE ENERGY RATIO CONCEPT

A distress plaguing the many highways is top-down cracking. FDOT has reported that over 90% of crack-related distresses in the state are top-down in nature (3). The exact mechanism initiating top-down cracking is a complex interaction of load, thermal, and aging effects on the roadway, and researchers have failed to find a single mix property to help designers eradicate this problem (4).

Due to the absence of material properties that could discern between cracked and non-cracked pavements, Roque et al. (4) developed the concept of a fracture energy ratio (ER) which could possibly predict top-down cracking potential. It had been proposed (5; 6; 7; 8) that an indirect tension test could be used to evaluate cracking potential by quantifying an asphalt mixture's energy dissipation and energy threshold. When the amount of energy dissipated by a pavement reached or surpassed the given threshold, cracking would occur. Therefore, if one were to design a pavement with a higher energy ratio, the pavement should be more resistant to top-down cracking (4).

FDOT sponsored two sections (Figure 3.1) at the Test Track during the summer of 2006 to help validate the energy ratio design concept. The first section (N1) was built with a PG 67-22 binder while the second section used a PG 76-22 binder. The PG 76-22 binder was predicted to increase the ER of the mixture, given the same aggregate structure and structural design (9).

These two sections were subjected to the accelerated trafficking patterns defined earlier. Once trafficking began, performance differences were quickly noted between the two sections as cracking began to propagate through N1. Later in the experiment, N2 began to crack as well. However, while differences in the cracking pattern were observed, it was important to clearly identify differences in ER as the primary cause cracking performance differences.

During construction, it was noticed that a material transfer device (MTD) operated on one of the paving lanes while laying the mix for section N1. The vehicle picked up tack on its tires which might have caused bond failure to occur in this section. Previous research at the Test Track has found relationships between poor bond and premature cracking (10; 11). Therefore, to

completely validate the energy ratio concept, a forensic investigation and mechanistic analysis was initiated (9).

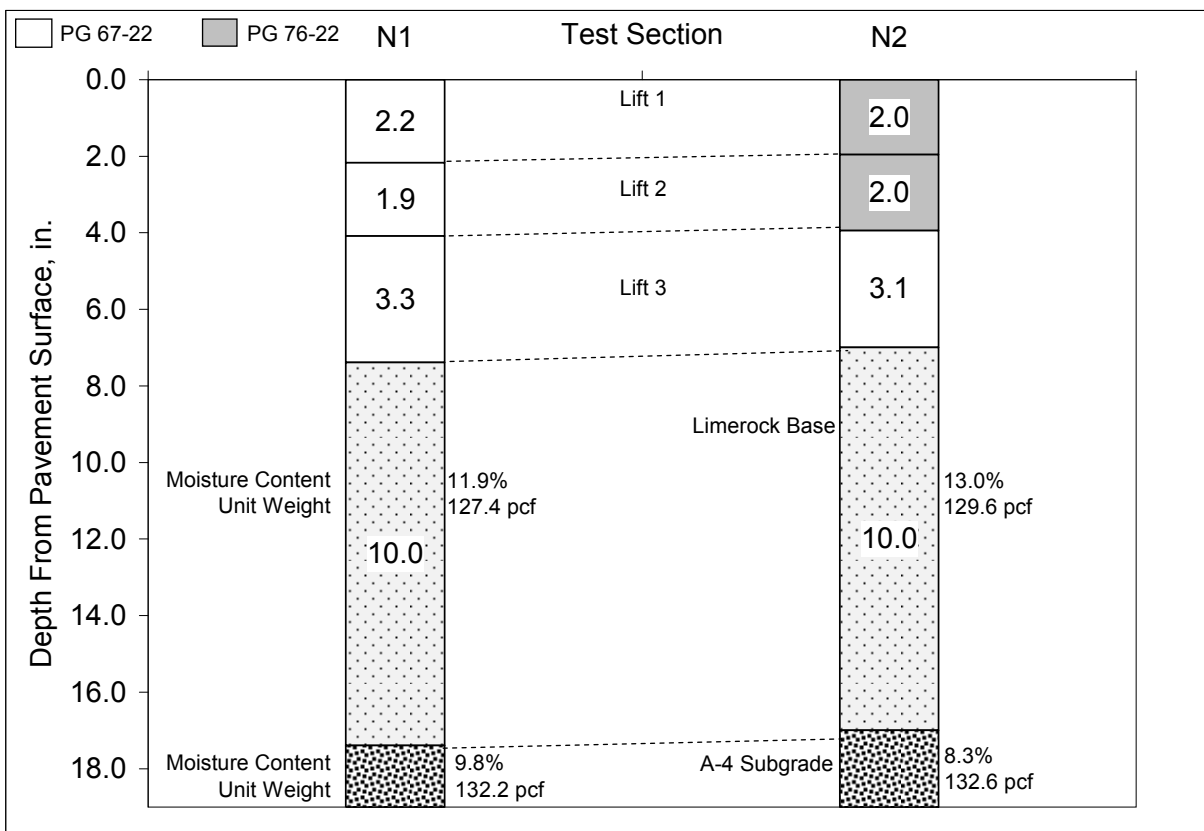


Figure 3.1. FDOT Test Sections (9)

Laboratory Energy Ratio Determination

The tests needed to calculate an energy ratio are laboratory indirect tension, creep strain and resilient modulus tests. These tests were performed on mix design samples. The energy ratios from duplicate tests for section N2 (i.e. the polymer modified section) were about 2.4 times higher on average than the energy ratios for N1; therefore, it was expected that N2 would be more resistant to top-down cracking (9).

Observed and Mapped Cracks

Cracking was first observed in section N1 on April 9, 2007. Approximately 200,000 ESALs later, cracking was observed in N2. The cracks began transversely and soon interconnected throughout the wheelpaths. This crack progression was not consistent with other forms of top-down cracking; however, coring did confirm the cracking was only within the upper two HMA layers (9).

The cracks that progressed through N1 were, initially, not very wide; however, the cracking spread quickly throughout N1, and by January 28, 2008, the entirety of the lane was cracked. A

shallow mill and inlay was used to repair the cracking in N1 using similar materials, and the same type of cracking was soon observed in the section again (9).

In-Situ Pavement Response

As will be described extensively in Chapter 4, asphalt strain measurements are collected weekly under full-scale loading from asphalt strain gauges embedded at the bottom of the HMA layer. These measurements are then compiled into a database where a representative strain response (95th percentile strain) was calculated for a given axle type each day of testing. Having these recorded mechanistic responses allows comparisons to be made between test sections. This data was used to validate that differences in pavement response did not cause section N1 to crack first (9).

Comparing the strain and temperature measurements of the two sections in question for single axles (Figure 3.2), similar strain magnitudes despite having slightly different as-built properties were observed. The strains in N1 become more erratic once cracking has propagated throughout the section. Once cracking has damaged the top layer of the pavement, the effective pavement depth has decreased causing an increase in the strain magnitude. Finally, the strains in N1 remained greater than those for N2 even after the mill and inlay occurred (9).

Core Observations

Cores were taken from both test sections to conduct a visual investigation into crack type. The cores validated the hypothesis of top-down cracking. The cores taken from N1 had cracks ranging from hairline surface fractures to cracks that propagated through the upper two inches of the pavement. However, below the top two inches, the cores were fully intact (9).

Bond Strength Testing

Bond strength tests were conducted on the cores using a Marshall device and test procedures described elsewhere (9). Table 3.1 shows the bond strength results. While one core from N1 showed atypically low bond strength, an ANOVA statistical test ($\alpha=0.05$) showed that the two sections did have statistically similar means (F-statistic 0.376, F-critical = 7.7). Thus, different bond strength was not a contributing factor to N1's early cracking relative to N2 (9).

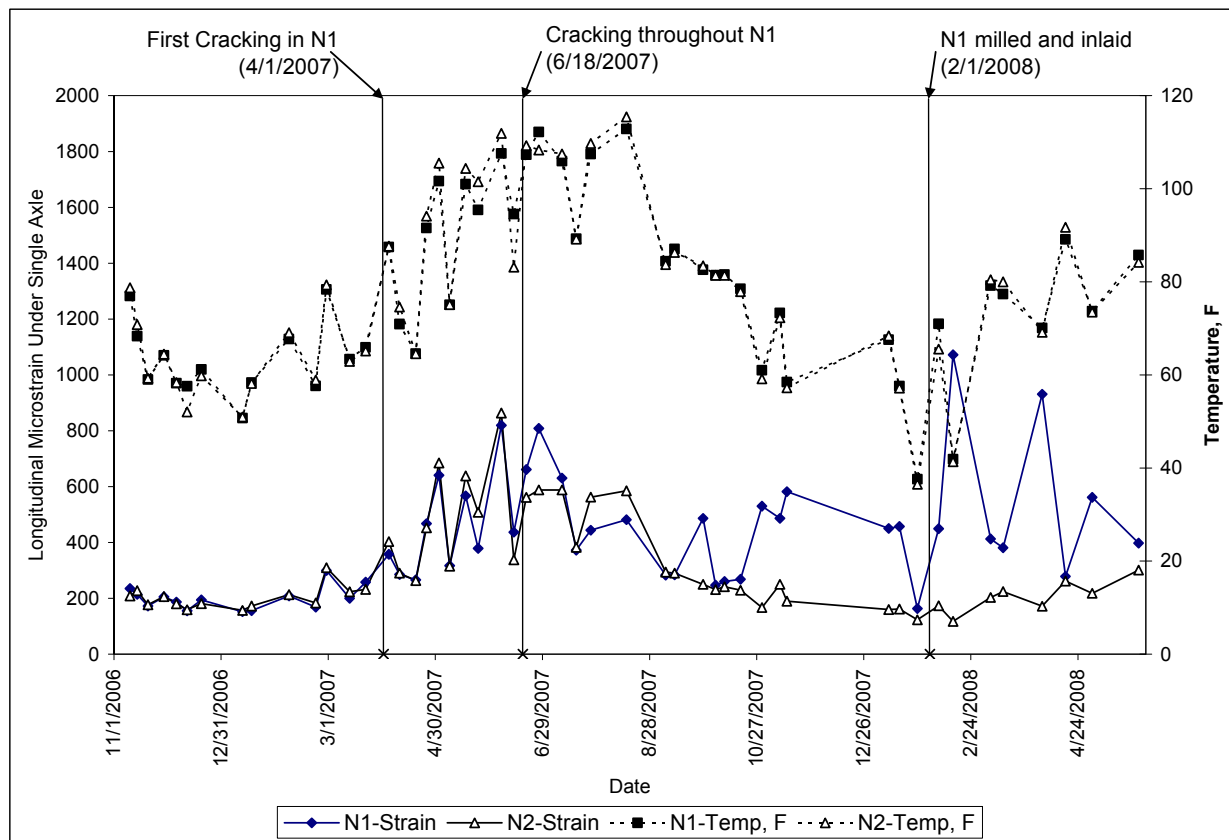


Figure 3.2. Measured Strain and Temperature versus Date (9)

Table 3.1. Bond Strength Test Results (9)

Section	Core	Shear Stress at Failure, psi
N1	1	84
	2	154
	3	197
	4	157
N2	1	149
	2	163
	3	186

Energy Ratio Conclusions

This study investigated two sections designed to validate the ER concept. The following conclusions can be drawn from this research.

- Section N2 was designed with nearly double the ER as section N1, and it proved to be more resistant to top-down cracking.
- The consistency between the two sections in both bond strength and strain magnitude provided evidence that bond strength was not the cause of one section’s early failure.
- Cores taken from the sections confirmed that the cracking was confined to the top of the pavement structure (9).

LABORATORY AND APT TESTING OF MODERATE AND HIGH RAP CONTENT MIXES

The interest in increasing RAP contents in HMA is driven by escalations in asphalt binder prices and the desire to conserve non-renewable resources. Many highway agencies currently limit RAP contents to 15 percent or less. The FHWA RAP Expert Task Group (ETG) identified two reasons higher RAP contents are not allowed are 1) the lack of documentation of high RAP mixes field performance and 2) the lack of research on the selection of appropriate virgin binder grades (12). High RAP mixes were defined by the RAP ETG as mixes containing 25 percent or more RAP by weight of aggregate.

To study both the constructability and performance of moderate and high RAP content mixes, six test sections (Table 3.2) were incorporated into a RAP experiment during the 2006 Test Track. The six test sections were built using a 50 mm mill and inlay with RAP mixtures as noted in the table. Beneath the RAP inlay is a 560 mm HMA structure on top of an aggregate base and Track subgrade (13). The virgin control section was the mill/inlay placed on section N5.

Table 3.2. Summary of Test Sections and Binder Test Data (13)

Section	%RAP*	%RAP Binder**	Virgin Binder		Virgin Binder + RAP	
			PG Grade	True Grade	Predicted Grade	Recovered Grade
W3	20%	18.2%	PG 76-22	78.1 -23.8	80.1 -22.4	78.1 -30.3
W4	20%	17.6%	PG 67-22	68.4-31.2	72.0 -28.6	74.2 -29.7
W5	45%	42.7%	PG 52-28	54.7-32.8	69.4 -25.8	74.1 -30.2
E5	45%	41.0%	PG 67-22	68.4-31.2	76.9 -25.1	80.9 -26.2
E6	45%	41.9%	PG 76-22	78.1-23.8	82.7 -20.7	85.5 -25.7
E7	45%	42.7%	PG 76-22 +1.5% Sasobit	83.2 -20.6	85.7 -18.8	86.3 -24.3
N5	0%	0%	PG 67-22	68.4-31.2	68.4 -31.2	71.1 -32.4

*by weight of aggregates **by weight of binder

Quality control data showed slight deviations in both air voids and voids filled with asphalt (VFA) in the three test sections in the West curve. The air void contents were approximately 2%, and the VFA percentages were about 10% higher than the design range for heavily trafficked pavements. These discrepancies were due to differences in the gradations of the RAP stockpiles used for design and production (13).

During construction, the 20% RAP test sections were easily compacted under the first few roller passes. Compactability of the 45% RAP test sections was influenced by binder grade. The sections with the softest binder exhibited the least compaction resistance. The two sections which required the most compactive effort were the 45% RAP sections which contained the PG 76-22 binder and the PG 76-22 + Sasobit. The Sasobit was added to aid in compaction, not for the reduction in production in temperature. However, the additive did not appear to improve the compactability of the RAP mat.

Field Performance

Four primary areas of concern were investigated in terms of the RAP sections' performance: rutting, texture change, roughness, and cracking. Figure 3.3 shows the measured rut depths of the seven test sections in the RAP experiment upon the completion of trafficking. Minor rutting occurred in most of the test sections with the exception of the 20% RAP, PG 67-22 test section. 8.5 mm of rutting was measured in this section. However, these rutting measurements were taken after two very warm summers. Since very little future rutting is expected in these sections, with the exception of the 20% RAP, PG 67-22 test section, the RAP mixes performed well despite the low air voids and high VFA percentages (13).

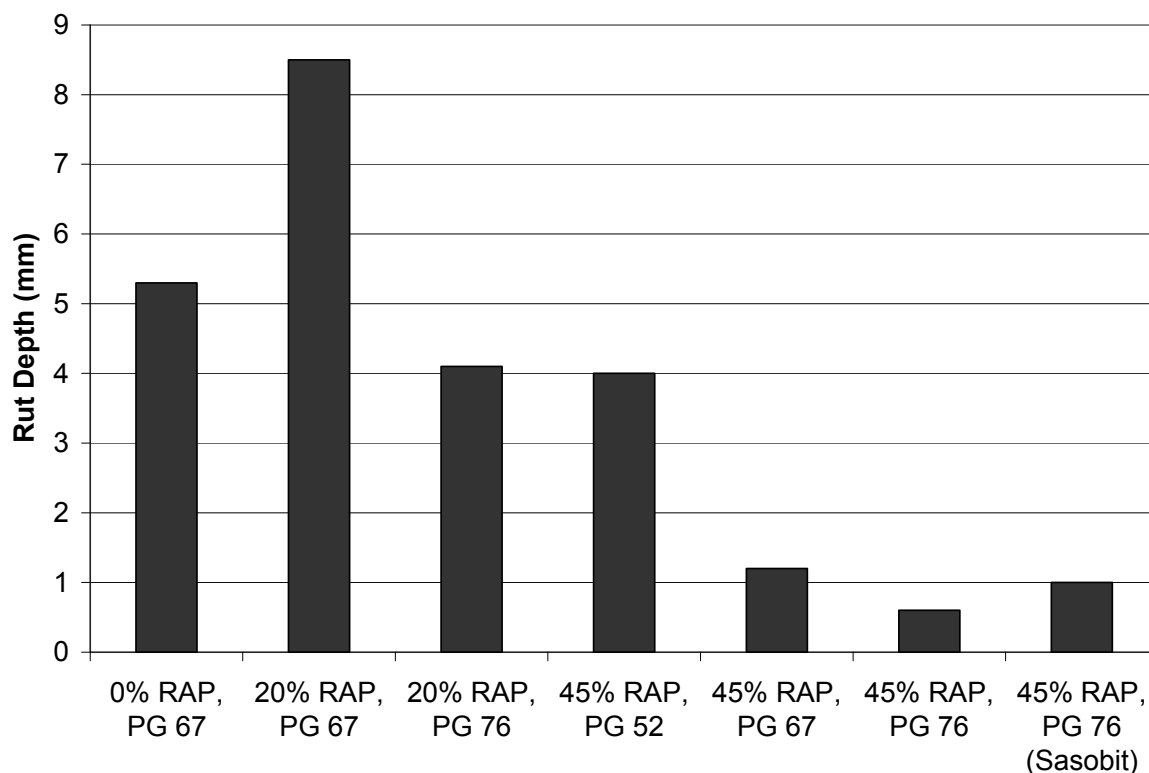


Figure 3.3. Field Rut Depths after 10 Million ESALs for the RAP Experimental Sections

Raveling has been linked to macrotexture changes in previous Test Track experiments. The ARAN van measured macrotexture using a high-frequency profile laser in the center of the right wheelpath. While two of the 45% RAP sections (PG 76-22 + Sasobit, PG 67-22) exhibited the greatest increase in texture, the textural increase was within the range typically observed under trafficking at the Test Track; therefore, these sections are expected to resist raveling (13).

Roughness was measured using inertial profiler technology described in AASHTO R 43-07. Over the course of testing, the 45% RAP sections' international roughness index (IRI) values remained relatively constant. Two sections (control and 20% RAP, PG 67-22) in the RAP experiment showed gradual increases in IRI; however, further investigations have removed this fault from the RAP mixtures. Both sections have showed increased rutting which would, in turn, increase the roughness number measured by the inertial profiler (13).

Two sections in the RAP study have experienced minor cracking; however, the cracks in these sections have been linked to either reflective cracking (45% RAP, PG 76-22+Sasobit) or segregation during construction (20% RAP, PG 76-22). More details regarding the crack mapping of the sections in the RAP study are given by West et al. (13).

Laboratory Testing

Laboratory testing was also conducted as part of the research to test rutting potential and durability using popular mixture testing techniques. Cores were taken from the RAP sections, and plant produced mix samples were also collected during the construction of these seven sections for laboratory testing.

Laboratory-created specimens were tested in the APA to quantify the rutting potential of the mix. Generally, the test results from the APA (Figure 3.4) validated the field performance of the test sections with the exception of the control section. A Fisher's least significant difference test showed that the control test section had statistically higher APA rut depths than the RAP mixes. This statistical analysis also showed the 20% RAP, PG 67-22 mix had greater rut depths than the other RAP mixes.

Reheated samples were used to conduct dynamic modulus testing using the Asphalt Mix Performance Test (AMPT). The temperatures of the test were 4.4, 21.1, and 37.8°C while the frequencies were 0.5, 1, 2, 5, 10, 20 and 25 Hz. The results of the mixes (Figure 3.5) generally follow the expected ranking of stiffness. The lone exception to this occurred when the 45% RAP mix with a PG 52-28 binder was ranked the stiffest at the low temperature (13).

A third test, beam fatigue, was run on reheated plant mix using AASHTO T 321-07. The tests were conducted on long-term aged specimens at 20°C and a constant strain of 500 microstrain. Failure was considered a 50% reduction in stiffness with original stiffness determined at the 50th loading cycle. The results are given in Figure 3.6 (13).

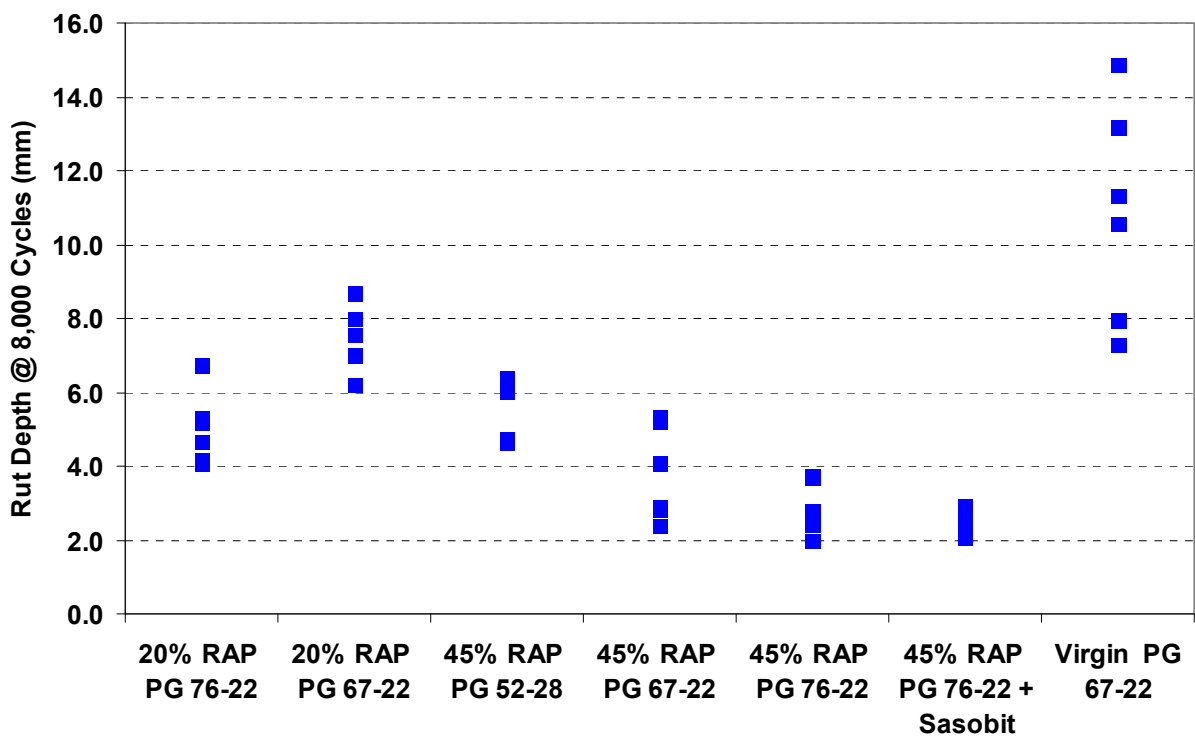


Figure 3.4. Rut Depths from APA Testing (13)

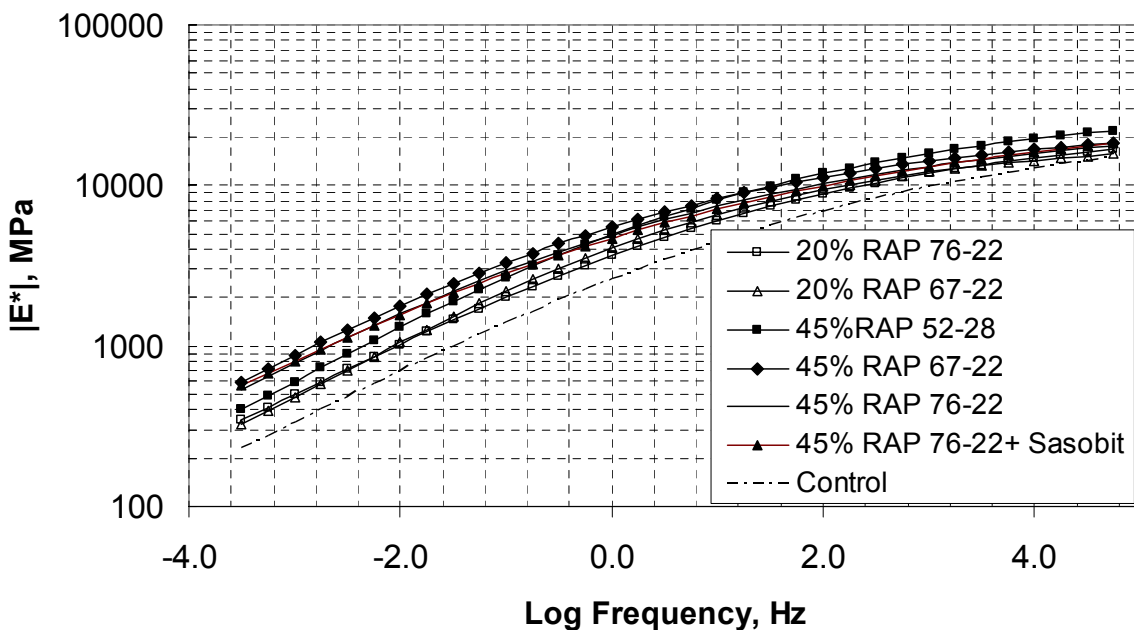


Figure 3.5. Master Curves of Dynamic Moduli for the RAP Experimental Sections (13)

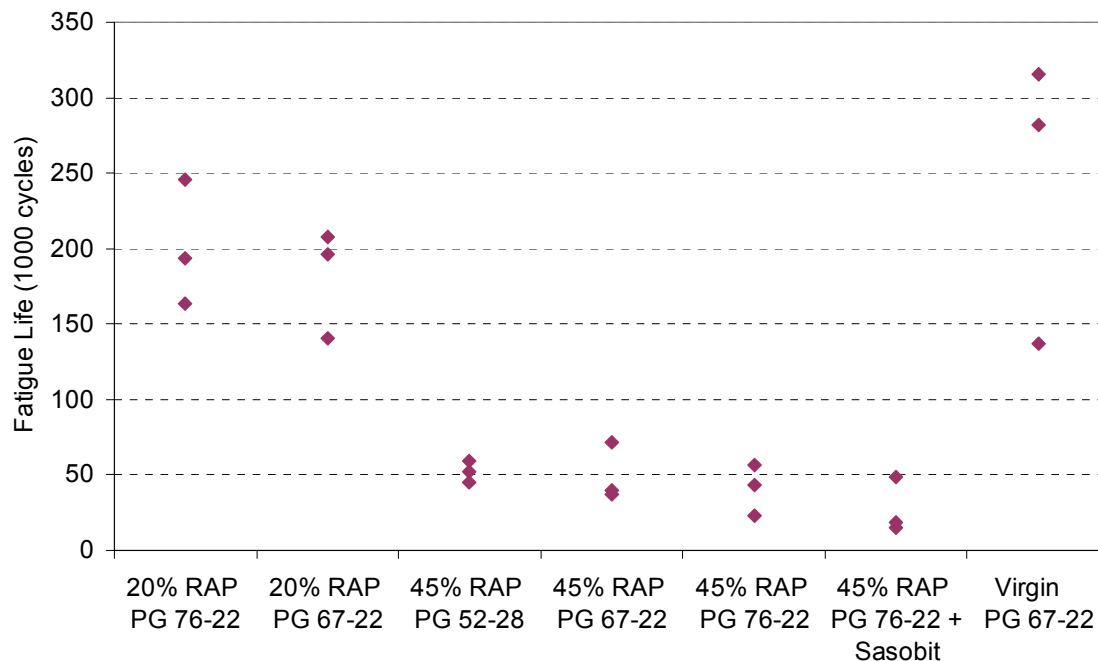


Figure 3.6. Plot of Beam Fatigue Test Results for the RAP Experimental Sections (13)

An ANOVA statistical analysis indicated statistical differences existed between all the datasets. Tukey’s pair-wise comparison was further used to confirm that a statistical difference was observed between the 20% and 45% RAP test sections. The 45% RAP mixes has a significantly lower number of cycles to failure than the 20% sections. However, binder grades did not significantly influence the beam fatigue results; therefore, it suggests that the binder volume plays a larger role in fatigue life than binder stiffness (13).

Summary

Additional laboratory work is being conducted to further analyze the effects of virgin binder grade on RAP mixes. When considering the field and laboratory test results from this study, the following conclusions can be inferred.

- Overall binder stiffness has an impact on the compactability of RAP mixes in the field.
- Despite low air voids and high VFA, the RAP mixes performed well in the field at the NCAT Test Track in regards to rutting.
- The minor cracking in test sections in the RAP experiment was not related to the structural properties of the RAP mixture.
- With the exception of the virgin test mix, rutting results from the APA matched field rut measurements.
- Master curves show that binder stiffness greatly influences mix stiffness. Softer grades of binder decrease the mix stiffness with could decrease a pavement’s durability.
- Differences in beam fatigue results appear to be more affected by binder volume content than by binder stiffness.

- Based upon laboratory and field data collected at the NCAT Test Track, there does not appear to be a strong case for supporting the use of softer binder grades in high RAP mixes (13).

LOW NOISE PAVEMENT STRUCTURES

An evaluation of tire-pavement noise was conducted with different surface mixes. Test sections consisting of coarse- and fine-graded mixes, SMA, and single and double layered open graded friction course mixtures were paved on the inside lane of the north and south tangents at the Test Track. NCAT Report 07-02 (14) reports on the design and testing of these test sections.

Low Noise Pavement Design

Materials

Seven different pavement sections were constructed on the inside untrafficked lanes on the south tangent of the NCAT test track. Asphalt mixtures used for the sections included three SMA's with varying nominal maximum aggregate sizes, two dense-graded asphalt mixtures, a micro-surfacing and an open-graded friction course (OGFC) (Table 3.3).

Table 3.3. Mix Designs for Noise Study (15)

Section	S2	S4	S5	S6	S7	S8	S9
Layer 1 (2 in)	OGFC	4.75 DGA	9.5 DGA	<4.75 SMA	4.75 SMA	9.5 SMA	Micro
Layer 2	Existing Track Milled Surface						

The various mixtures were paved to a thickness of two inches over existing dense-graded asphalt (DGA), which was milled. All mixtures were comprised of a PG 76-22 SBS polymer modified asphalt binder and granite aggregate from Georgia (15).

Surface Macrotexture Measurements

The macrotexture of the surfacing layers were evaluated using the circular texture meter (CTM) and the ultra-light inertial profiler (ULIP). These techniques are reported elsewhere (16). Replicate CTM texture measurements were completed at five random locations on both surfacing layers. Statistics of the macrotexture measurements using the CTM are shown in Table 3.4. ULIP texture measurements are documented elsewhere (15).

Table 3.4. Surface Macrotexture (MPD, mm) of Noise Sections Using the CTM (15)

Section	S2	S4	S5	S6	S7	S8	S9
Description	OGFC	4.75 DGA	9.5 DGA	<4.75 SMA	4.75 SMA	9.5 SMA	Micro
Mean Profile Depth, mm	1.19	0.11	0.12	0.10	0.15	0.58	1.04
Standard Deviation, mm	0.26	0.02	0.02	0.05	0.03	0.15	0.25

Sound Testing

Sound measurements on the sections included sound pressure and on-board sound intensity (OBSI) evaluations using the NCAT CPX trailer as detailed in NCAT Report 07-02 (14). Repeated sound measurements (at least 3 runs) were done on each section. Testing was done with the Michelin standard reference test tire (SRTT) at speeds of 45 and 60 mph.

Sound intensity testing with a NCAT triple trailer truck was also completed by attaching a frame around the rear wheels on the rear trailer. Sound intensity microphones could be mounted to record leading-edge and trailing-edge measurements. Details of the configuration used are given in NCAT Report 07-02 (14). Sound absorption measurements with the 6 inch diameter impedance tube were done in the field. Window putty was used to seal the base of the tube that is placed directly onto the tested surface during measurements. This procedure was evaluated in lieu of coring specimens and testing these in the laboratory.

Sound Pressure and Intensity Measurements

The sound pressure and intensity measurements on the low noise sections were completed on March 3, 2007. The mean air temperature during noise measurements was 69°F. Results of the sound pressure measurements on the low-noise sections measured using the CPX trailer with SRTT tires are illustrated in Figure 3.7. For the sake of brevity, only the A-weighted global sound pressure levels (SPL) calculated by logarithmic addition of the sound levels between the third octave band frequencies of 316 and 3981 Hz are reported. The data for the sound pressure measurements collected for the three runs at the front and rear microphones are tabulated elsewhere (15).

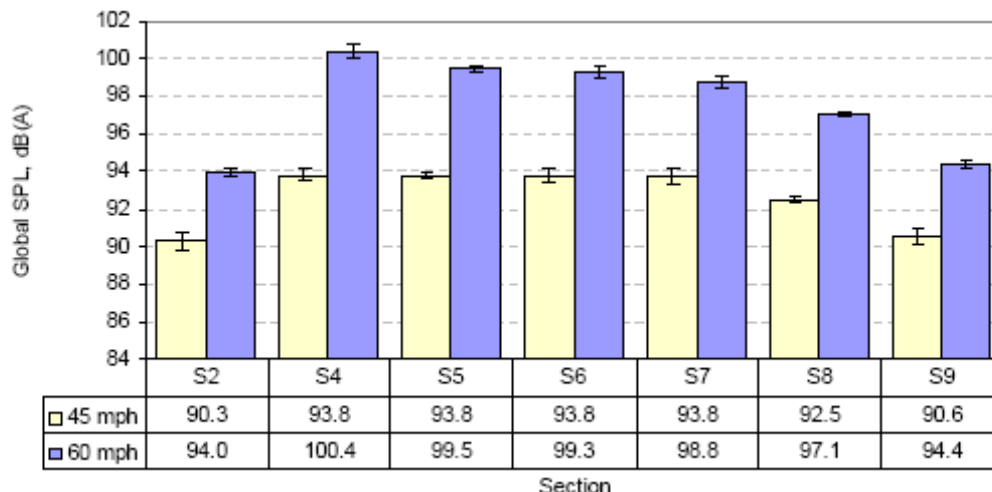


Figure 3.7. Summary of Global Sound Pressure Levels at 45 and 60 mph (15)

Figure 3.8 summarizes the sound intensity measurements on the low noise sections done using the CPX trailer at speeds of 45 mph and 60 mph and the NCAT semi trailer at a speed of 45 mph. The data for the sound intensity measurements collected for the three runs at the leading- and trailing-edge microphones are tabulated by Smit and Waller (15).

The noise spectra from the CPX sound pressure measurements and sound intensity measurements at speeds of 45 and 60 mph with the SRTT tires have been documented elsewhere by Smit and Waller (15).

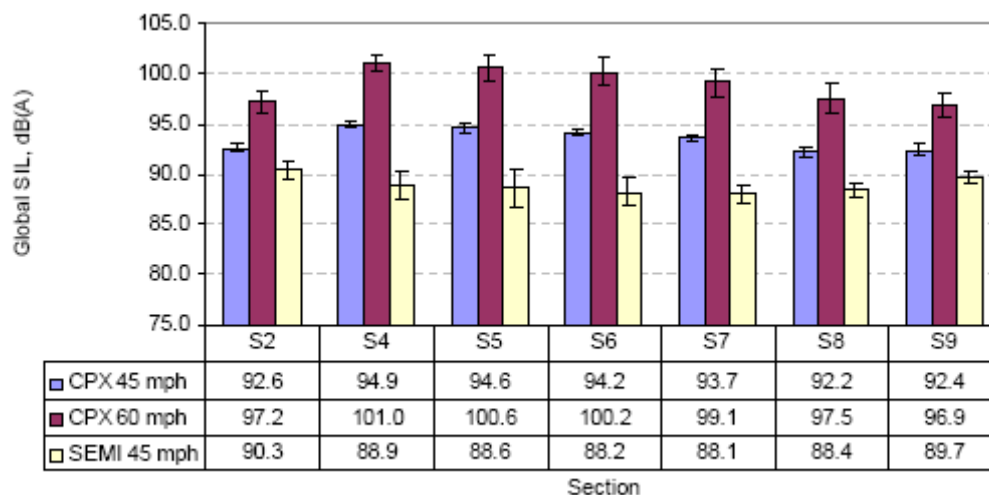


Figure 3.8. Summary of Global Sound Intensity Levels (15)

Findings

Macrotexture

Although macrotexture significantly influenced the sound measured at the tire-pavement interface, the relationship between macrotexture and noise is not well defined. This might be because macrotexture is masked by other influence factors such as the porosity and stiffness of the pavement mixture. It was reported that surfaces with the coarser Porous European Mixture (PEM) were noisier than those with the finer OGFC (16).

It is proposed that the surface profile as defined using the ULIP be used to differentiate the positive and negative texture on the road surface. This may be done, for example, by applying a root-mean square (RMS) filter to the surface profile as shown in Figure 3.9. This would allow a differentiation of positive and negative texture profiles.

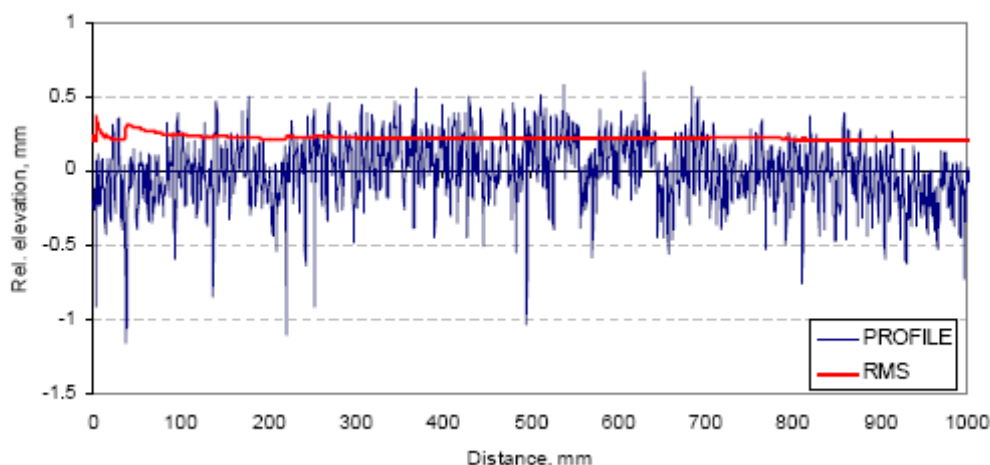


Figure 3.9. RMS Filter Applied to ULIP Surface Profile (15)

Sound Pressure

Figure 3.7 shows the mean sound pressure levels for the different mixtures tested at 45 mph and 60 mph. Contrary to expectations, the sound levels on the smoother surface mixtures are higher than those on a coarser surface texture. An observation made when examining these smooth surface mixtures in the field was that they would “squeak” or generate a high pitch noise if the rubber soles of one’s shoes were dragged across the surface. Although this is not an objective test, it indicates possible noise effects under rolling tires. A possible consequence of this phenomenon is the unusual peak sometimes seen in the data. It can be seen that for the smoother surface mixtures on sections S4, S5, S6 and S7 that in addition to the typical peak in the data observed at 1,000 Hz, an additional peak in the sound level data is apparent at a third octave band frequency of 1,585 Hz and 1,995 Hz at 45mph and 60 mph, respectively. The peak at the higher frequency could be indicative of a tonal noise generated on these smoother surfaces. One possible explanation for this observation is that thin binder films coating the surface aggregates were still present as these pavements were not subjected to traffic before testing. The sound pressure spectra also indicate that the smoother surface mixtures generate lower sound levels at the lower frequencies but higher noise levels at the higher frequencies compared to the coarser

surface mixtures. This partly explains why these mixtures appear noisier as the human ear is more sensitive to higher frequency sound levels and the A-weighting factors effectively filter out the lower frequency sound levels. The better performing mixtures in terms of sound pressure level are the OGFC mix on section S2 and the micro-surfacing on section S9.

Sound Intensity

Figure 3.8 shows the mean global sound intensity levels measured using the CPX trailer at speeds of 45 mph and 60 mph and those measured from an NCAT semi trailer at 45 mph. The sound intensity measurements with the CPX trailer rank the surface mixtures in terms of noise in the same order as the sound pressure measurements but are 1 to 2 dB(A) higher as has been observed in previous studies (14). As with the sound pressure measurements, a secondary peak in the sound intensity spectra is apparent at frequencies of 1,585 Hz and 1,995 Hz at test speeds of 45 mph and 60 mph respectively. Particularly high low frequency (316 Hz) sound levels are apparent in the sound intensity spectra plots. This is probably related to external noise influences resulting from possible vibration of the OBSI bracket.

Sound Absorption

The sound absorption plots (15) indicate negligible sound absorption for the dense-graded and SMA mixtures, as expected. Sound absorption is apparent for the open-graded mixture on section S2 and the microsurfacing mixture on section S9, albeit that the absorption coefficients on the latter mixture vary considerably depending on where on the mat the absorption testing was done. Low but discernable levels of absorption are apparent from two tests on the 9.5 mm SMA mixture on section S8, probably related to surface scatter of the sound waves from the coarser surface texture. This is emphasized to highlight the corresponding trend observed in the sound level data. Surface mixtures with higher sound absorption characteristics (such as open-graded mixtures) generally present lower CPX trailer noise levels. This does not, however, explain the lower noise levels observed for the denser mixtures under the NCAT trucks. This finding suggests that noise levels generated by heavier vehicles or higher tire pressures are perhaps more influenced by the surface macrotexture present at the tire pavement interface in contrast to lighter passenger vehicles, whose noise levels are more influenced by the porosity of the surface mixture. The interaction between surface macrotexture and porosity and the influence of these parameters on noise generated at the tire-pavement interface is not clear. Intuitively one could speculate that vehicle tires at higher pressures and under heavier loads would apply greater horizontal forces to positive texture presented from coarser surface mixtures at the tire-pavement interface compared to lighter vehicles with lower tire pressures traveling at the same speed. Hence the lower noise levels of the heavier vehicles on the smoother surfaces. Further research is needed, however, to better understand these influences.

Summary

- The noise levels generated at the tire-pavement influence on roads is related to both the macrotexture and porosity of the surface mixture. The degree to which these factors influence the noise levels appears to be related to the weight of the vehicle on the road and possibly tire pressure. For lighter passenger vehicles, the porosity of the surface and the corresponding degree of noise attenuation as observed from noise absorption testing appears to be the more dominant influencing factor. For heavier vehicles (or higher tire

pressures), the macrotexture of the surface and the positive texture presented at the tire pavement interface has a greater influence.

- To better understand the nature of the factors that influence road noise, it is recommended that additional research be done to better define the interaction at the tire-pavement interface.
- Having defined the positive and negative texture present at the tire-pavement interface, these profiles may be used to investigate these influences separately. The positive texture affords a degree of “stiffness” representing the obstacle in the tires path that would generate noise (possibly related to the forces applied at the surface) and the negative texture represents “porosity” that would serve to attenuate noise levels.

TEST TRACK FRICTION

The test sections at the NCAT Test Track have been measured for friction properties since inception of the 2000 Test Track. Similar to rutting, each new surface mixture placed on the track initiates a new set of measurements for friction. In the Test Track database, there are six unique sets of friction data.

19 surfaces trafficked from 2000 to 2002

14 surfaces trafficked from 2000 to 2005

11 surfaces trafficked from 2000 to 2008

8 surfaces trafficked from 2003 to 2005

13 surfaces trafficked from 2003 to 2008

19 surfaces trafficked from 2006 to 2008

All of the sections have been measured for friction properties with standard skid trailers operated by the Alabama DOT. In general, the frequency of friction measurement was monthly, but a few periods extended further due to scheduling conflicts with the skid trailers. In addition to the standard skid trailer friction measurements, the Dynamic Friction Tester (DFT) and CTM were used on the Test Track sections. These devices are small portable devices with a footprint of approximately 18 inches by 18 inches that measure the friction resistance and macro-texture of a defined circular path. The DFT and CTM are American Society for Testing and Materials (ASTM) standard tests. The amount of DFT and CTM measurements on the Test Track sections is lower and less consistent than the skid trailer measurements.

To compare skid trailer measurements and DFT measurements, the international roadway safety community developed the universal International Friction Index (IFI). Through correlation studies, the IFI was intended to compute comparable friction values from various friction measurement devices. Research papers examining the application of IFI have had mixed results. The friction study at NCAT will utilize the controlled traffic conditioning and multiple HMA surfaces at the Test Track to further examine the use of IFI.

A global analysis of the friction performance of the sections at the Test Track has not been undertaken until recent months. NCAT research in this area is still in its early stages. Most of the emphasis is on developing a laboratory conditioning and testing protocol. With a practical laboratory protocol, highway agencies will be able to evaluate HMA mixture surface friction

performance in a matter of weeks, instead of the three to five years needed to gather data from full scale field test sections.

NCAT is currently working on a second phase study to calibrate and validate a laboratory conditioning and testing program using the three-wheel polishing device (TWPD), DFT and CTM. The TWPD was developed in an earlier NCAT study. A preliminary step of the current research is to better define the friction performance of the Test Track sections and select appropriate sections for the laboratory study. This effort is underway.

The initial focus of the Test Track friction analysis is to define each test section based on the section's long-term friction performance. The boundaries for the study are the friction measurements between the 2-million ESAL and 10-million ESAL traffic levels. Defining friction relative to ESALs is comparable to using the real parameter (wheel passes). The three parameters that will be determined from this initial analysis are:

- Long-term friction loss trend (linear best fit)
- Seasonal impact (polynomial best fit)
- Measurement variation (distribution about the seasonal best fit)

The friction data from initial construction to 2-million ESALs accounts for the dramatic change in friction associated with friction increase as the asphalt binder film wears away and the steep friction loss due to initial aggregate polishing. Most of the Test Track sections display this friction pattern. After the initial aggregate polishing, the surface friction performance stabilizes. The initial analysis of the study focuses only on the long-term (stable) friction performance. A generic friction performance curve is given in Figure 3.10.

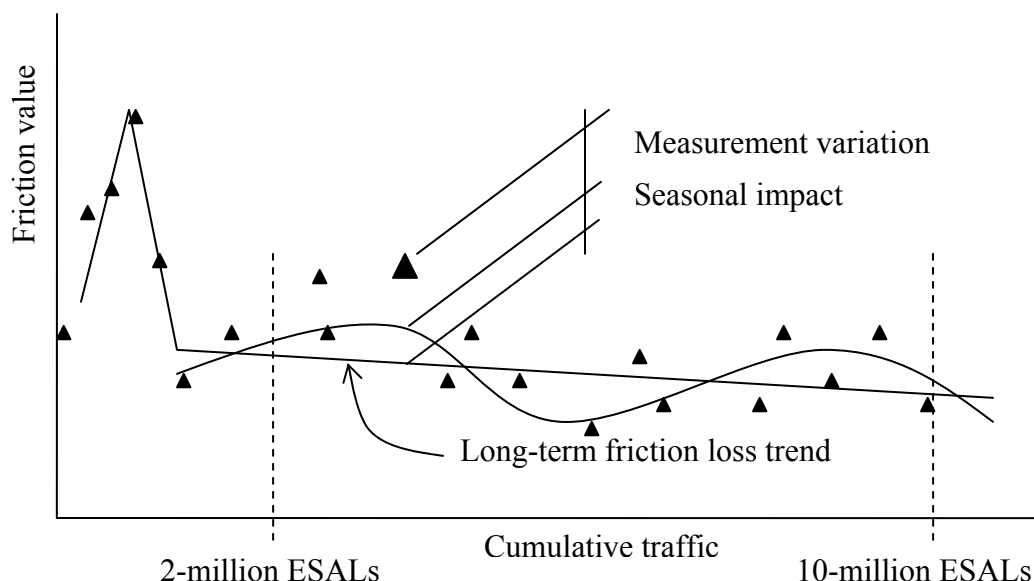


Figure 3.10. Generic HMA Surface Friction Performance Curve

CONSTRUCTION AND PERFORMANCE OF PERMEABLE SURFACE MIXES

Sponsors typically fund research on two or more sections to compare the performance of paving alternatives. In Phase III, GDOT sought to compare the construction and performance of permeable surface mixes containing two different aggregate sources and to compare permeable surface courses placed with conventional and dual layer paving equipment.

Permeable mixes with two different aggregate sources were studied to compare the effects of aggregate shape (percentage of flat and elongated particles) on drainage characteristics and performance. Currently, Georgia specifications require that aggregates used for porous mixtures have LA Abrasion values of 50 or less. Georgia’s flat and elongated specification limits 5:1 flat and elongated particles to 10 percent. A favorable comparison between the single and dual layer pavements could result in improved performance with respect to drainability, noise, etc. Constructability issues with the dual layer paver during construction were also of interest to GDOT.

Experimental Design

All three sections were placed on perpetual foundations to ensure that distresses would be isolated to the experimental surface mixes. Two porous pavement sections were placed with a conventional single layer paver, one containing cubical aggregate (15% 3:1 flat and elongated in section N11) and the other containing a higher percentage of flat and elongated particles (29% 3:1 flat and elongated in section N12). The third section (N13) was built using the same slightly flat and elongated aggregate; however, the surface consisted of a thin 9.5 mm NMAS porous mix over the same 12.5 mm NMAS porous mix. The purpose of the 9.5 mm NMAS upper mix was to prevent debris from potentially clogging the void structure of the lower 12.5 mm NMAS mix. Figure 3.11 shows the aggregate gradation of the sections. N13-1 and N13-2 in the chart refer to the mixture used in the top and bottom layers of section N13, respectively. The DGA mix (S11) has been shown for comparison purposes.

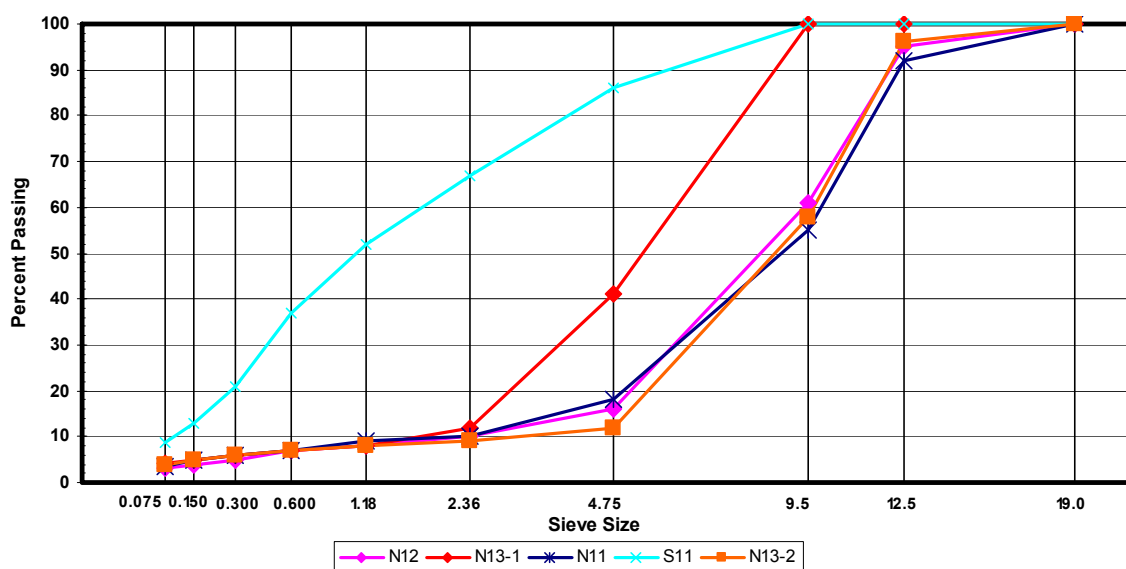


Figure 3.11. Aggregate Gradations of the Sections

Drainable surface mixes on sections N11 and N12 were supported by 38 mm of conventional GDOT dense-graded mix, while section N13 was supported by 54 mm of the same dense-graded mix. The planned thickness of the 12.5 mm NMAS porous mix on all three sections was 32 mm; however, section N13 also included 16 mm of 9.5 mm NMAS porous surface mix. The job mix formulas are documented elsewhere ([14](#)).

Placement

Sections N11, N12 and N13 were milled beforehand to depths that would facilitate the planned mat placements. A conventional paver was used to place all the lifts in sections N11 and N12, as well as the lower lift of dense-graded mix in section N13. A European dual layer paver with a German crew was provided by Dynapac for the simultaneous placement of both drainable mixes on the surface of section N13. The dual-layer paving machine (Dynapac F-300 C/S) was manufactured in Germany, disassembled, shipped to the Track then reassembled for use. Before being used to place mix on the track, the newly reassembled machine was first used to simultaneously place two lifts of uncoated aggregate materials at an off-track location. The dual layer paver was then moved to section N13 for placement of the experimental mixes on the surface of the track. No tack coat was necessary between the two porous mixes.

Dual layer paver technology has been used in Europe for approximately 10 years ([18](#); [19](#)). The lower layer hopper was reported to have a 45 ton capacity, while the upper layer hopper was reported to have a 25 ton capacity. One of the challenges in building the dual layer section was filling of the paver's upper hopper. Because the Dynapac material transfer device designed to feed the upper hopper of the dual layer paver was not available, a temporary ramp had to be built on the track so that the Roadtec SB2500 material transfer device in use at the Track could reach the upper hopper. Compactive effort was adjustable on both the lower and upper screeds, with the amount of effort controlled by the crew. The reported cost of the unit used at the Track was between \$1.2 and \$1.4 million ([Nittinger, Unpublished Data](#)).

After work on all test sections was completed, the NCAT profiler was used to assess the smoothness of the experimental mats. As seen in Figure 3.12, the smoothness of section N13 (placed with the dual layer paver) compared well with the smoothness of sections N11 and N12 (placed with a conventional single layer paver). Additionally, mat densities were determined by volumetric analysis of cut cores. Air voids in the mat (shown in Figure 3.13) generally met GDOT's expectations for porous surface mixes.

Laboratory Performance

Cores were also obtained for permeability testing and interlayer bond strength measurements. Bond strength measurements are presented in Figure 3.14 while laboratory permeabilities are shown in Figure 3.15. It is seen in Figure 3.14 that bond strengths between the dual layer pavements were comparable to bond strengths between tacked layers. Further, it is seen in Figure 3.15 that permeabilities measured for the porous mixtures were very good.

Field Performance

After 10 million ESALs, very little rutting had occurred in any of the three test sections. Changes in roughness and macrotexture resulting from the application of traffic are presented in Figures 3.16 and 3.17, respectively. The lower macrotexture results for Section N13 are due to the smaller NMAAS gradation used as the surface of that section.

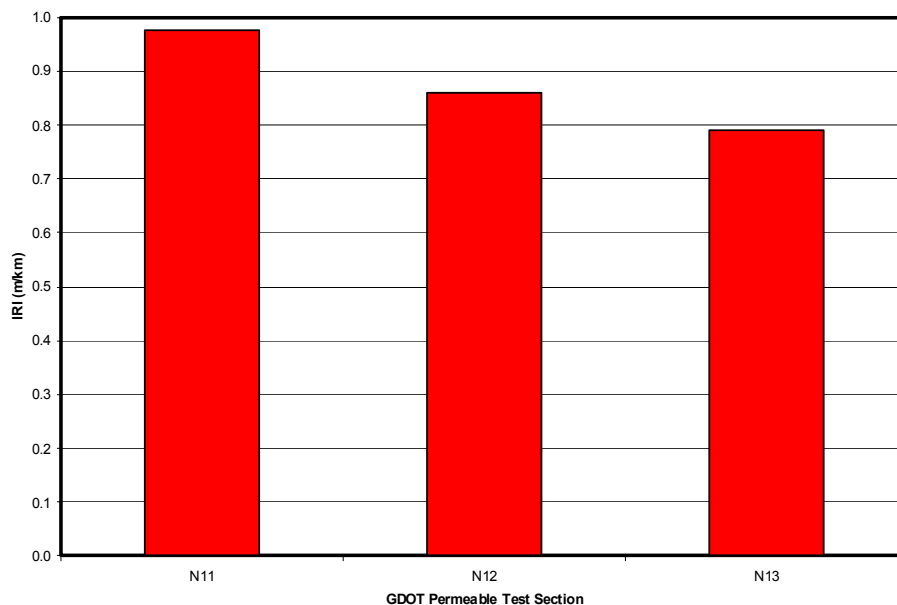


Figure 3.12. Post-Construction Smoothness Comparison (14)

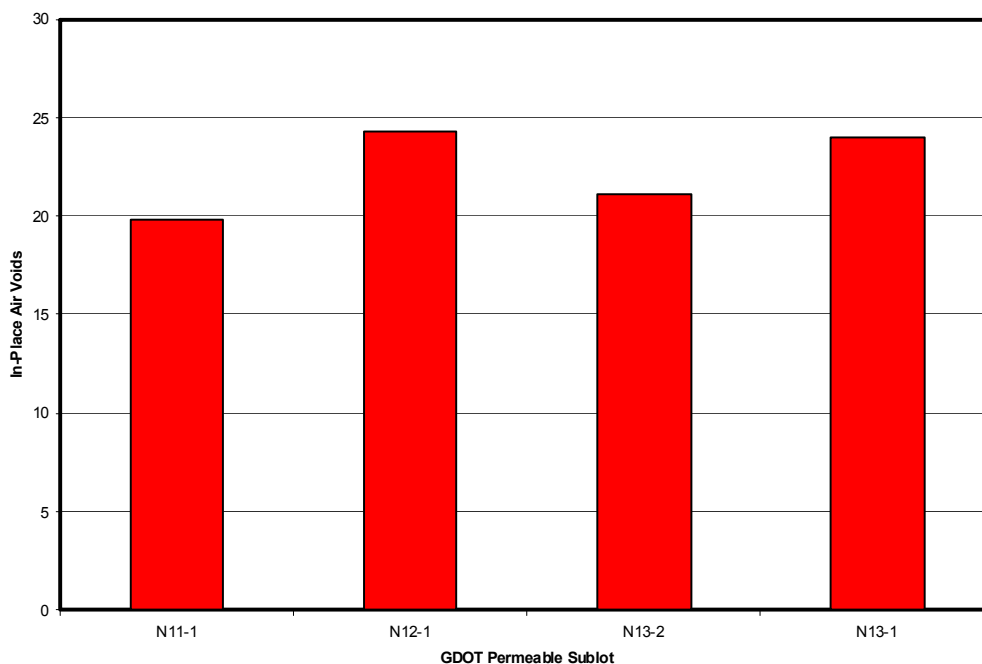


Figure 3.13. Post-Construction Air Voids for all Porous Surface Lift Sublots (1 = Upper Lift, 2 = Lower Lift) (14)

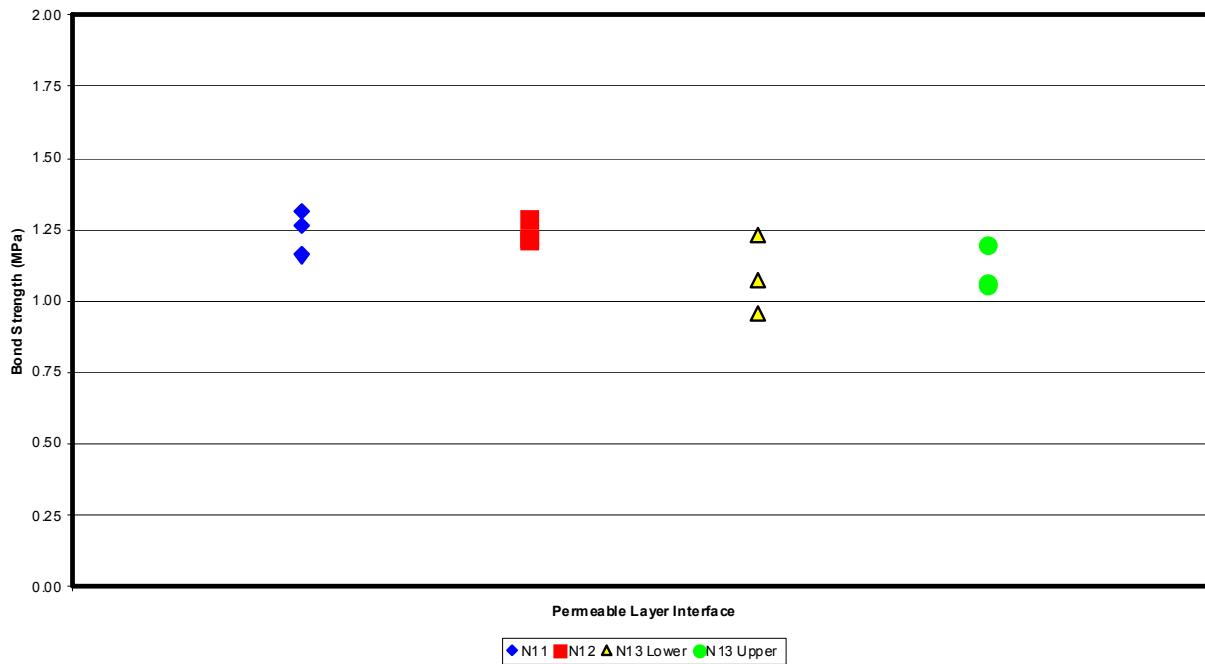


Figure 3.14. Interlayer Bond Strength Measurements from Mat Cores (14)

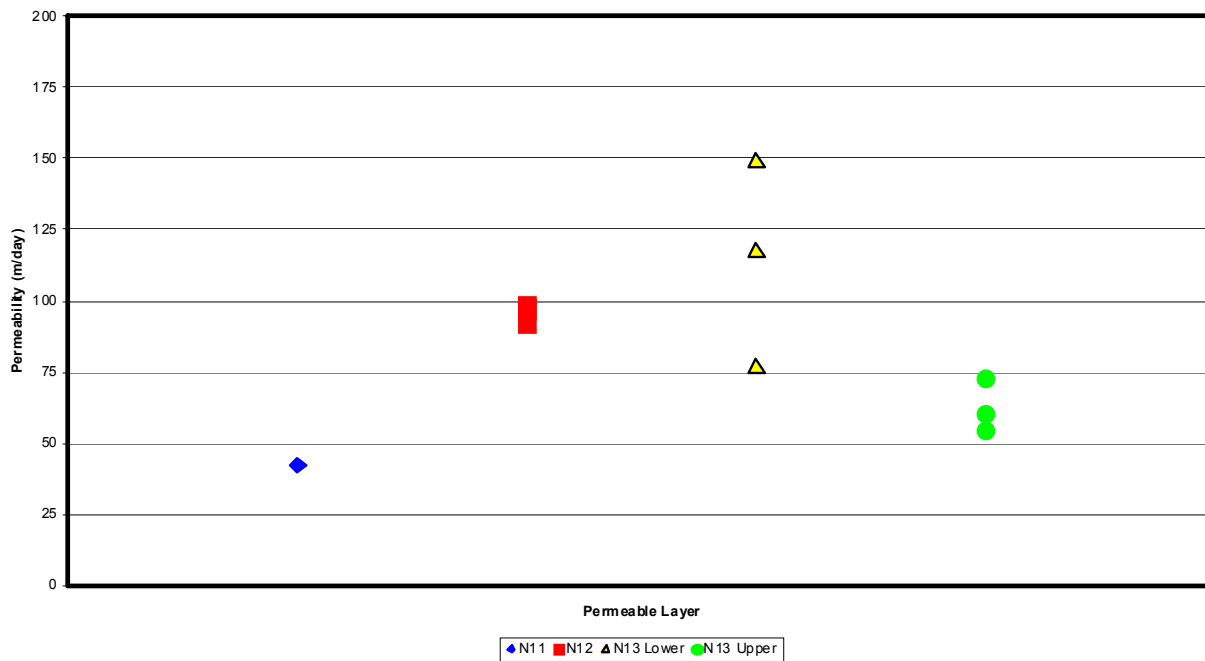


Figure 3.15. Laboratory Permeability Measurements from Cut Cores (14)

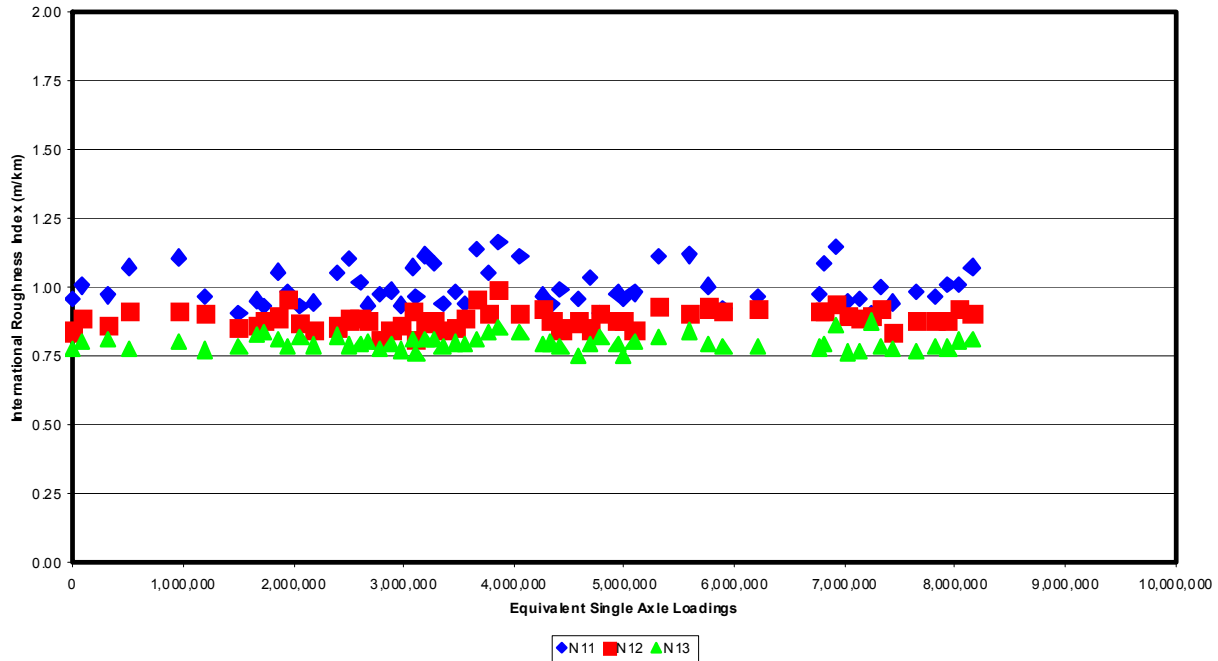


Figure 3.16. Roughness Measurements as a Function of Truck Traffic (14)

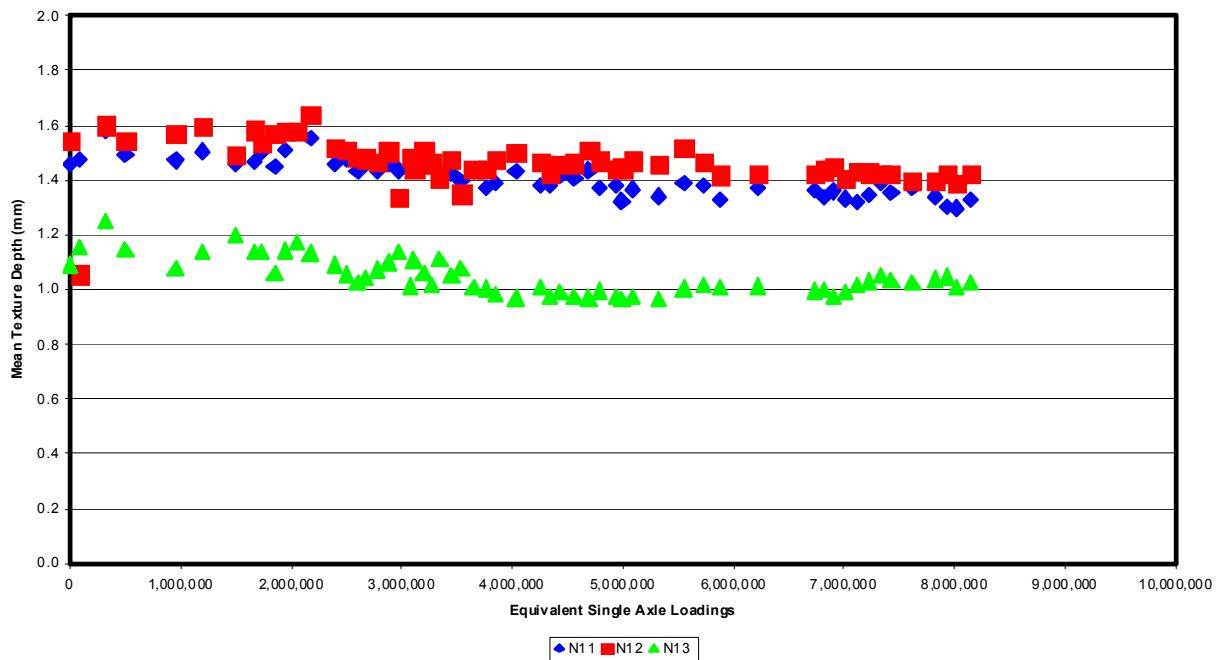


Figure 3.17. Macrotexture Measurements as a Function of Truck Traffic (14)

Noise

Sound level measurements were performed approximately quarterly following construction, beginning in December 2006. Table 3.5 includes the date of the measurements, noise level recorded, and the amount of traffic (cumulative) that each section received prior to the measurement. Data from the fine-graded HMA surface on section S11 is provided as a control comparison. Figure 3.18 shows the sound pressure measurements through this roughly two -year cycle.

Table 3.5. Summary of the Noise Measurements and Traffic

Date	Traffic (ESAL)	Sound Pressure Level (SPL), dB(A)			
		N11	N12	N13	S11
15 Dec-06	410,690	96.1	95.1	89.0	94.4
7 Mar-07	1,412,107	94.9	94.4	88.5	92.4
22 May-07	2,520,987	94.8	94.5	90.0	93.2
14 Dec-07	5,163,668	96.0	95.5	90.9	94.4
17 Mar-08	6,215,771	95.6	94.8	90.5	94.8
9 Jan-09	10,017,560	96.3	94.6	91.3	95.5

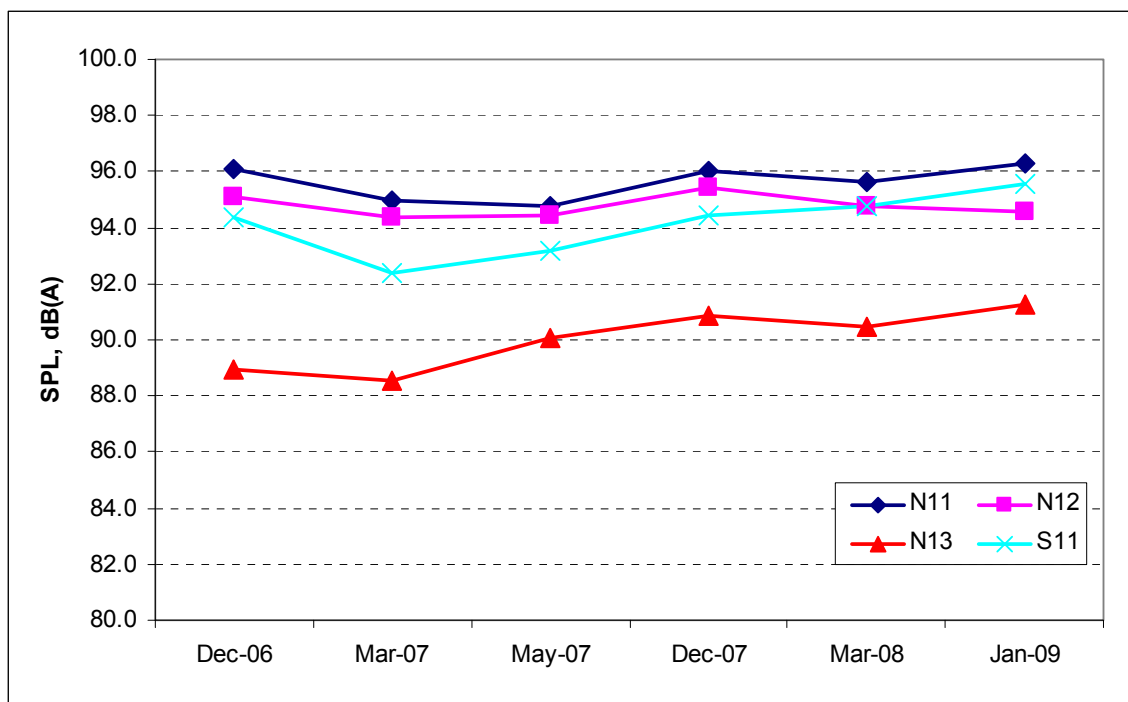


Figure 3.18. SPL of the Sections over Time

Section N13, the double-layer porous surface, shows a very gradual increase in sound pressure level over the two year period, but remains the quietest of the four sections. Higher noise levels were measured on the fine-graded Superpave surface mix on S11, and the 12.5 mm NMAS single-layer porous surface mixes in N11 and N12. These results show some variations in the

noise levels over time which may include aggregate reorientation, surface wear and aging affects, as well as possible seasonal effects.

To better understand the noise absorbing characteristics of these test sections, Figures 3.19 to 3.24 show noise spectra measurements over this time period. Porous surface course sections, N11, N12, and N13, revealed typical bell-shaped spectra. The double-layer surface on section N13 shows lower amplitude values at each frequency band compared to the single-layer porous surface sections. Section S11 was characterized by a spectrum shifted toward higher frequencies which are more annoying to the human ear.

Analysis of the noise-frequency spectra for the double-layer porous surface, N13, through each plot shows the low frequency (less than 1000 Hz) sound pressure measurements are consistently lower than those of the N11 and N12 spectra.

Comparison of the noise spectra from sections N11 and N12 shows that the results were similar except between 800 and 1600 Hz, where N12 (built with a higher percentage of flat and elongated particles) was consistently quieter. This difference may be attributed to the slight differences in particle shapes and gradations for these two porous friction courses. However, the average difference over that frequency range was 0.8 dB (A) which is not significant within human auditory perception.

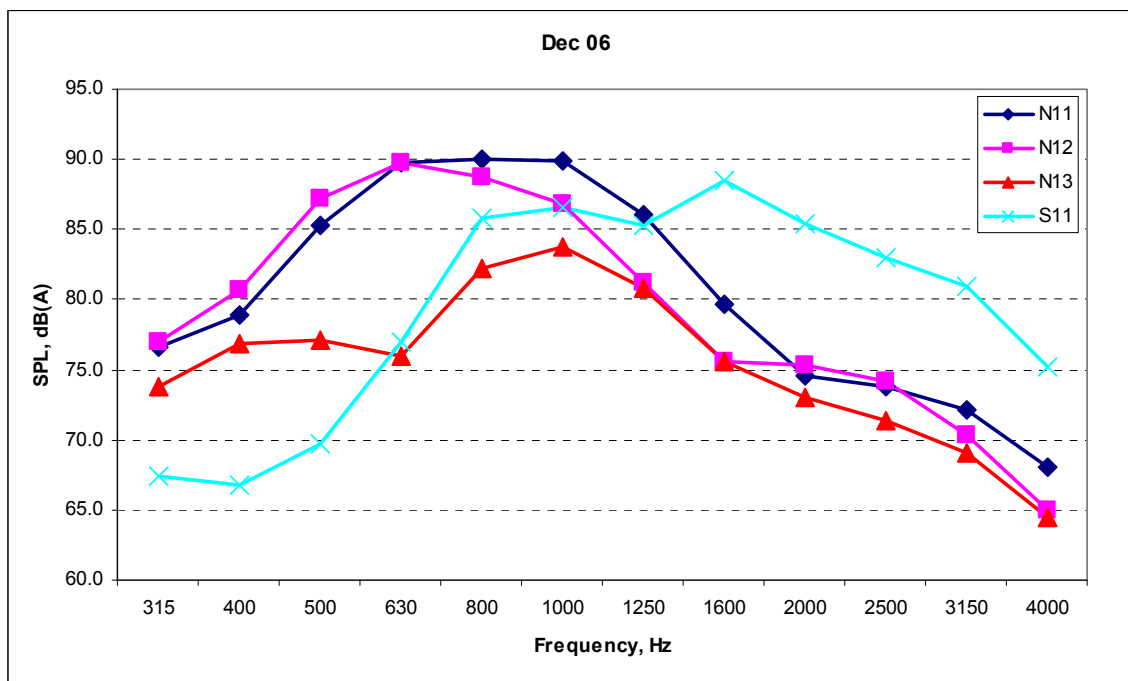


Figure 3.19. Noise Spectra – Dec-06 Measurements

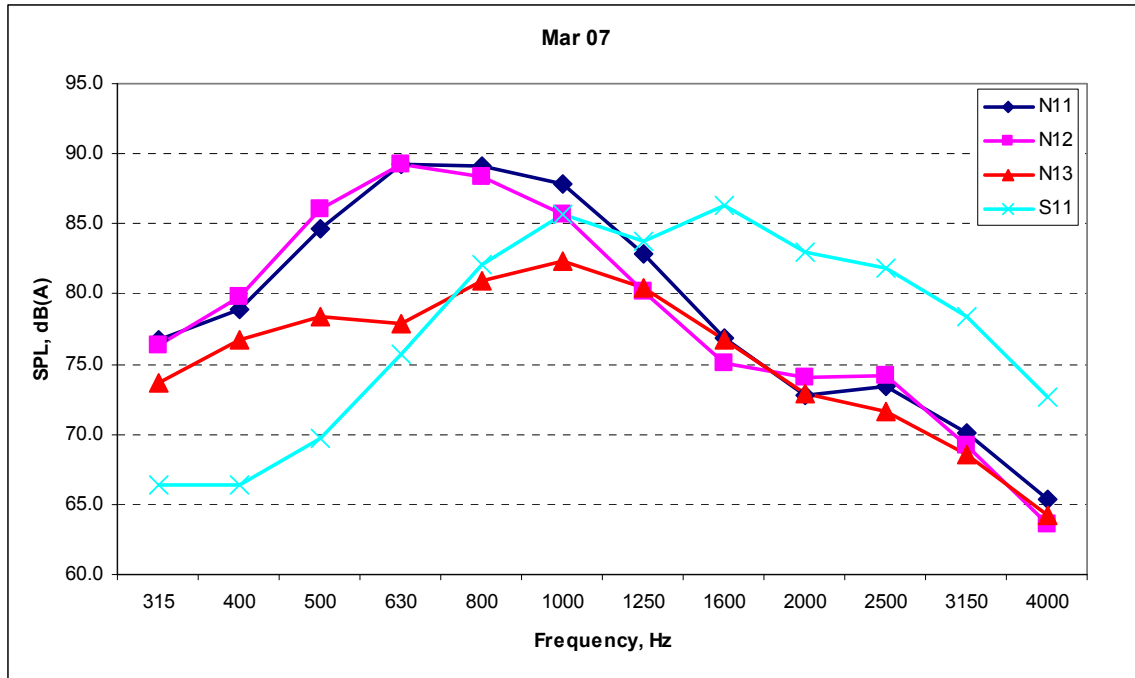


Figure 3.20. Noise Spectra – Mar-07 Measurements

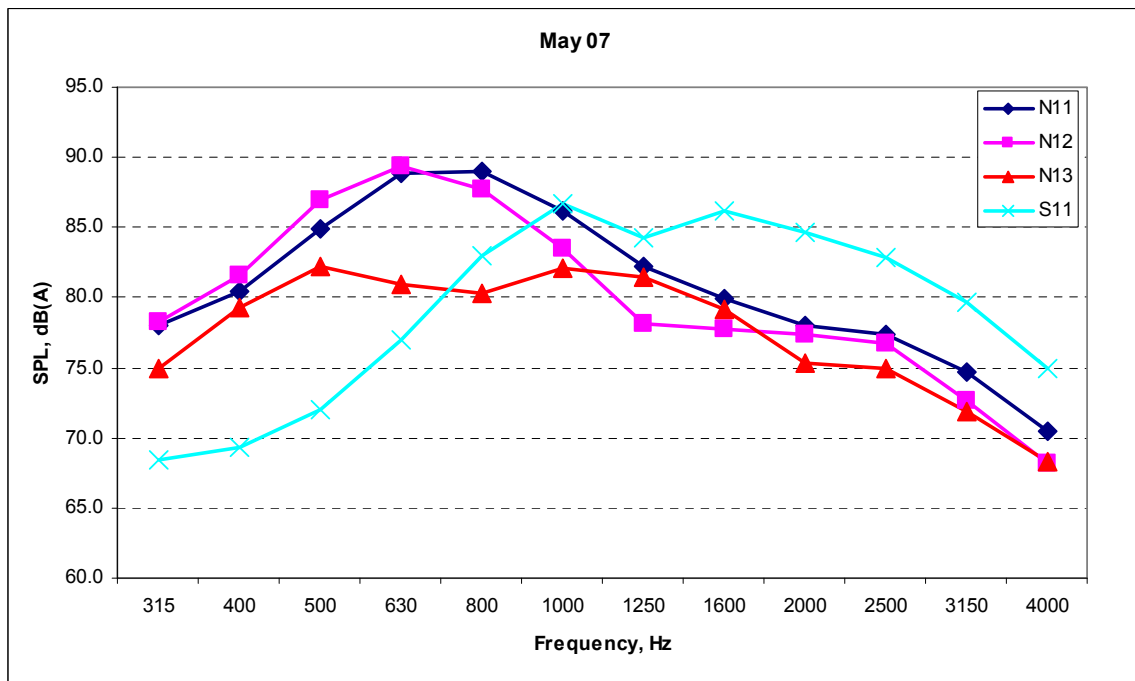


Figure 3.21. Noise Spectra – May-07 Measurements

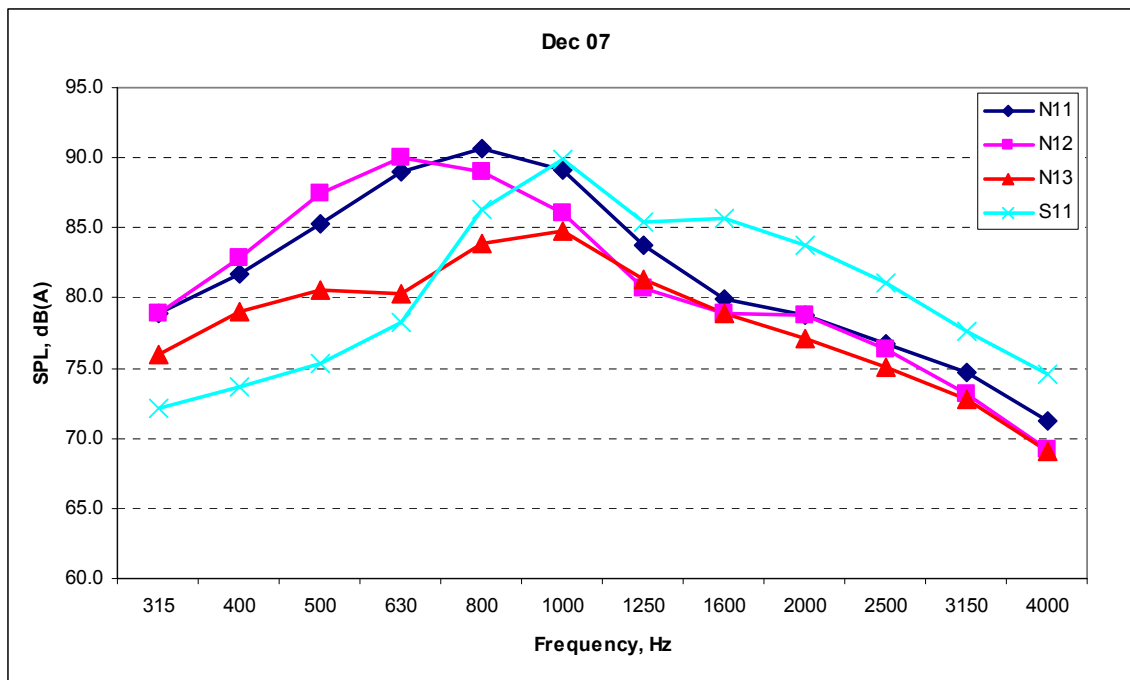


Figure 3.22. Noise Spectra – Dec-07 Measurements

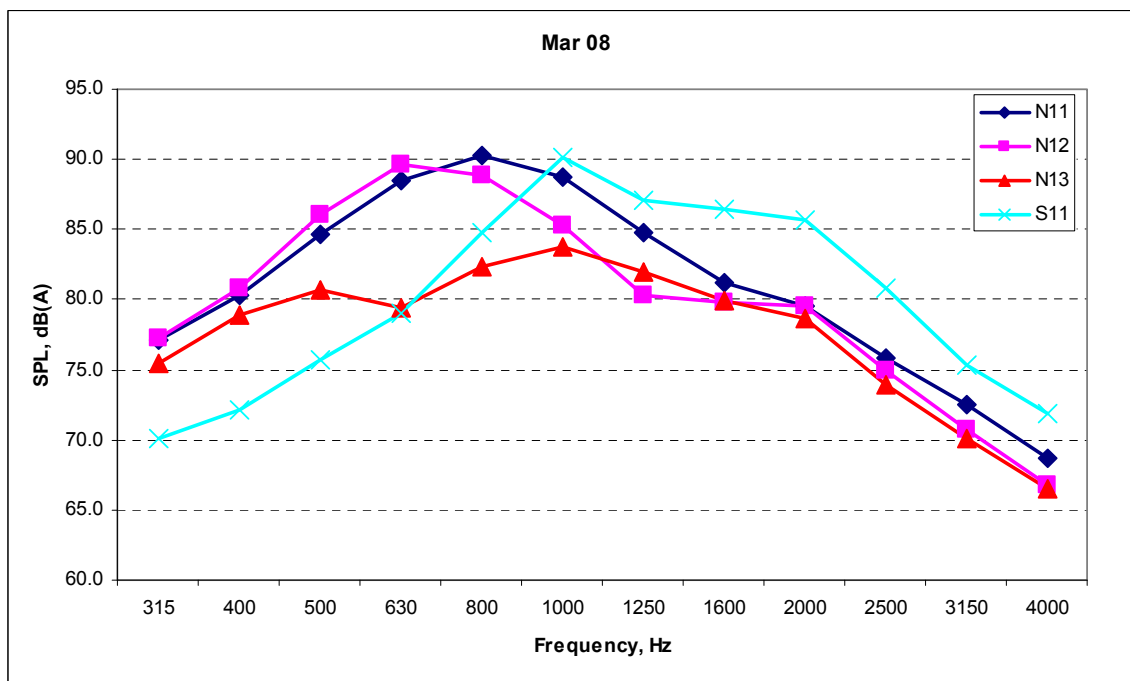


Figure 3.23. Noise Spectra – Mar-08 Measurements

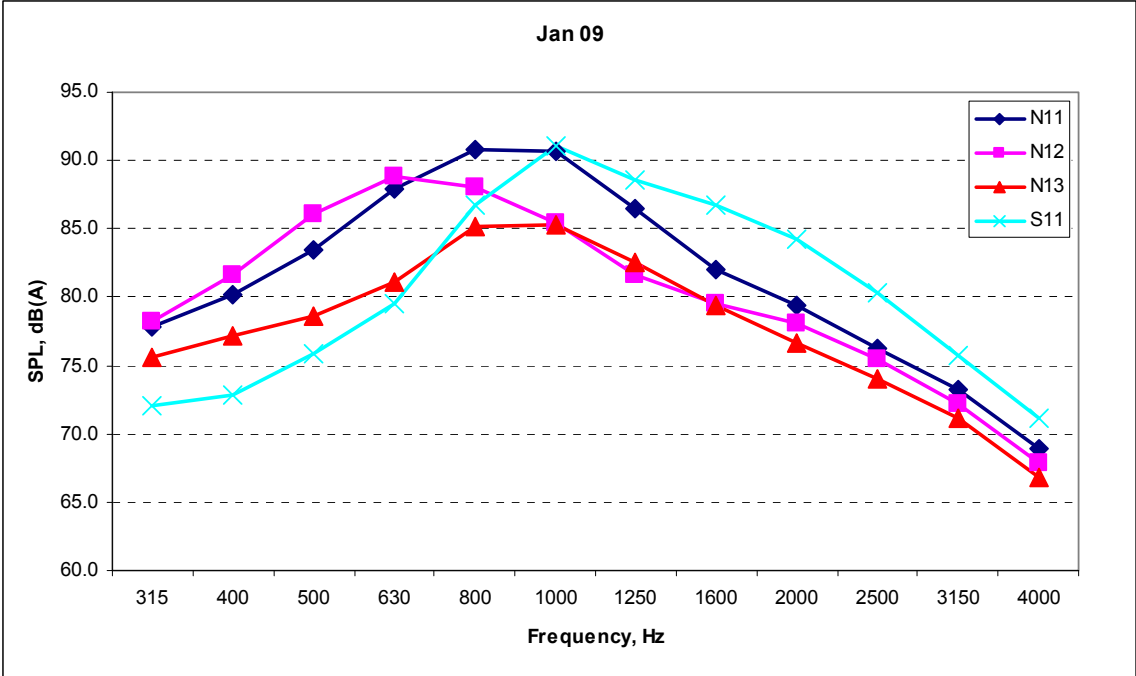


Figure 3.24. Noise Spectra – Jan-09 Measurements

Drainage

Observations of the drainage performance of the porous mixes were made at times when natural rainfall presented the opportunity. Following extended rainfall events, videos were made while following one the Track’s heavy trucks as it drove across all 46 test sections. Still pictures clipped from a road spray video file recorded on May 15, 2008 after four hours of rain falling at a rate of approximately 6 mm per hour are shown in Figure 3.25. Here, it is seen that the rain has exceeded the drainage capacity of the porous mix on N11 containing the most cubical aggregates. Water can be seen ponding in the wheelpaths. In comparison, the porous mix on N12 containing a higher percentage of flat and elongated particles appears to be nearing capacity, with isolated areas of visible water. The dual layer porous surface appears to still be functioning very well.



Figure 3.25. Road Spray Observed Following Four Hours (6 mm per hour) of Rain During Fleet Operations (14)

Conclusions and Recommendations

The following conclusions and recommendations can be made based on the results of this comparison study that will be useful to both the highway industry and roadway construction practitioners:

- The construction quality of all three sections was generally very good, with mat air voids and roughness values approximately equal. Besides the ramp improvisation necessary for the MTD boom to load the upper hopper, no special problems were encountered with the dual layer paver.
- The interlayer bond strengths for all the porous mixes were excellent, including the bond strength between the 9.5 and 12.5 mm dual layer lifts in section N13. Laboratory permeabilities were also very good for all test mixes.
- The field drainability exhibited by the section built with slightly flat and elongated aggregate appeared to function better than the section built with the more cubical aggregate after prolonged rain.
- The field drainability exhibited by the dual layer pavement appeared to be better than the conventional single layer drainable surface after prolonged rain.
- At lower noise frequencies, the porous layer with more flat and elongated particles showed lower sound amplitudes than the section with more cubical aggregate. This aspect may be related to the volume and shape of the voids and their capabilities in limiting resonance effects. These hypotheses require additional studies specifically on the texture and its variability on the three porous surface sections.
- Drainability, durability (as indicated by change in MTD) and sound should be monitored with additional traffic in order to document any changes in performance that could result from the accumulation of debris within the internal void structure of these three porous pavement test sections.

DETERMINATION OF RUT DEPTH CRITERIA FOR LABORATORY PERMANENT DEFORMATION EVALUATION

The Superpave mix design procedure was originally envisioned to consist of a volumetric design procedure and performance tests (20). The volumetric mix design process has been adopted by most state agencies, and the Superpave gyratory compactor (SGC) has been used to determine volumetric properties for the general acceptance of HMA mixes. However, the performance tests using the Superpave shear tester and the indirect tensile tester developed for use in the Superpave mix design procedure are expensive and require extensive operator training. Hence, these tests have not been adopted by state agencies for routine testing (21).

Increasing truck traffic has contributed to the demand for rut-resistant HMA on major highways. Therefore, there is a need for a test that can indicate the rutting resistance of mixes and that can be conducted in a timely manner during mix design processes or for quality assurance purposes. For these reasons, loaded wheel testers (LWT), such as the APA and Hamburg Wheel Tracking Device (HWTD), have been adopted for checking the rutting resistance of HMA during the mix design process in many states.

The LWT rut depth has a reasonable correlation with field performance on an individual project basis. However, prediction of field rut depths using LWT results for a given project based on

relationships developed from other projects with different geographic locations and traffic is not generally reliable (22). In addition, LWTs do not provide a fundamental property that can be used with an advanced material characterization model to account for any specific stress state and temperature. Thus, research has been initiated to develop a new performance-related test for permanent deformation for incorporation in the Superpave volumetric mix design method and pavement structural design.

Under NCHRP Project 9-19 (23), the dynamic modulus (E^*) and flow number (F_n) tests were selected as simple performance tests for permanent deformation. However, the E^* test has been used mainly as the prime test method for HMA materials characterization for pavement structural design in the Mechanistic-Empirical Pavement Design Guide (MEPDG) developed under NCHRP Project 1-37A (24), and the F_n test has been considered as a potential performance test for permanent deformation. Commercial testing equipment, the AMPT or formerly known as Simple Performance Tester (SPT), is available for possible adoption of the F_n and E^* tests for routine use in the Superpave mix design method and in HMA materials characterization for pavement structural design (25).

One objective of the NCAT Pavement Test Track study was to evaluate correlations between laboratory permanent deformation measurements using APA and F_n tests and field rutting performance for a variety of HMA mixtures used at the NCAT test track. Based on these correlations, rut depth criteria were determined and proposed for future implementation.

Experimental Plan

The experimental plan is shown in Table 3.6. Ten test sections shown in the first column of Table 3.4 were selected for this study. Sections S7 and S8 were divided into two 100-foot subsections (S7A, S7B, S8A and S8B), and a unique HMA mixture was utilized for each subsection. Thus, twelve plant-produced mixes were sampled.

Specimen Preparation

All mixes used for preparing specimens in the laboratory were plant-produced and sampled during the construction of the test sections. Twelve mixes were sampled, of which nine mixes were 12.5 mm nominal size and three mixes were 9.5 mm nominal size. Two test sections used 15 percent RAP.

Table 3.7 shows the quality control gradation and binder content of the twelve mixes. A detailed description of HMA mixture properties for each test section/subsection is available on the NCAT Pavement Test Track website (26).

For each HMA mixture, twelve test specimens were prepared for the APA testing at the test track laboratory immediately after sampling. Six replicates were compacted to N_{des} gyrations with a final height of 115 ± 5 mm. These test specimens were not cut to a height of 75 ± 1 mm but tested using molds that can accommodate 115 mm high compacted specimens. The other six replicates were prepared for target air voids of 7 percent. The sample mass used for preparing these specimens was calculated based on the research team experience with mixtures used in the NCAT laboratory. Most of the samples had the air voids between 6 and 7 percent.

Three replicates were prepared of each HMA mix for F_n tests by reheating the plant-produced mixes in the laboratory. For each test replicate, a cylinder 180 mm high and 150 mm in diameter was first compacted in an SGC. The compacted specimen was then cored at the center, and both ends of the core were trimmed. The final test specimen was 150 mm high and 100 mm in diameter. The target air void level for these test specimens was $7 \pm 0.5\%$. Table 3.8 shows a summary of the average and standard deviation of air voids for each set of specimens tested in this study.

Laboratory Testing

All APA testing was conducted at 64 C (147 F). This is the high temperature of the standard Superpave performance grade (PG) binder determined using the LTPP Binder software for the test track location in Opelika, Alabama. After seating the test specimens, tests were run for 8,000 cycles. A hose pressure of 830 kPa (120 psi) and a wheel load of 533 N (120 lb) were used to test all of the specimens that were compacted to N_{des} . These conditions were recommended in NCHRP Report 508. For the group of specimens compacted to the target air voids of 7 percent, a hose pressure of 690 kPa (100 psi) and a wheel load of 445 N (100 lb) were used in accordance with AASHTO TP 63-07. Both automatic and manual rut-depth measurements were taken for each test.

The F_n tests were conducted using an AMPT. The specimens were tested at a deviator stress of 70 psi and a confining pressure of 10 psi. The tests were terminated when the samples had deformed to 100,000 microstrain. Some F_n tests were first conducted at the same temperature as the APA test (64°C); however, the specimens failed quickly. Thus, the research team decided to reduce the testing temperature from 64 C to 58 C. The flow number was determined using two model forms—power and Francken models. The non-linear regression analysis used to fit both models to the test data was performed within the AMPT testing software.

Test Results and Analysis

Table 3.9 shows 1) the average APA rut depths measured manually and automatically; 2) the average flow numbers determined using the power and Francken models; and 3) the rut depths measured in the field for approximately 5 and 10 million ESALs.

The correlations between the APA rut depths/flow numbers and field rutting performance were shown in Tables 3.10 and 3.11 for 5 and 10 million ESALs, respectively. The most common measure of correlation between data is Pearson's correlation (Pearson's r) with p -value. Pearson's correlation reflects the degree of linear relationship between two variables. It ranges from -1 to +1. A correlation of -1 or +1 means that there is a perfect negative or positive linear relationship between variables. If the probability value (p -value) is lower than 5 percent (p -values < 0.05), the correlation coefficient (Pearson's r) is considered statistically significant.

As shown in Table 3.7, the APA automated measurement using 7 percent void specimens and flow number determined using the Francken model exhibited reasonably good correlations with the rut depths measured in the field for 5 million ESALs. These correlations were significant (p -value < 0.05). The correlations between the laboratory and field rutting performance for 10 million ESALs were not as strong as those for 5 million ESALs and not significant (p -value > 0.05).

Table 3.6. Experimental Plan

Sect.	Sponsor	Mix Type	Binder	RAP%	NMAS	APA		F _n
						Ndes 120lb / 120psi	7% 100lb / 100psi	7% 70psi / 10psi
N1	FL	Super	67-22	0	12.5	6	6	3
N2	FL	Super	76-22	0	12.5	6	6	3
N8	OK	SMA	76-28	0	12.5	6	6	3
N10	MO	Super	70-22	0	12.5	6	6	3
S2	MS	Super	76-22	15	9.5	6	6	3
S6	TN	411-D	64-22	15	12.5	6	6	3
S7A	IN	Super	64-22	0	12.5	6	6	3
S7B	IN	Super	64-22	0	12.5	6	6	3
S8A	IN	Super	64-22	0	12.5	6	6	3
S8B	IN	Super	64-22	0	12.5	6	6	3
S11	AL	Super	76-22	0	9.5	6	6	3
S12	TX	D-A	76-22	0	9.5	6	6	3
No. of Test Specimens						72	72	36

Table 3.7. Quality Control Gradation and Binder Content of 12 HMA Mixtures

Sieve Size	Percent Passing											
	N1	N2	N8	N10	S2	S6	S7A	S7B	S8A	S8B	S11	S12
1"	100	100	100	100	100	100	100	100	100	100	100	100
3/4"	100	100	100	99	100	100	100	100	100	100	100	100
1/2"	97	97	93	96	100	96	98	100	97	98	100	100
3/8"	82	85	71	83	99	88	90	91	88	88	100	97
No. 4	59	61	31	52	76	69	71	76	66	63	86	65
No. 8	49	50	22	33	48	49	58	53	53	49	67	38
No. 16	39	39	17	21	33	36	45	42	41	38	52	36
No. 30	30	31	15	14	24	26	32	30	30	28	37	18
No. 50	22	23	13	9	13	14	18	17	18	18	21	11
No. 100	14	15	12	7	8	9	12	11	11	12	13	10
No. 200	8.8	9.6	10.5	5.4	6.0	7.3	8.0	7.4	7.5	7.8	8.6	7.4
%AC	4.9	4.8	6.9	5.6	7.4	6.3	6.5	6.1	6.2	6.1	6.9	7.4

Table 3.8. Average and Standard Deviation of Air Voids

Section	APA Test				F _n Test	
	N _{des}		7% Target Voids		7% Target Voids	
	Avg.	Std. Dev.	Avg.	Std. Dev.	Avg.	Std. Dev.
N1	2.1	0.08	6.4	0.29	7.0	0.30
N2	2.5	0.14	6.4	0.24	6.9	0.30
N8	5.4	0.38	6.3	0.27	6.7	0.30
N10	5.0	0.28	6.6	0.46	7.0	0.15
S2	2.6	0.15	6.4	0.14	6.9	0.40
S6	2.1	0.27	6.0	0.36	6.7	0.29
S7A	0.8	0.10	6.1	0.10	7.0	0.17
S7B	2.6	0.26	6.5	0.16	7.0	0.35
S8A	2.0	0.13	6.5	0.17	7.0	0.31
S8B	1.1	0.10	6.3	0.33	6.8	0.10
S11	3.8	0.10	6.9	0.23	6.8	0.06
S12	1.9	0.20	6.7	0.34	7.0	0.20

Table 3.9. Average APA Rut Depth Measurements and Flow Numbers

Section	APA Test				Fn Test		Field Rut	
	N _{des} 120lb/120psi		7% Voids 100lb/100psi		7% Voids 70psi/10psi		~ 5 mil ESAL	~ 10 mil ESAL
	Manual (mm)	Auto (mm)	Manual (mm)	Auto (mm)	Power (cycle)	Francken (cycle)		
N1	3.76	2.55	3.65	4.99	493	493	1.40	N/A
N2	3.04	1.45	3.43	4.26	726	1121	1.50	3.7
N8	3.99	3.45	2.04	2.12	1877	1840	2.00	2.3
N10	4.74	2.99	3.85	4.42	500	618	8.30	12.3
S2	1.71	2.91	5.67	6.48	878	1110	0.70	0.7
S6	3.46	4.49	4.31	4.95	1615	1177	1.30	2.3
S7A	11.30	7.48	8.85	10.91	350	348	33.40	N/A
S7B	6.59	4.15	5.05	6.76	351	407	21.30	N/A
S8A	2.09	3.78	6.60	8.82	302	301	23.00	N/A
S8B	5.08	2.82	6.19	8.23	274	280	24.60	N/A
S11	7.26	5.71	5.93	6.89	656	752	6.80	11
S12	3.57	2.05	4.25	4.68	613	731	13.80	19.5

Notes: N/A = not available because the surface mixes of these sections were replaced after approximately 5 million ESALs due to excessive cracking and rutting

Table 3.10. Correlations between Lab and Field Rutting Performance for 5 Million ESALs

Correlation Statistics	APA Test				Fn Test	
	N _{des} 120lb/120psi		7% Voids 100lb/100psi		7% Voids 70psi/10psi	
	Manual	Auto	Manual	Auto	Power	Francken
Pearson's r	0.612	0.499	0.751	0.795	-0.637	-0.879
p-value	0.035	0.099	0.005	0.002	0.026	0.004

Table 3.11. Correlations between Lab and Field Rutting Performance for 10 Million ESALs

Correlation Statistics	APA Test				Fn Test	
	N _{des} 120lb/120psi		7% Voids 100lb/100psi		7% Voids 70psi/10psi	
	Manual	Auto	Manual	Auto	Power	Francken
Pearson's r	0.465	-0.08	-0.015	-0.060	-0.623	-0.713
p-value	0.293	0.865	0.975	0.898	0.135	0.072

Figure 3.26 shows a comparison of rut depths measured in the field after 5 and 10 million ESALs. For all of the sections that survived 10 million ESALs, the rate of rutting was higher for the first 5 million ESALs from the start of traffic in November 2006 through the end of 2007. Figure 3.26 also showed that if the critical rut depth in the field was 12.5 mm, all of the mixes that performed well for the first 5 million ESALs would perform well in terms of rutting for 10 million ESALs. In other words, the rut-susceptible HMA mixtures exhibited rut depths that were greater than the critical rut depth of 12.5 mm within the first 5 million ESALs. Thus, in order to determine critical rut depth criteria for rutting evaluation using the APA and F_n tests in the laboratory, correlations between the laboratory and field rutting performance for 5 million ESALs were developed. Figure 3.27 shows the correlation between the average APA rut depths measured automatically using 7 percent void specimens and the rut depths measured in the field. The correlation between the average flow numbers determined using the Francken model and the field rut depths is presented in Figure 3.28.

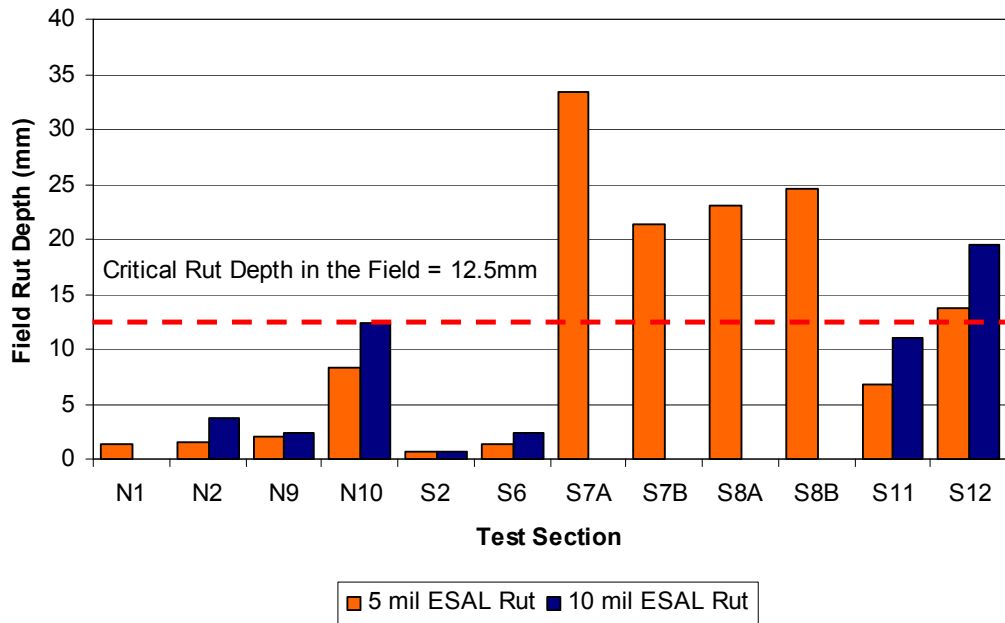


Figure 3.26. Comparison of Field Rut Depths after 5 and 10 million ESALs

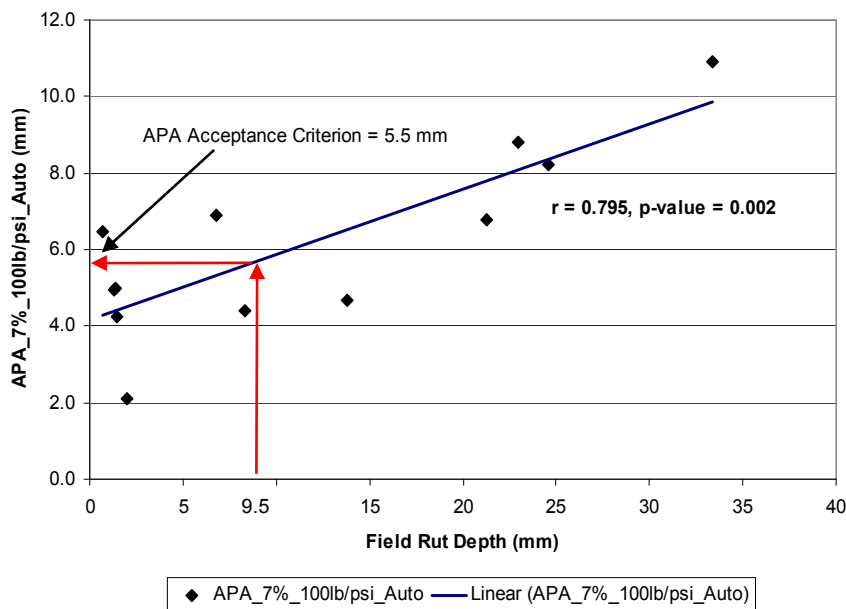


Figure 3.27. Correlation between APA Rut Depths and Field Rutting Performance

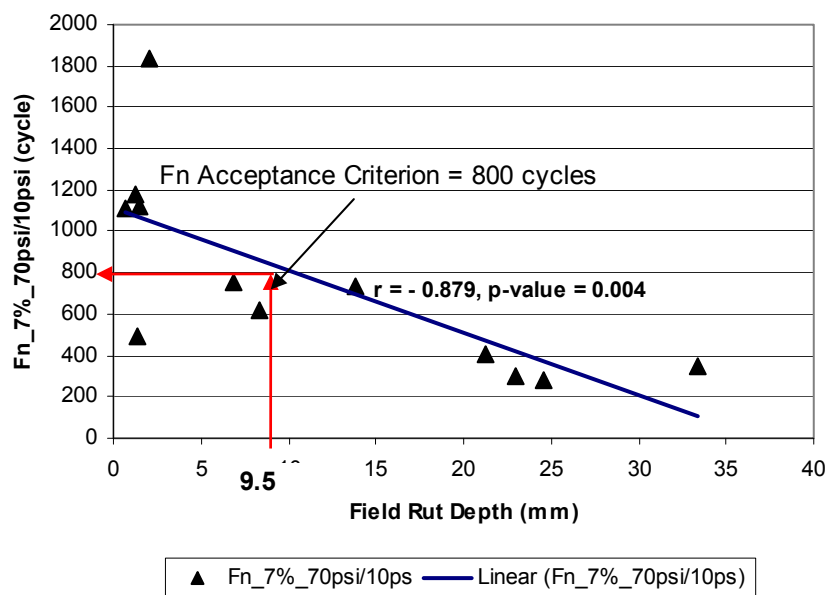


Figure 3.28. Correlation Between Flow Number and Field Rutting Performance

Conclusion

Based on the correlations shown in Figure 3.28 and 3.29, the following conclusions are drawn:

- The maximum acceptance criterion for APA tests should be 5.5 mm.
- The maximum acceptance criterion for Fn testing should be 800 cycles.
- These criteria were developed based on the laboratory test conditions presented in this study and a conservative critical field rut depth of 3/8 inch (9.5 mm).

LOW AIR VOIDS EXPERIMENT

The low QC air voids experiment sponsored by INDOT also yielded very interesting results. INDOT reported in their research plan for the study that the implementation of volumetric acceptance of HMA mixtures has exposed risks to the department and contractors. Prior to this acceptance implementation, it was believed that mixtures placed on the roadway were generally in accordance with design criteria; however, once volumetric acceptance was implemented, problems involving the control of air voids began to surface.

Data from their QC program showed that the magnitude of variation for air voids was $\pm 4\%$, four times greater than the $\pm 1\%$ commonly believed. This means that in some cases Superpave mixtures designed for 4.0% air voids were placed with nearly 0% air voids due to construction variations. At the time the low QC air voids experiment was initiated at the Test Track, mixtures placed with less than 2.0% air voids risked removal and replacement and mixtures placed with air voids between 4.0% and 2.0% were accepted with monetary adjustments. INDOT was

concerned with the performance of low air void mixtures left in-place while contractors were concerned with the monetary ramifications incurred through removal and replacement.

The performance risk to INDOT versus the monetary risk to the contractors needed to be evaluated. The risk of pavement failure for INDOT when HMA with less than 4.0% air voids is left in-place needed to be evaluated and compared to normal construction variation. The monetary risk to contractors needed to be evaluated to determine if low air void HMA could remain in-place and provide acceptable performance, thereby, reducing the removal and replacement risks and resulting in lower HMA costs. For example, the following outcomes were needed to address these issues:

- Development of a rutting model for asphalt pavements with air voids between 0% and 4%,
- Validation of tests for assessing the rutting potential of HMA, and
- Development of an acceptance pay structure for low air void mixtures based on performance models.

To address this need, two 200 foot test sections were divided into four 100 foot subsections. Transitional paving was accomplished by emptying the paver hopper at each marked 100 foot point and refilling with new mix containing slightly different aggregate and binder blends. Three sections were produced with low QC voids by increasing the asphalt content, and one section was produced by increasing the asphalt content and adjusting the aggregate blend percentages. Another test section built with the same materials and similar gradation was used as an experimental control. All mix was produced using an unmodified PG 64-22 asphalt binder (designated as a PG 67-22 in some states).

The first four subsections were placed in the fall of 2006 and performed well under traffic throughout the winter and early spring. As seen in Figure 3.29, significant rutting was observed when pavement temperatures increased in May of 2007 (after approximately 2.4 million ESALs). Rutting was allowed to progress throughout the summer and into winter of 2008. In February of 2008 (at approximately 5.6 million ESALs), all four experimental subsections were replaced with new mixes at QC air voids levels that were intended to better define the relationship with rutting performance. Rutting was again observed beginning in May 2008 (at approximately 7 million ESALs).

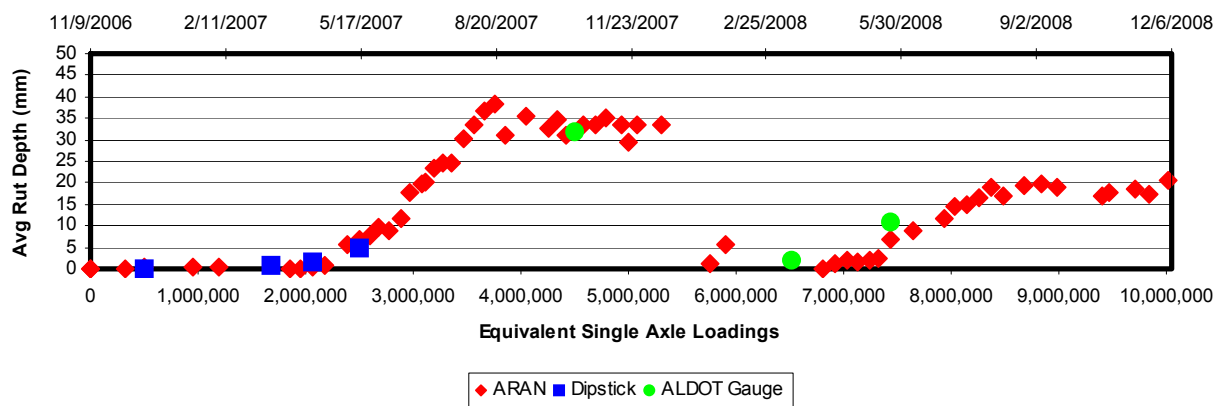


Figure 3.29. Rutting Progression in Section S8B Showing Replacement Mix

As seen in Figure 3.30, rutting for both the original and the replacement mixes progressed at a more or less linear rate. In order to define the relationship between rutting performance and QC air voids, the rate of rutting for the original and replacement subsections was plotted against the corresponding QC air voids measured during construction. The plot also includes results from the 2000 Track (also funded by INDOT) with slag and limestone mixes produced with unmodified binder in which the asphalt contents were intentionally increased by 0.5 percent. The resulting relationship is provided as Figure 3.30. Results from high RAP content sections produced with unmodified virgin binder are also included in order to demonstrate the broad relevance of these findings.

From a purely performance based perspective, it does not appear that any adjustment in pay is required above approximately 2.75 percent QC air voids; however, the rutting rate increases dramatically below this level and removal/replacement may be necessary. Please note that Track data from the 2000, 2003 and 2006 research cycles all indicate that a completely different relationship is expected for polymer-modified binders (with greater tolerance for lower QC air voids).

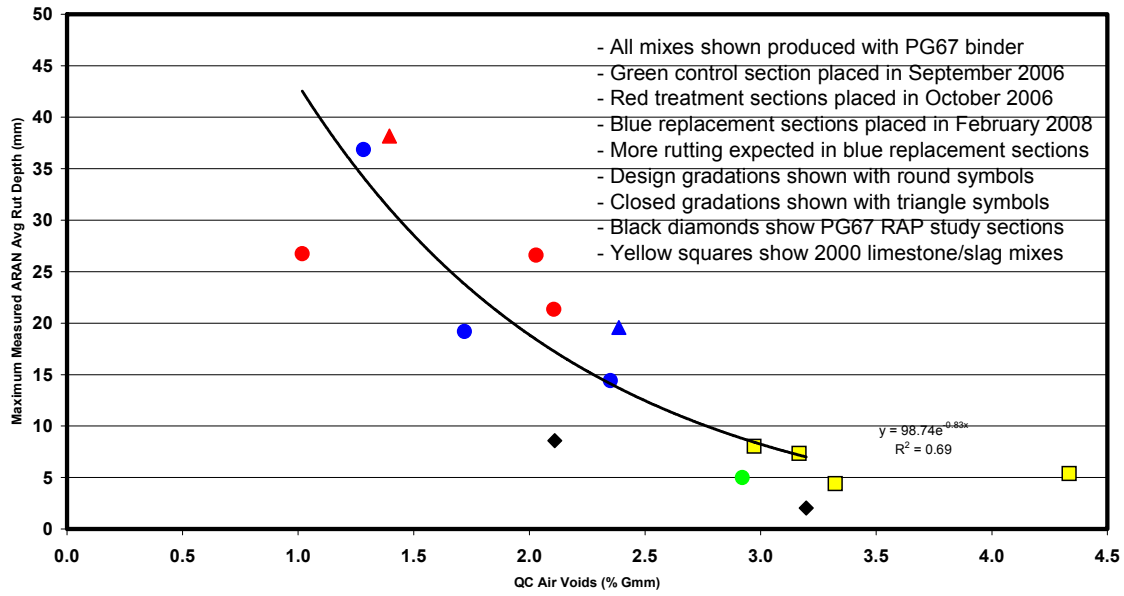


Figure 3.30. Relationship Between Rutting and QC Air Voids

CHAPTER 4 - STRUCTURAL STUDY

The structural study at the NCAT Test Track began as part of the 2003 Test Track experiment with eight instrumented test sections. These sections were designed to meet the needs of M-E design validation by studying the interaction between pavement response and performance for pavement structure constructed with different materials and thicknesses. The study was expanded in the 2006 Test Track to eleven sections where four test sections were left in-place from 2003, one section was rehabilitated, and six sections were completely reconstructed. This chapter provides details about the pavement sections, instrumentation used, mechanistic pavement properties, and pavement performance.

EXPERIMENTAL OBJECTIVES

To address the needs stipulated above, a number of broadly-defined experimental objectives were developed for the 2006 Test Track structural experiment. These objectives, with brief explanations, included (2):

- **Further validate and calibrate new transfer functions for M-E design.**
On sections left in place from the 2003 experiment, initial transfer functions had been developed. These models require further refinement and validation before they can be widely applied. Additional calibration activities on new test sections will increase the size of the calibration data set which can then be applied to a wider set of real world design scenarios.
- **Develop recommendations for mechanistic-based material characterization that yields accurate pavement response predictions.**
To optimize pavement design it is important to accurately characterize the material properties which directly affect predictions of pavement response under load. There are currently many methods of material characterization in the context of M-E design. These methods range from laboratory-based to field-based and include direct measurement versus correlation equations. Furthermore, the methods can often produce conflicting sets of information regarding the same material. Therefore, there is a need to investigate the various methods and recommend best practices toward mechanistic characterization of material properties.
- **Characterize pavement response in rehabilitated flexible pavement structures.**
Many agencies are faced with rehabilitating flexible pavements, typically with overlay or mill and inlay techniques. There is a need to validate pavement response predictions made in rehabilitation design methodologies to improve and/or refine these methods.
- **Determine field-based fatigue response thresholds for perpetual pavements.**
Many state agencies have begun to design and construct so-called perpetual pavements (a.k.a., long-life pavements). A critical component of the design process is the selection of the fatigue threshold. Most laboratory fatigue testing of asphalt mixtures have set a conservative strain threshold of 70 microstrain ($\mu\epsilon$) to prevent bottom-up fatigue cracking. However, it is believed that the threshold may be much higher due to rest

periods and other differences between the field and lab. Pavement response and performance measurements can help refine and update the strain threshold for fatigue performance.

2006 TEST SECTIONS

As noted above, the sections comprising the 2006 structural study were a blend of new construction, left-in-place and rehabilitated sections. Figure 4.1 illustrates the average as-built thicknesses and the constituent materials, in each section.

There are five different types of unbound materials that are utilized for the structural study at the Test Track (27). A Florida limerock base was utilized as the base layer material in sections N1 and N2. This material was quarried in Alachua, Florida, and is commonly utilized by the Florida DOT. The granite graded aggregate base material supplied by Vulcan Materials, Inc. was utilized as the base layer material in section N3, N4, N5, N6, N7, and S11. This material is commonly used by ALDOT in the southeastern part of the state and was quarried in Columbus, GA. The Type 5 material supplied by the Missouri DOT was used as the base material in section N10. This material is a dolomitic limestone that was quarried in Maryland Heights, Missouri, and is commonly used by the Missouri DOT. The Seale subgrade material was employed by the Oklahoma DOT as the subgrade layer in sections N8 and N9. This material is high clay content borrow material imported from Seale, Alabama. This soil is classified as an A-7-6 material by American Association of State Highway and Transportation Officials (AASHTO) soil classification. Finally, the metamorphic quartzite soil excavated from the Test Track property was utilized as the fill material in every section except N8 and N9. This material was used as the base layer material for N8 and N9 to simulate lime stabilization often used in Oklahoma and formed the deep subgrade material for each structural section. This material is classified as an A-4(0) soil.

Florida DOT: Sections N1 and N2

FDOT sponsored two structural sections (N1 and N2) consisting of approximately seven inches of HMA over ten inches of limerock base. The main difference between the sections is that N2 included an SBS modified PG 76-22 binder in the upper four inches of HMA, whereas N1 used an unmodified PG 67-22 throughout the full seven inches of HMA. The upper lifts from the two test sections were designed to yield significantly different resistance to cracking as indicated by their indirect tension (IDT) energy ratios. It was expected that section N1 would crack before N2. Also, the introduction of a base material different from the other structural test sections allows for interesting comparisons between the performance of granular base layers.

Alabama DOT and FHWA: Sections N3 – N7

As noted previously, sections N3 through N7 were left in place from the 2003 Test Track. They all share the same high-quality subgrade and 6 inch unbound granite base layer. Sections N3 and N4, both consisting of 9 inches of HMA, are companion sections with the binder type as the main experimental variable. N5 and N6 were also companion sections consisting of 7 inches of HMA, though N5 was milled 2 inches and inlaid with new HMA to mitigate the top-down cracking problem. N7 was also left in place and features SMA as the surface course.

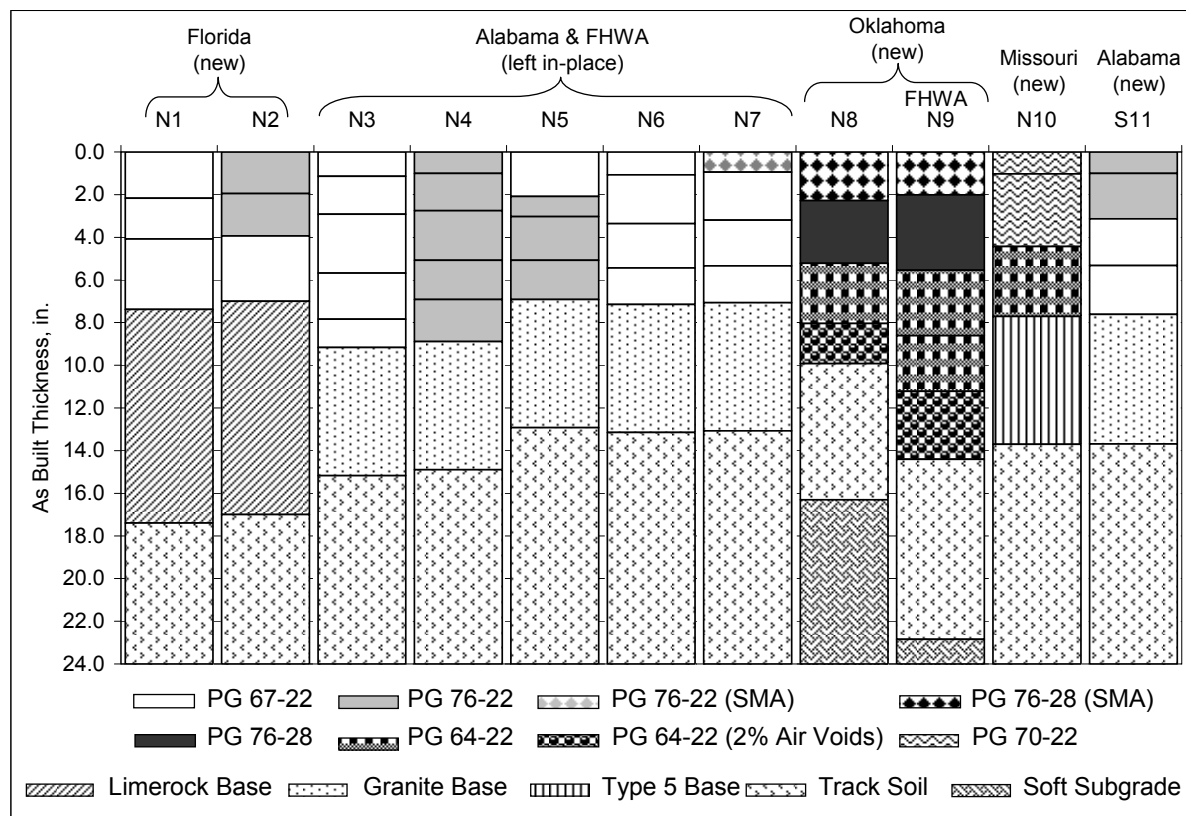


Figure 4.1. As-Built Pavement Cross Sections (2)

Oklahoma DOT: Sections N8 and N9

ODOT also sponsored two new structural test sections (N8 and N9) intended to study the perpetual pavement concept. These sections represent the thickest cross-sections built, to date, as part of the structural experiment. The ODOT sections feature a soft subgrade which was more representative of some soils in Oklahoma. Section N8, the first of the two ODOT sections, has ten inches of asphalt which is made up of a two inch rich bottom layer, six inches of Superpave mix, and capped with a two inch layer of SMA. The second section, N9, has a total HMA thickness of fourteen inches. The rich bottom layer was increased to three inches and an additional three inch Superpave lift was added for this section. It should be noted that the so-called “rich-bottom” was simply a mixture designed to 2% air voids rather than 4%. The net result was a 6% design asphalt content in the rich-bottom.

FHWA: Supplemental N9

Accounting for the viscoelastic nature of hot-mix is a critical component of any M-E design methodology. Specifically, it is important to account for pavement temperature and loading frequency (i.e., truck speed) when predicting pavement response using a mechanistic model. While viscoelastic properties of individual mixtures can be readily measured in the laboratory through dynamic modulus testing, translating the results into a form useful for predicting pavement response can be complicated due to differences in mode of loading, rest periods and other factors. There is an added level of complexity due to the layered nature of flexible

pavements with each layer potentially having different viscoelastic properties. Furthermore, temperature and loading frequency change with depth through the layers so establishing representative temperatures and frequencies can be particularly challenging.

Methods for handling the above complexities of mechanistic modeling have been well-documented and even implemented within design programs such as the MEPDG. However, there are a large number of simplifying assumptions that require validation to ensure maximum accuracy within the design system. Therefore, the supplemental section sponsored by FHWA was intended to provide a model validation data set for evaluating the accuracy of various material characterization and modeling approaches currently available. One feature of this investigation was embedment of strain gauges at lift interfaces to a minimum depth of five inches to quantify pavement response with depth. N9 was selected for this supplemental investigation because it was the thickest HMA section available and allowed for the greatest strain and temperature profiles to be developed. The supplemental instrumentation used in section N9 is shown in Figure 4.2. Full details regarding instrumentation are provided later in this chapter.

Missouri: N10

The Missouri DOT has sponsored a structural section (N10) which was designed to address the broad needs of mechanistic-empirical pavement design. N10 features a Missouri Type 5 granular base material beneath eight inches of HMA which are commonly used in Missouri.

Alabama DOT: S11

A new section was sponsored by ALDOT meant to build on previous work in the 2003 Test Track. In the 2003 structural sections, the same binder grade was used for all layers in a given test section. In practice, however, agencies typically use higher binder grades near the pavement surface where HMA rutting is more likely to occur and lower binder grades lower in the pavement where temperatures are not as extreme and rutting less likely to occur. Section S11 was built to more closely replicate typical pavement cross sections upper three inches contained a PG 76-22 binder and the four inches contained a PG 67-22 binder.

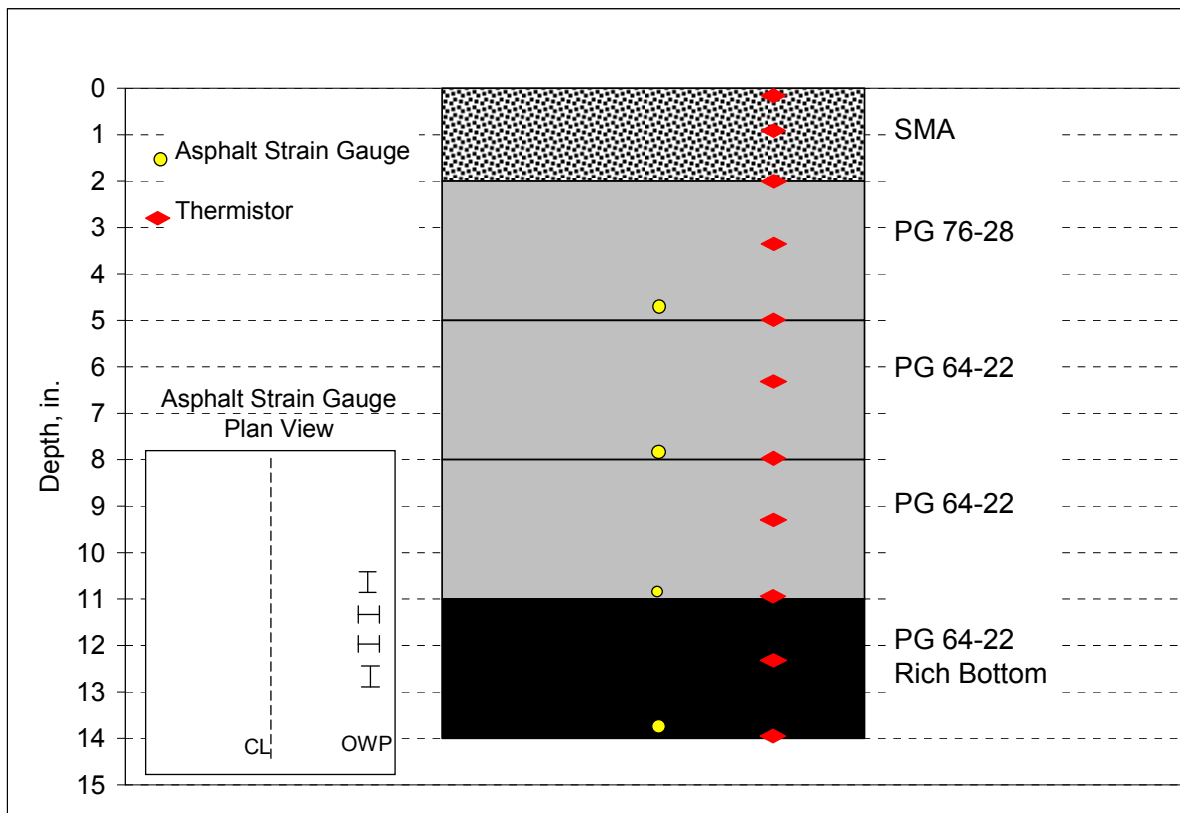


Figure 4.2. N9 Supplemental Instrumentation (2)

INSTRUMENTATION

The instrumentation system developed and deployed for the 2003 structural study had proven itself to be reasonably robust and effective in gathering the requisite pavement response data needed for M-E investigations. Therefore, essentially the same system, with a few exceptions, was used for the 2006 investigation. This also maintained continuity between the two research cycles in terms of equipment, data collection and data processing schemes. This testing plan and methodology has been documented by Timm (2).

CHAPTER 5 - MECHANISTIC PAVEMENT ANALYSIS

A primary objective of the 2006 Structural Study was the analysis of mechanistic pavement design concepts. This was accomplished by embedding instrumentation into the pavement structure of eleven sections at the 2006 NCAT Test Track. Two major studies have been completed and documented relating to different components of M-E design to date. The first study synthesized in this chapter determined the effects that temperature and speed have on the mechanistic responses of flexible perpetual pavements. The second study developed cumulative distributions of strains for twenty-one test sections (six built in 2000, seven built in 2003, and eight built in 2006) and compared the distributions to pavement performance. Both studies have been documented in detail elsewhere (28; 29).

TEMPERATURE AND SPEED EFFECTS

M-E design procedures such as the MEPDG utilize material characteristics, climate, and layer thickness to predict pavement responses under loading (30; 24). Transfer functions are then employed to predict pavement performance based on the computed responses. Responses that are essential to the successful prediction of load repetitions to failure include the horizontal tensile strain at the bottom of the HMA layer to predict fatigue cracking, and the vertical compressive strain at the top of the subgrade layer to predict rutting.

The horizontal tensile strain is of particular interest for the design of perpetual pavements which have come to the forefront of the asphalt industry in recent years. One key feature of these long lasting pavements is that each layer is designed to resist specific distresses. In particular, the bottom layer is designed to resist bottom-up fatigue cracking by considering the flexibility and thickness of the HMA (31). Fatigue cracking is dependent on the horizontal tensile strain induced at the bottom of the HMA. If these strains are kept below a maximum value it is believed that the pavement can sustain an infinite number of load repetitions without failing by fatigue (31). Early estimates of the threshold were approximately 70 $\mu\epsilon$ while more recent observations have reported a threshold of 100 $\mu\epsilon$ (32; 33). As a result of the zero damage incurred, the number of load repetitions that occur at or below the strain threshold can be ignored in determining the load repetitions to fatigue failure, ultimately reducing the required layer thickness. Therefore, properly predicting the tensile strains at the bottom of the HMA is critical to designing a successful and cost-efficient perpetual pavement.

Recent research efforts at the NCAT Test Track have included investigations of perpetual pavements. ODOT has sponsored perpetual pavement sections at the Test Track to examine their behavior in an accelerated loading environment. One of the long-term goals of this research is to characterize the performance of their perpetual sections so that the relevant mix design and structural design procedures can be refined prior to widespread implementation throughout Oklahoma. Central to this effort is characterizing a field-based threshold for structural design. To accomplish this goal, both pavement response and performance require characterization. As described below, this investigation focused primarily on pavement response characterization.

Objectives

Given the needs regarding perpetual pavement design thresholds stipulated above, the objectives of this study were:

- Characterize the effects of temperature and speed on measured perpetual pavement response.
- Describe the strain history of the perpetual pavement in the context of existing response thresholds.

Field Testing

Test Section

This experiment consisted of the application of live loads at a minimum of 4 different speeds on 4 different dates to measure the strain induced throughout the N9 test section. During the testing, temperatures throughout the pavement structure were also monitored. Section N9 was a perpetual pavement section and was comprised of approximately 14 inches of asphalt concrete over a 9.6 inch granular base.

Testing Dates and Speeds

Testing was conducted on April 6, 10, 25 and May 2, 2007. On each date, the trucks traveled at four speeds: 15 mph, 25 mph, 35 mph, and 45 mph. On the first two dates, data were also gathered at 55 mph. However, for safety reasons, it was decided to discontinue testing at this speed on the remaining dates (the Test Track is designed for 45 mph). For each speed tested, the trucks adjusted to the test speed prior to traveling over the test section, such that once over the test section, the speed was constant. It should be noted that section N9 was subjected to “routine” traffic at 45 mph as part of the overall Test Track trucking operation. The various test speeds used in this particular investigation were intended to provide a wider range of conditions and therefore more applicability to potential lower-speed conditions of actual roadways.

Field Results and Discussion

The results of the tests were processed and transformed into useable data to analyze the pavement’s response due to the speed at which the load was applied and the in-situ temperature of the pavement. The useable data was in the form of strain traces, which plotted the strain ($\mu\epsilon$) versus time. These strain traces allowed for the definition of the induced strain under dynamic loading and for the analysis of strain due to vehicle speed and pavement temperature.

Strain Definition

In investigating the effects of speed and temperature on strain within the pavement, focus was placed on the tensile strain induced at the bottom of the HMA, where the maximum tensile strain occurs. The tensile strains captured for all three passes of the trucks at a particular speed and date were compiled separately by direction and axle type. Among the strains captured from the six longitudinal and six transverse gauges, the maximum of the strains induced under each axle type was selected for the date and speed in question, resulting in one longitudinal tensile strain and one transverse tensile strain for each date, speed, and axle type. Selecting the maximum strain gave the best hit on the gauge array, such that the strain selected was that induced by the axle

group pass that came closest to traveling directly over the strain gauge. It was imperative that the strains compiled included all six gauges in each direction as wheel wander was a factor.

Strain vs. Speed

The strains determined from the best hit selections were investigated to determine the relationship between vehicle speed and tensile strain. For the first two dates, April 6, and April 10, 2007 the induced longitudinal strain decreases with an increase in speed. The same trend exists for the last two dates; however, the strain decreased at a greater rate than on the first two dates for each increase in speed. In looking at the rate of strain change due to vehicle speed relative to mid-depth temperature it was found that at high mid-depth temperatures the longitudinal strain was reduced at a greater rate, whereas at colder mid-depth temperatures, the rate of reduction nears zero. Therefore, at warmer temperatures, vehicle speed has a greater influence on the tensile strains at the bottom of the HMA than at colder temperatures. This was to be expected since warmer temperatures induce a greater viscoelastic behavior from the HMA thus increasing the impact of vehicle speed.

For all test dates and axle types the same general trend existed: increasing the vehicle speed resulted in a decrease in the amount of strain that was induced. Attaching a trend line to the data, it became evident that the longitudinal strain was proportional to the natural logarithm of the speed of the applied load, modeled by Equation 5-1. The goodness of fit, corresponding to the trend line for each axle type on each test date revealed that Equation 5-1 models the relationship very well, returning R^2 values ranging from 0.80 to 0.99 with the majority of the R^2 values greater than 0.90. The same trends existed for strains under each axle type in the transverse direction. Equation 5-1 can also be used to describe those strains, returning relatively high R^2 values.

$$\varepsilon_t = a \ln v + b \quad (5-1)$$

where:

- ε_t = tensile strain (microstrain)
- v = speed of applied load (mph)
- a, b = regression coefficients

Strain vs. Temperature

By conducting the experiment on four different dates throughout the month of April and beginning of May, a wide range of in-situ pavement temperatures were experienced. Pavement surface temperatures ($^{\circ}\text{F}$) ranged from the low 70s to low 120s. Temperatures from all probes were recorded prior to the start of each test. As to be expected, the temperature throughout the structure rose as the experiment progressed throughout the month of April and into the month of May. Additionally, surface temperatures were significantly higher than temperatures at the bottom of the asphalt concrete. Mid-depth temperatures were chosen for the analysis of the strain-temperature relationship under each axle type and speed tested. A previous investigation at the Test Track also selected mid-depth temperature as the best predictor of strain (33, 29).

To further investigate the effect of temperature on strain, the maximum tensile strain was plotted against the mid-depth temperature. In general, an increase in mid-depth pavement temperature resulted in a very large increase in tensile strain, a relationship that can be described by an exponential function, of the form listed in Equation 5-2. Regression equations and coefficients of determination (R^2) were generated for the strain due to temperature at all vehicle speeds, returning consistently high R^2 values for all four speeds, ranging from 0.96-0.99. These high R^2 values indicate that Equation 5-2 describes the temperature-strain relationship very well. Furthermore, the speed-strain relationship was reiterated in this comparison, such that the highest strain values were induced at the slowest test speeds. Thus, the largest longitudinal strain occurred under a single axle traveling at a speed of 15 mph, at the highest mid-depth pavement temperature, 99.47°F . These findings were also evident in the other two axle types: steer and tandem axles, however, the single axle consistently produced higher strain levels under loading. Similar trends were also found for the tensile strain induced in the transverse direction. The relationship described by Equation 5-2 was used to characterize the strain under any of the three axle types and the strain in either direction (longitudinal or transverse).

$$\varepsilon_t = ce^{dT} \quad (5-2)$$

where:

ε_t = Tensile strain (micro strain)

T = Mid-depth Temperature (F)

e = constant, with approximate value = 2.71828183

c, d = regression coefficients

Combined Effect

It is of some benefit to know the effect of speed and temperature combined, as independently these variables greatly influence the amount of tensile strain induced in a pavement. The investigations into the effects of speed and temperature revealed that tensile strain is directly proportional to the natural logarithm of the vehicle speed and directly proportional to the exponential function of temperature. To determine the combined effect, DataFit, a regression analysis software program, was utilized to linearly combine the above equations into regression equations of the form:

$$\varepsilon_t = f \ln v + e^{gT} + h \tag{5-3}$$

where:

ε_t = tensile strain (micro strain)

v = speed (mph)

T = mid-depth pavement temperature (F)

e = constant, with approximate value = 2.71828183

f, g, h = regression coefficients

The above equation was selected to represent the effect of speed and temperature based on the coefficients of determination and the significance of each coefficient. The regression coefficients for each axle type and gauge orientation are listed in Table 5.1 and the coefficients of determination were consistently very high for each regression equation. Although not shown, each coefficient was found to be statistically significant with all p-values reported as less than 0.001.

Table 5.1. Regression Coefficients by Axle Type and Direction of Strain (28)

Gauge Orientation	Axle Type	Regression Coefficients			R ²
		f	g	h	
Longitudinal	Steer	-24.25	0.047	108.81	0.955
Longitudinal	Tandem	-34.67	0.051	172.93	0.970
Longitudinal	Single	-40.57	0.053	206.67	0.983
Transverse	Steer	-19.70	0.050	101.40	0.986
Transverse	Tandem	-15.05	0.500	112.57	0.971
Transverse	Single	-16.23	0.051	102.18	0.986

Application of Regression Models

The regression models described above serve two functions. The first is to characterize the effects of vehicle speed and mid-depth temperature for the pavement section investigated. The second is to provide a way to predict the tensile strains under a variety of conditions. Both are beneficial for perpetual pavement design in that the regression models can be used to determine the conditions that induce strains beyond the laboratory-established threshold limit. Further analysis stemming from these developed equations can also be utilized to assess the relevance of laboratory-established thresholds to field conditions.

To determine the most critical conditions for the perpetual pavement investigated, five speeds (15, 25, 35, 45, and 65 mph) and five mid-depth pavement temperatures (40, 60, 80, 100 and 120°F) were selected to predict tensile strains from the aforementioned regression equations. The vehicle speeds were representative of those included in the experiment, with the addition of one speed (65 mph) outside the range that was selected to reflect highway speeds. For the mid-depth pavement temperatures chosen for this analysis, three temperatures were experienced in the experiment and the two additional temperatures (40 and 120°F) allowed for extrapolation of strains to temperatures experienced at the Test Track but not specifically part of this experiment.

The longitudinal tensile strains predicted for a single axle were plotted in Figure 5.1, as well as a threshold level of 100 $\mu\epsilon$. As expected, a vehicle speed of 15 mph is most critical for the N9 test section, inducing strains above the threshold for all of the selected temperatures. The critical mid-depth pavement temperature was found to be approximately 78°F for vehicle speeds of 65 mph or less. At these conditions the predicted strains were equal to the threshold value of 100 $\mu\epsilon$; therefore, at lower mid-depth temperatures, zero damage would theoretically be incurred under an infinite number of load applications.

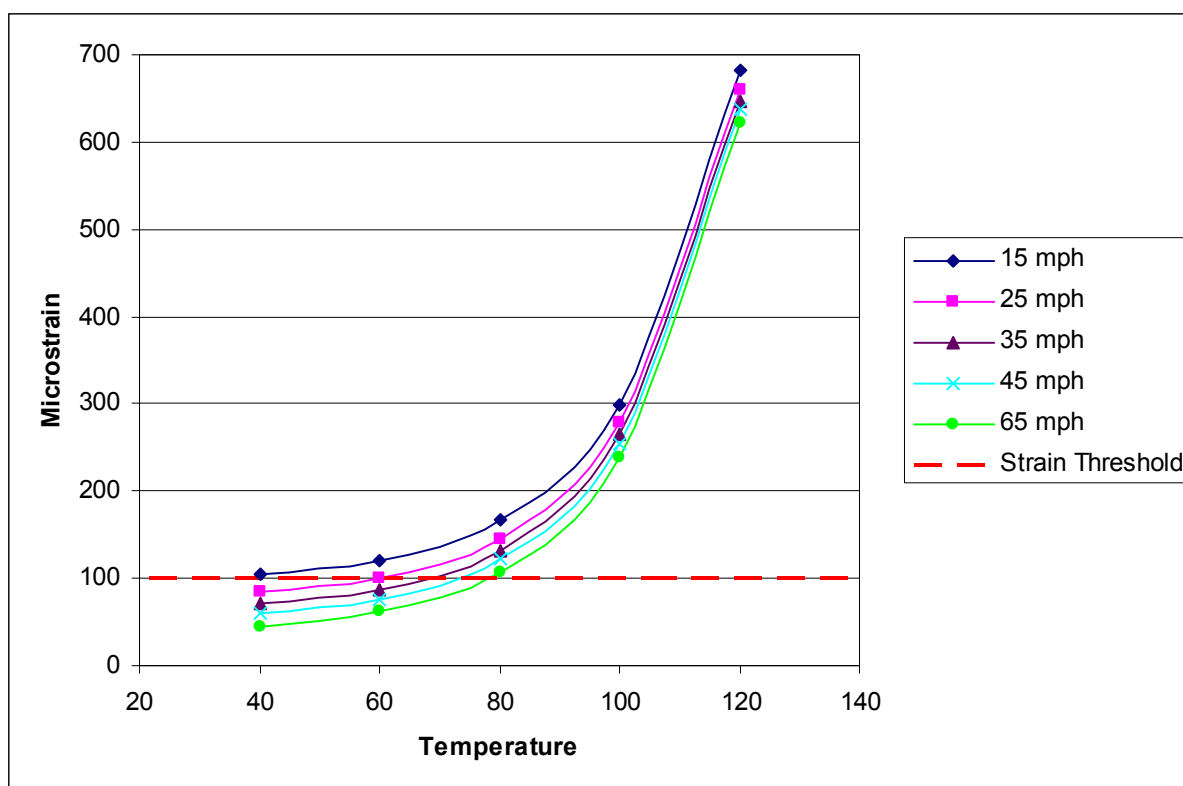


Figure 5.1. Predicted Strain by Temperature for a Single Axle

To investigate the relevance of the laboratory established thresholds, it is important to consider how frequently the critical conditions occur or are surpassed. As noted earlier, section N9 was also subjected to routine traffic at 45 mph for 16 hours per day, 5 days a week, as part of the overall trucking operation for the Test Track. This operation, which commenced in November, 2006 and continued to the end of the Test Track cycle, provided a range of temperatures experienced over a much broader time period. Temperatures were recorded on a minute-by-minute basis from which hourly summaries were stored. From the available temperature data, the average mid-depth temperatures were retrieved from November 7, 2006 to January 14, 2008. Using the regression equation developed above, the tensile strains at the bottom of the HMA were calculated for the recorded temperatures and a vehicle speed of 45 mph.

Figure 5.2 depicts the calculated longitudinal strain under a single axle for the average mid-depth pavement temperature data ($T2_avg$) and vehicle speed of 45 mph for the hours of operation (5:00AM to 11:00PM). Using the same regression equation for the longitudinal strain under a single axle, the critical temperature for a vehicle speed of 45 mph was found to be 72.83°F.

Figure 5.2 illustrates that on a large number of occasions mid-depth temperatures far surpassed this critical temperature, with maximum mid-depth temperatures approaching 118°F. Corresponding to these high temperatures were elevated tensile strains well above the strain threshold level of 100 $\mu\epsilon$, with maximum strains near 575 $\mu\epsilon$. For the dataset that spanned just over a year, approximately 55% of the calculated strains fell below the 100 $\mu\epsilon$ threshold level. To date, this section has exhibited only minimal amounts of rutting (< 5mm) and no cracking. Given the high strain levels and good performance thus far, it may suggest that the field strain threshold could be greater than 100 $\mu\epsilon$. However, further traffic and testing is certainly warranted to confirm or refute this statement. The strain regression equations developed in this study can be used to further study this test section through the remainder of the trafficking cycle.

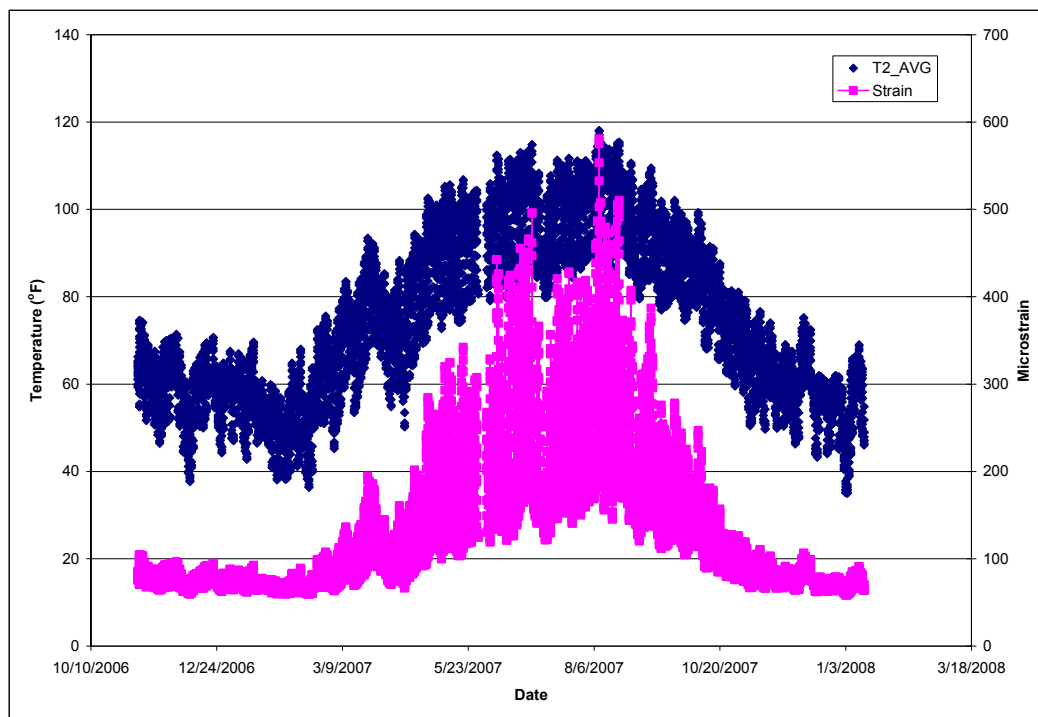


Figure 5.2. Measured Strain and Mid-Depth Temperatures for the N9 Test Section (28)

Summary

Investigations at the Test Track helped characterize those effects on pavement response for a perpetual pavement section, using the N9 test section. Results from this investigation revealed the following:

- The rate of strain reduction was more sensitive to vehicle speeds at warmer temperatures.
- The tensile strain at the bottom of the HMA layer was found to be proportional to the natural logarithm of the vehicle speed.
- The mid-depth pavement temperature correlated best with the induced tensile strain.
- Increasing the mid-depth temperature resulted in an exponential increase in tensile strains. The combined effects were correlated to the measured strain levels, resulting in a regression equation of the form:

$$\epsilon_t = f \ln v + e^{gT} + h \tag{5-4}$$

- This comparison between predicted strains and an established laboratory strain threshold indicated that the critical mid-depth pavement temperature for vehicle speeds of 65 mph or less was approximately 78°F. Generally speaking, for vehicle speeds of 65 mph or less, the strains induced at temperatures greater than this critical temperature will be greater than the threshold level, causing damage to the pavement that must be accounted for.
- For a time period of just over a year it was found that less than 55% of the estimated strains were below a threshold value of 100 $\mu\epsilon$.
- Based on these analyses, monitoring of strain levels and performance of section N9 should be continued to determine if a threshold level of 100 $\mu\epsilon$ is conservative for the section.

FIELD-BASED PERPETUAL PAVEMENT STRAIN THRESHOLDS

M-E pavement design and analysis has recently made advances toward widespread implementation throughout the United States. As the new MEPDG is being completed and implemented, more attention is being spent on proper material and pavement response characterization (34). Material properties are needed in this design framework to determine theoretical load-induced responses in pavement structures. These responses are then used in transfer functions to predict the life of the pavement through Miner's Hypothesis (35). Transfer functions rely on theoretical strains and pressures to estimate the design life of pavement structures. If these values are accurately estimated, the transfer functions will provide the engineer with a pavement of optimized thickness.

Since perpetual pavement design relies on maintaining pavement responses below some critical thresholds, it is well suited to M-E pavement design. To capture the fatigue life of pavements, engineers can estimate pavement responses so the pavement will have sufficient life. In perpetual pavement design, the determination of fatigue life is controlled by the tensile strain at the bottom of the HMA. This mechanistic response is limited to mitigate the possibility for bottom-up fatigue cracking (31; 36; 37). The longitudinal strain at this pavement location has proven to be critical in thinner pavements, and in a fully-bonded pavement, it is always the location of highest tensile strain (38).

In a 2006 survey of APT facilities in the United States, 85.7% of the responding facilities measured horizontal strain at the base of the HMA layer to study fatigue life (39). Other projects on actual highways, such as I-5 in Oregon and the Marquette Interchange, have also incorporated measuring strain at the base of the HMA into their research (40). In protecting a perpetual pavement against fatigue cracking, engineers typically design the pavement so that the tensile strain at the base of the HMA remains below 70 $\mu\epsilon$ (37). Other engineers suggest that the strain threshold be between 60 to 100 $\mu\epsilon$ based upon laboratory testing (41). A recent experimental pavement project in China allowed perpetual pavement design to reach the seemingly unconservative value of 125 $\mu\epsilon$ (42).

It is important for engineers to determine an appropriate and reliable value to use as a strain threshold in M-E perpetual pavement design. While many engineers currently use a 70-100 $\mu\epsilon$ fatigue threshold, these values come from laboratory testing at one temperature with no rest periods. It is difficult, if not impossible, to relate these values and correlate them to field testing.

If the field design threshold could be raised, based on sound research and engineering, highway agencies would be able to build thinner pavements. A perpetual pavement experiment in China reduced its thickness from 20 to 15 inches when the fatigue threshold limit was increased from 70 to 125 $\mu\epsilon$ (42). This would reduce the construction and material costs for highway agencies at a time where funding is extremely limited during these frugal economic conditions. This would also substantially reduce the amount of non-renewable natural resources consumed for road construction. In the end, the pavement system as a whole would be more efficient.

Objective and Scope

The main objective of this research was to recommend strain criteria for fatigue cracking in perpetual pavements. This was completed by correlating simulated and measured strains at the bottom of the HMA layer to field performance over three cycles of the Test Track. For the 2000 Track experiment, strain distributions were estimated using PerRoad, a mechanistic modeling software package, for six sections along the North and South tangents. For the 2003 cycle, direct strain measurements from the base of the HMA were used to develop strain profiles for seven structural sections. Direct strain measurements for eight sections from the 2006 Test Track were also analyzed.

2000 Test Track

Six thick (greater than 24 inches) test sections built in the summer of 2000 were selected for a theoretical strain analysis: N11, N12, S2, S9, S10, and S13. These six sections were chosen because they had all experienced at least 20 million ESALs without showing signs of fatigue cracking. Since pavement response instrumentation was not included in the 2000 experiment, strains were estimated using the mechanistic pavement modeling program PerRoad. Inputs for PerRoad include trafficking data, layer thicknesses, and material properties of the HMA and soil. Trafficking databases have been kept at the Test Track since its inception; therefore, the traffic could be divided into a load spectrum for the first 20 million ESALs of the experiment (2000-2005). This traffic division is documented elsewhere (29).

Once the load spectrum was determined, the exact layer thicknesses needed to be imported into the program so PerRoad would know where to calculate the desired strains. Each test section at the 2000 Test Track consisted of a 4 inch experimental surface mix on top of a perpetual buildup. The perpetual buildup was essentially the same for each section around the track with slight variations in constructed thickness. The subgrade for the experiment was an improved roadbed material, also documented as Track Soil, taken from rock formations in the West curve of the Test Track compacted to 95% of Proctor maximum density. Above the subgrade was another 12 inch lift of the improved roadbed material; however, this lift was compacted to 100% of Proctor for a higher density. A densely crushed granite base layer, often used by ALDOT, was built in a 6 inch lift above the Track soil. The final layer separating the unbound materials from the bound materials was a non-woven geotextile fabric. This layer was placed above the granular materials to allow the flow of water through the layer, but not allow fines to pump to the surface or through the pavement layers (1).

The perpetual buildup of the 2000 Test Track included three layers of bound materials as well as the previously mentioned unbound materials. The bottom layer of the bound materials was 4 inches of permeable asphalt treated base (PATB). While four inches of material was planned as a

part of the experiment, the thick spread rate made the build-up closer to 5 inches in most areas of the Track. Fifteen inches of Superpave mix was placed on top of the PATB layer. The bottom nine inches of the Superpave mix consisted of a mix design using a PG 67 binder. The top six inches used a PG 76 binder to increase the rutting resistance (1).

After building each section's cross-section, the stiffness of the HMA and the resilient modulus of the soil could then be characterized. This was accomplished using falling weight deflectometer data collected during 2001. The AASHTO two-layer backcalculation methodology was followed to determine the material properties in question on the days of testing (43). In this analysis, the division between the two layers occurs at the geotextile or beneath the PATB. Since the subgrade is a stiff material, it was put into one layer with the 12 inches of improved roadbed and 6 inches of granite base. Relationships were then developed between the HMA modulus and the temperature 10 inches into the HMA during the time of testing (Table 5.2). These relationships were used to create a cumulative distribution for the stiffness of the pavement during trafficking.

During FWD testing, temperatures were recorded 10 inches deep in the pavement. With these recorded data, non-linear regression was used to develop relationships between the backcalculated material properties and temperature at the time of the testing. Figure 5-3 shows one example of the relationship developed between temperature and the modulus of the hot-mix asphalt from section S10 on a semi-log plot.

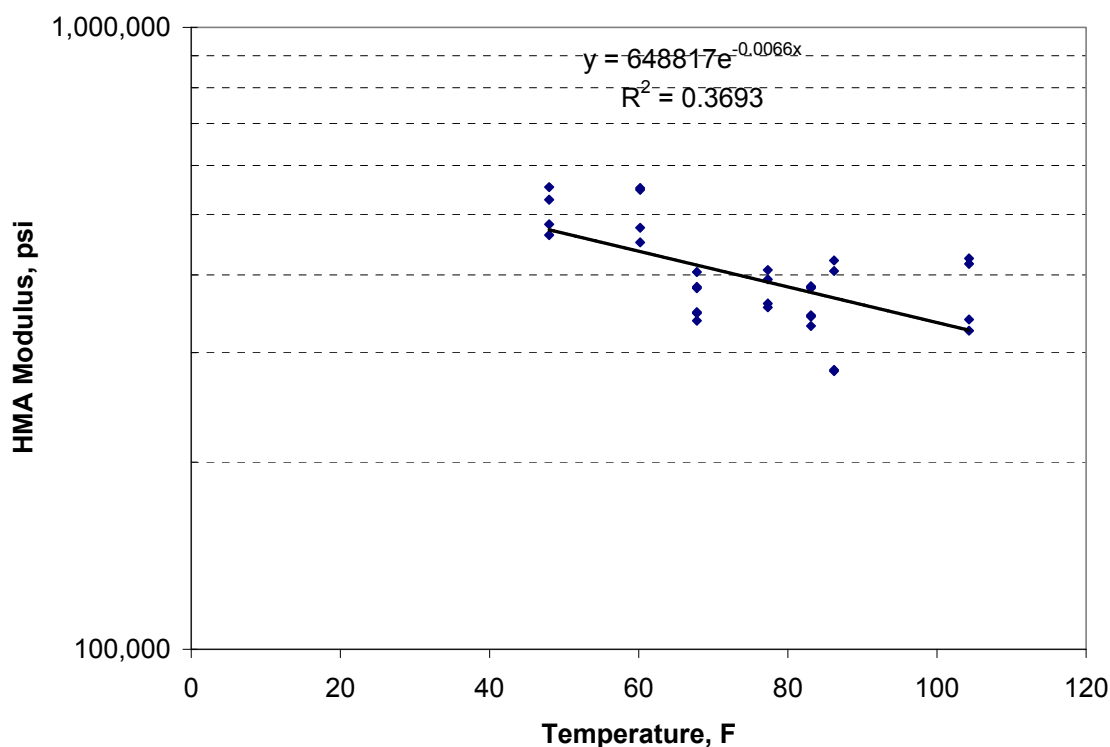


Figure 5.3. HMA and Temperature Relationship for S10 (29)

When comparing power, linear, and exponential relationships, negative exponential relationships returned consistently higher R^2 values. One would expect a negative relationship between temperature and HMA modulus because as the temperature in a pavement structure increases, the

pavement should become softer and its modulus would be reduced. Therefore, the equations developed for the six experimental sections follow the format of Equation 5-5, and Table 5.2 displays each equation's constants and R² value.

$$E_p = k_1 e^{k_2 T} \tag{5-5}$$

where:

- E_p = HMA modulus, psi
- k₁ = section specific constant
- k₂ = section specific constant
- T = temperature, F

Table 5.2. Constants for Equation 5-5

Section	k ₁	k ₂	R ²
N11	816061	-0.0087	0.73
N12	797238	-0.0091	0.47
S2	384073	0.0036	0.09
S9	605842	-0.0093	0.71
S10	648817	-0.0066	0.37
S13	747956	-0.0107	0.75

As Table 5.2 indicates, three of the sections maintained a relatively strong relationship (R²>0.7) between temperature and the modulus of the pavement. Two of the sections were weaker with R² values ranging from 0.37 to 0.47. Section S2 had no relationship that could be developed between its HMA modulus and the temperature. The lack of relationship prevented a multi-seasonal analysis from being conducted on section S2. This was also verified in laboratory experiments.

Upon the development of these relationships, cumulative distributions of the stiffness were developed by calculating stiffness based on the average hourly temperature under trafficking. These cumulative distributions were then divided into quintiles for PerRoad's five season temperature analysis.

PerRoad also required a characterization of the soil in each cross-section. Figure 5.4 shows the results of comparing S10's resilient modulus of the soil to the pavement temperature during the FWD testing. As can be seen, there is no real trend upwards or downwards with temperature for the soil's material properties. This was the case for each of the six sections analyzed from the 2000 Test Track. Since no relationship could be developed, the average modulus from the FWD testing was used along with the coefficient of variation of the backcalculated data to simulate the variability of each section's soil modulus.

With both the material properties of the pavement and soil characterized, the load spectrum accurately quantified, and cross-sections for each test section constructed, the needed dataset required for PerRoad to complete its mechanistic pavement analysis was complete. The program used the data created and coupled it with layered elastic theory to calculate horizontal strain at the base of the bound materials, the critical location for fatigue cracking.

Once these strains had been estimated, cumulative distributions were developed. Figure 5.5 presents the cumulative distributions for all the sections analyzed in the 2000 Test Track. This plot represents the percentiles of strains experienced at the base of the HMA layer in each section over six years of trafficking between 2000 and 2005.

As expected, these test sections proved to be overdesigned for fatigue cracking. At the 99th percentile, all six sections have strains below 9 $\mu\epsilon$. The maximum 50th percentile of the six sections is even below 4.5 $\mu\epsilon$. The 99th percentile value is 8 times smaller than the laboratory estimated fatigue threshold of 70 $\mu\epsilon$. The 50th percentile value is 15.5 times lower than the estimated laboratory fatigue threshold. Because these strains are so much lower than this estimated fatigue threshold, it is possible to see that pavements can be placed thinner than 23 inches with the possibility of having adequate fatigue protection as long as proper construction practices and mix design are considered. Exactly how thin was determined by examining sections in the 2003 and 2006 structural studies.

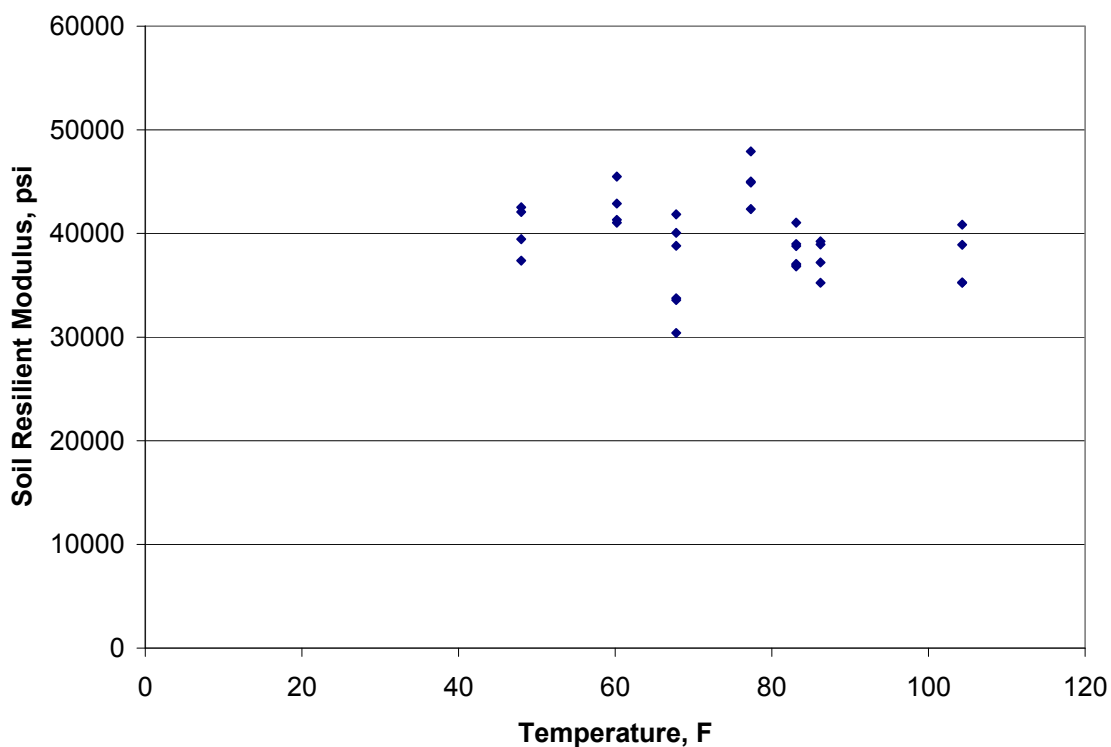


Figure 5.4. Soil Resilient Modulus and Temperature Relationship for S10 (29)

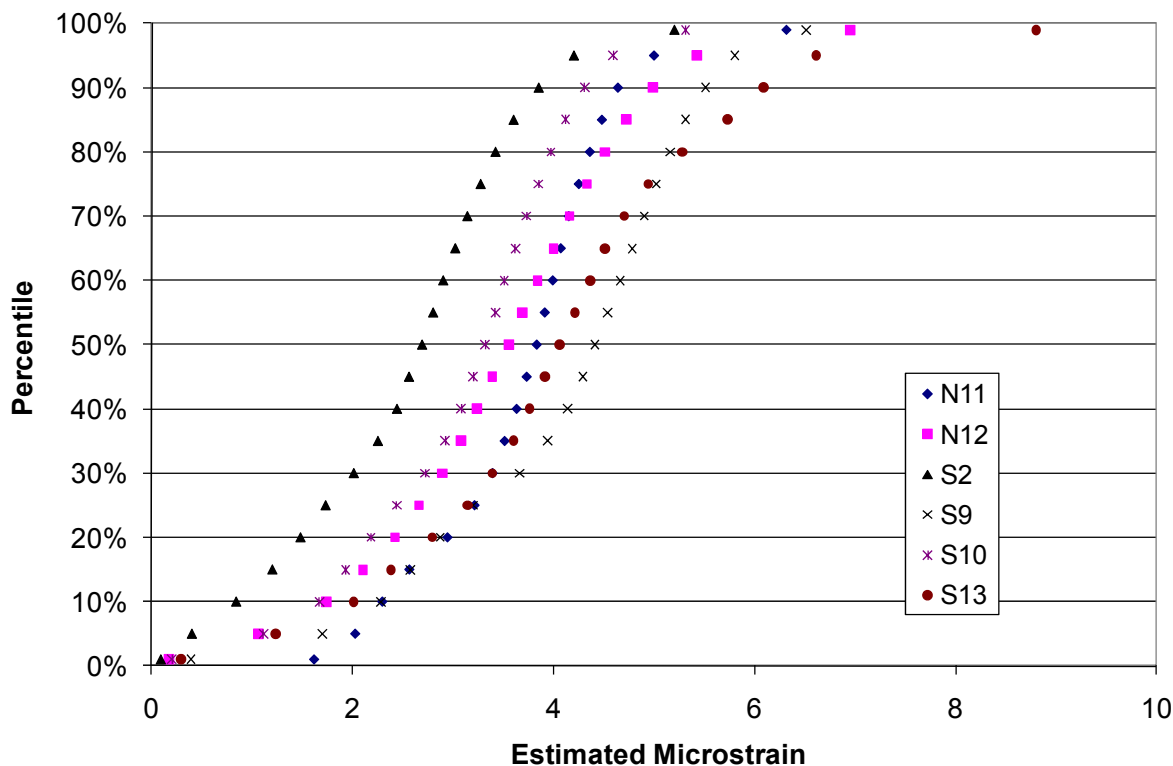


Figure 5.5. Cumulative Distributions of Strain for 2000 Test Track (29)

2003 Test Track

The 2003 Test Track introduced the structural study where embedded asphalt strain gauges measured strain at the base of the HMA layer of a pavement structure. PerRoad was not needed since strain levels were directly measured. The two components of the analysis requiring manipulation and study were the loading configuration and the pavement responses. Detailed trucking databases allowed precise loading configurations to be analyzed and weekly measured pavement responses were used to develop continuous strain distributions for the structural sections. These two design components were then linked to the observed pavement performance of the section to make correlations between pavement response and performance in seven of the eight structural sections. N8 was excluded from analysis due to the debonding that occurred during the 2003 Test Track (11).

The trafficking of the 2003 Test Track was completed using a fleet of four triple flat-bed trailers and one single box trailer. Previous research was conducted which developed relationships by section for each truck between a mechanistic pavement response (strain) and temperature (33). These relationships were used to develop cumulative distributions of strain for the life of the pavement (i.e. until cracking was observed).

While Priest and Timm’s work (33) developed strain-temperature relationships for the seven structural sections in this study, the work did not continue into developing cumulative strain distributions for each structural section. Figure 5.6 provides the methodology used in developing the strain distributions for this analysis. These calculations were made by linking the trafficking

database to the strain database to determine the number of times each strain magnitude occurred for each section.

Once the cumulative distributions were determined for each structural section, the 1st, 99th, and every 5th percentile were manually picked from the completed spreadsheets to develop cumulative distribution plots. Figure 5.7 provides the cumulative distribution functions by section graphically.

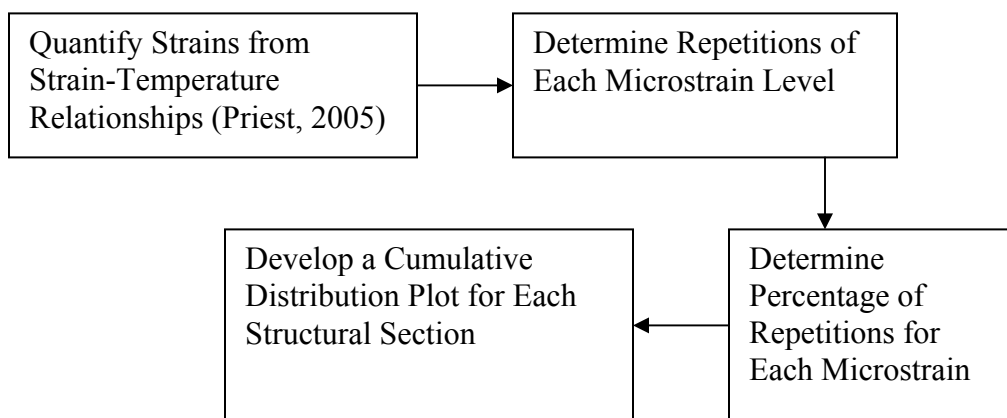


Figure 5.6. Developing Cumulative Strain Distribution Methodology

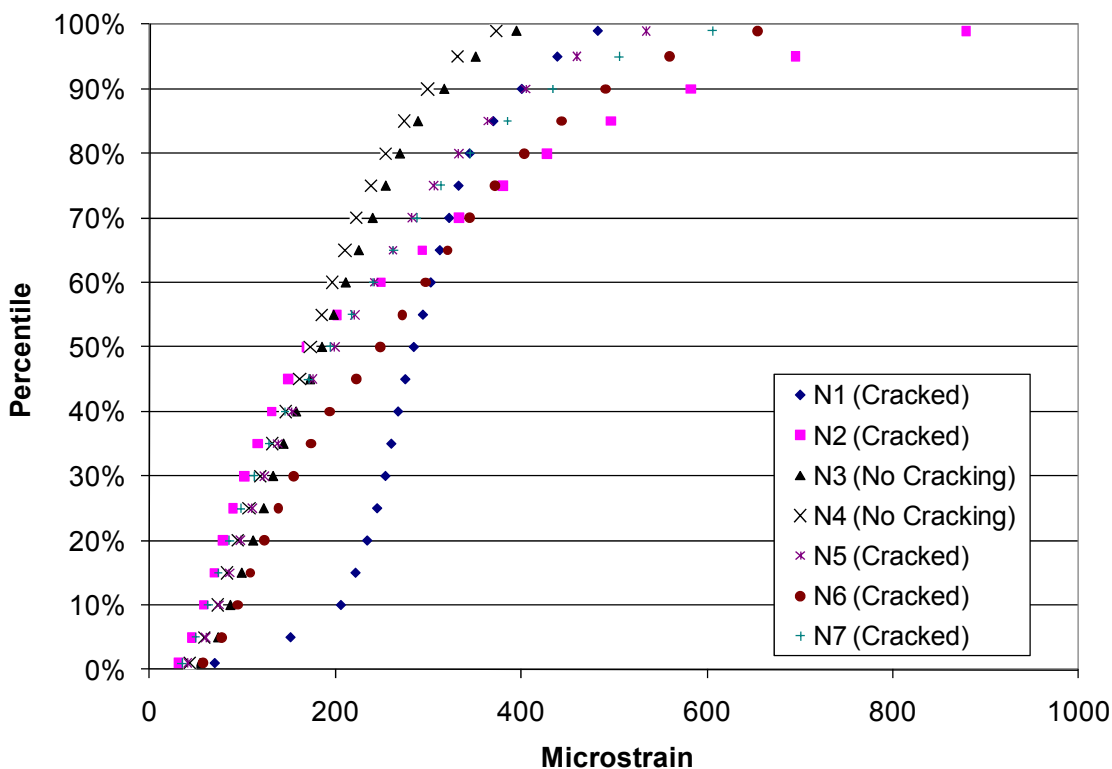


Figure 5.7. Cumulative Distribution Plots for 2003 Test Sections (29)

Of the seven sections analyzed in the 2003 analysis, five of the sections experienced fatigue cracking: N1, N2, N5, N6, and N7. N3 and N4 have not shown any signs of fatigue cracking after 20 million ESALs.

Comparing the cumulative distributions of these sections, section N4 has the lowest distribution strains at the high end of the cumulative distribution. However, until the 55th percentile strain, its strains are not the lowest. Those are found in N2, but the strains soon escalate in this thinner section.

The other section that did not show signs of fatigue cracking, N3, started out with low strains comparable to those in failed sections; however, from the 25th until the 50th percentile, its strains track very well with sections that failed in fatigue. The 55th percentile seemed to be the breaking point for sections N3 and N4 where failed sections began to escalate into higher strain levels.

While the breakpoint where the cumulative distribution functions of the cracked sections are greater than those of the non-cracked occurs at the 55th percentile, clear deviations between the sections that performed well and those that did not are present after the 60th percentile where the difference between the maximum non-cracked sectional strain and minimum fatigue cracked sectional strain jumps from 4 $\mu\epsilon$ at the 55th percentile to almost 30 $\mu\epsilon$ at the 60th percentile.

Comparing the cumulative distribution functions calculated for sections N3 and N4 to the often used laboratory fatigue thresholds of 70 or 100 $\mu\epsilon$, one would find that for both sections, less than 10% of the strain measurements fall below 70 $\mu\epsilon$. In section N3, less than 15% of the strain measurements were below 100 $\mu\epsilon$, and this value was under 25% for section N4. Therefore, it can be inferred that measured strains in the field can exceed the laboratory fatigue threshold without fatigue damage occurring. This will allow for the design of thinner pavement structures in the future.

These limited data suggested that pavements can be designed to withstand higher magnitude strains in the field than previously speculated from laboratory testing. Further investigation of the 2006 structural sections was needed to more precisely quantify acceptable strain levels.

2006 Test Track

In 2006, the Structural Study at the Test Track grew to 11 sections as previously noted in Chapter 4. Since instrumentation was incorporated into these sections, actual strain measurements could be taken at the base of the HMA. Only eight sections were included in the 2006 analysis because sections N5-N7 had already experienced cracking.

The methodology followed to create the cumulative strain distributions for the 2006 Test Track was similar to that of the 2003 Test Track; however, previous research had not been done to develop strain-temperature relationships. In 2006, it was decided to develop relationships between strain and temperature by axle for each section instead of by truck. When analyzing pavement response by axle, each steer and tandem axle was processed for every truck pass; however, of the five trailing single axles, only the axle with the “best hit” was processed. The “best hit” was defined as the axle yielding the highest recorded strain. This was believed to be the axle which most directly hit a strain gauge. The best hit single axle is circled in Figure 5.8.

Figure 5.8 also shows that the strain trace for the triple trailers predominantly used at the Test Track consisted of eight individual strain events. These were the results of one steer axle, one tandem, and five single axles loading the pavement. A double trailer resulted in six strain events, and a single trailer had four. In each case, no matter how many single axles were present, only the best hit was processed.

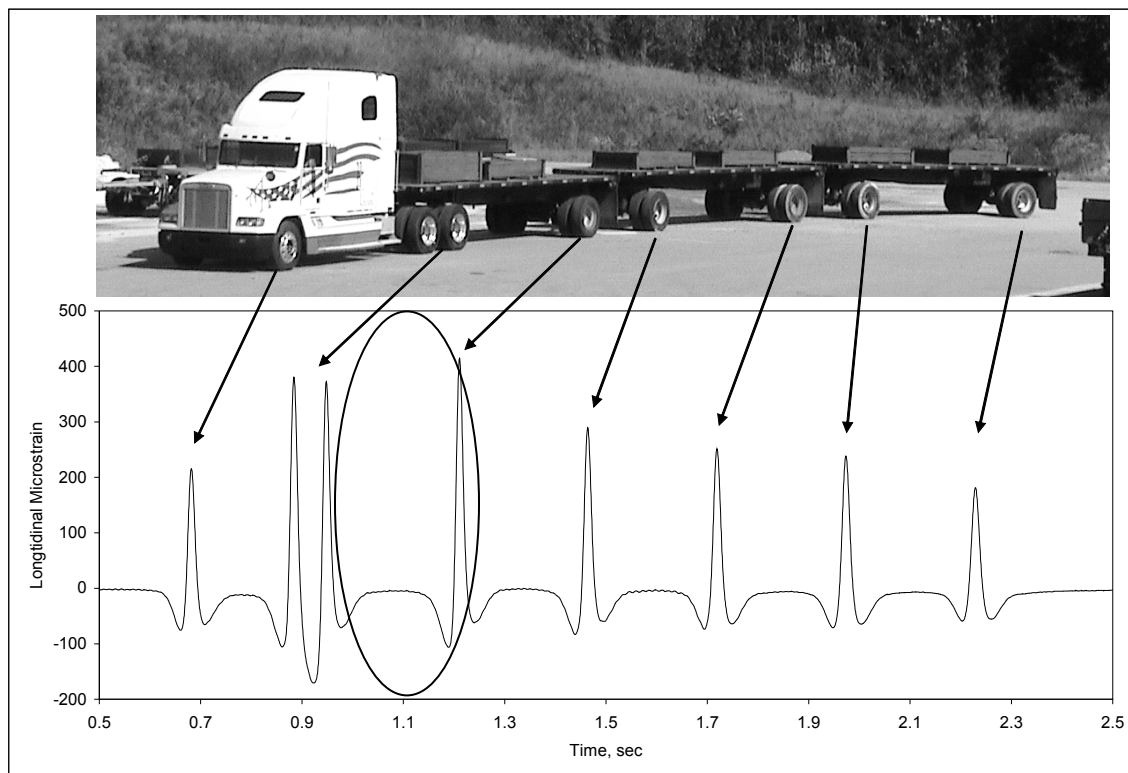


Figure 5.8. “Best Hit” Single Axle (29)

The 2003 Test Track strain-temperature relationships were developed using only longitudinal strains. When analyzing the data, longitudinal strains were typically larger than transverse strains at the same lateral offset, and a previous study (44) had shown longitudinal gauges were less influenced by wander and would better represent what is occurring at the base of an HMA layer under trafficking. Hence, longitudinal strains were used to develop strain-temperature relationships for the 2006 Test Track.

The next decision as to which strains to use in developing the strain-temperature relationships was what magnitude strain to incorporate in the analysis. While great care was taken to ensure only quality data were included in the strain databases, voltage spikes, faulty gauges, and processing errors occur in data processing. If the maximum longitudinal strain were chosen to develop the strain-temperature relationships, these errors might drive the strain temperature relationship development. Upon a thorough examination of the data, it was determined the 95th percentile strain would be appropriate strain magnitude to use for relationship development.

Previous researchers at the Test Track (33) developed strain-temperature relationships based on the mid-depth temperature. To remain consistent with the previous research, the mid-depth temperature was once again used to develop new strain-temperature relationships. The mid-depth temperature was directly measured in the newly constructed sections (N1, N2, N8, N9, N10, and S11), and linear interpolation was used to determine the mid-depth temperature for the sections remaining from the 2003 experiment (N3 and N4).

Figure 5.9 provides the methodology for developing the strain-temperature relationship. Queries were first developed in Microsoft Access which matched the 95th percentile strain for each axle and section to the temperature measured at the time of testing recorded in another database. These matched records were then exported to Excel where non-linear regression was used to determine the best relationship between the 95th percentile longitudinal strain and the mid-depth temperature.

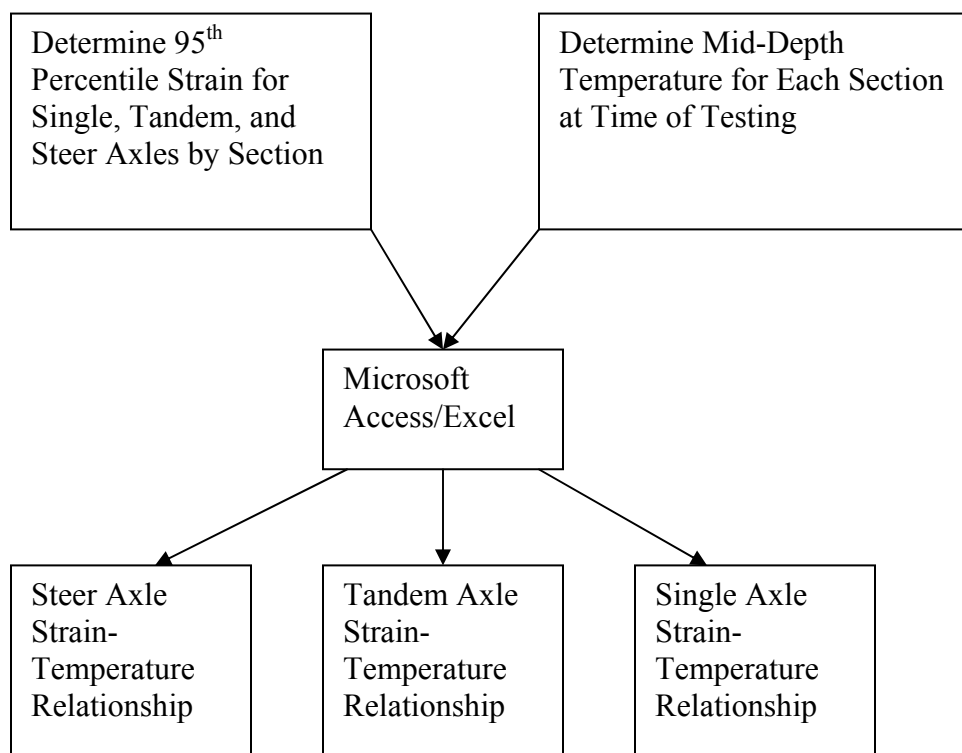


Figure 5.9. Relationship Development Methodology

To determine the best fit equation, Excel was used to fit power, exponential and polynomial functions to the data. The exponential equations returned the most consistently high R² values. Therefore, equation 5-6 was used as the backbone for the strain-temperature relationships in 2006.

$$\varepsilon = k_1 e^{k_2 T} \quad (5-6)$$

where:

- ϵ = strain, microstrain
- k_1 = sectional constant
- k_2 = sectional constant
- T = temperature, F

An example of a relationship developed for the steer axles is graphically provided in Figure 5.10. Table 5.3 provides an example of the relationship coefficients for steer axles. The other coefficients are documented by Willis elsewhere (29).

When looking at the coefficients, the thicker sections (N8 and N9) had the lower k_1 values in all three analyses. At lower thicknesses, the k_1 increased somewhat with the exception of S11 which was thinner than N3 and N4; however, these two sections have oxidized and become stiffer over the course of the previous trafficking cycle. The k_2 coefficients in the equation give the slope or rate of strain increase with temperature.

As can be seen in the Table 5.3, section N4 has a high k_1 coefficient; however, the low k_2 coefficient means that strain does not increase much with temperature. The opposite is seen in section N9. The k_1 value is lower than any other section, but it has the one of the highest k_2 values. Both of these sections were free of fatigue cracking. The two sections with the most fatigue cracking (N10 and S11) had comparatively high k_1 and k_2 coefficients; thus, as temperatures increase in these two sections, the strain magnitudes will escalate greatly.

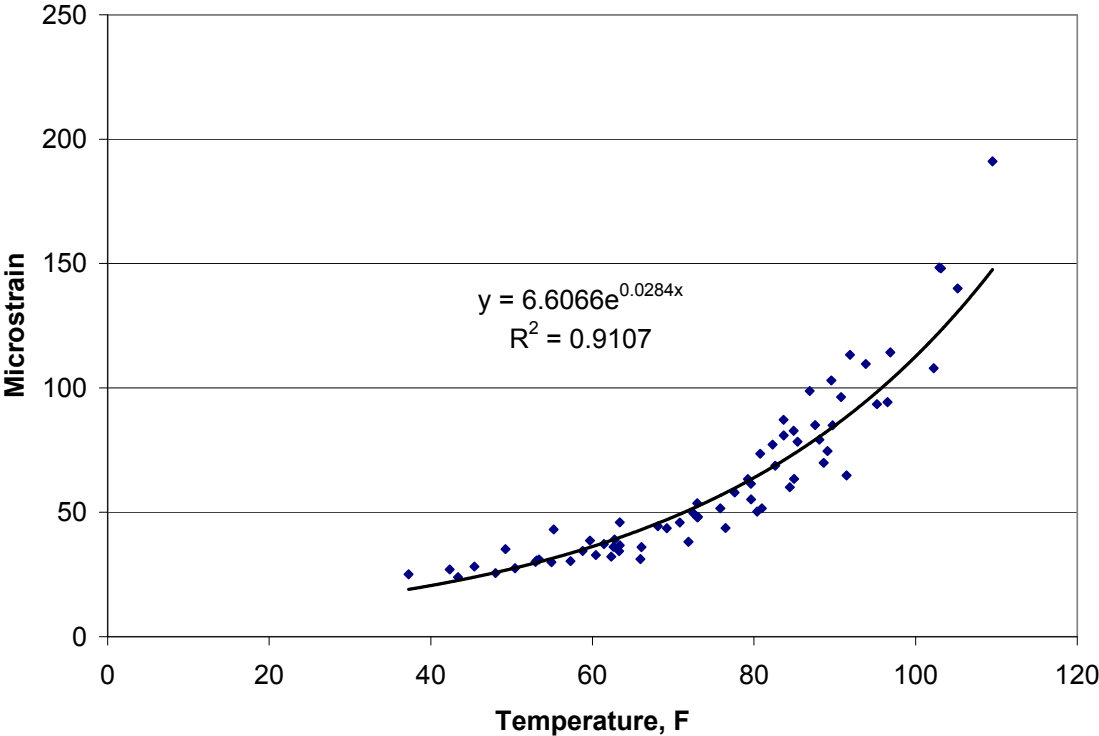


Figure 5.10. Strain-Temperature Relationship for Steer Axles in N9 (29)

After these relationships had been developed, the previously mentioned methodology was followed for linking the strain magnitudes to trafficking repetitions for the development of a cumulative distribution function. The cumulative strain distributions for the 2006 sections are provided in Figure 5.11.

Table 5.3. Equation Coefficients by Section for Steer Axles

Section	k_1	t-stat k_1	k_2	t-stat k_2	R^2
N1	21.58	7.30	0.0272	-3.82	0.84
N2	24.605	7.54	0.0264	-3.45	0.81
N3	10.543	13.15	0.0316	-7.51	0.80
N4	17.631	12.10	0.0225	-5.16	0.79
N8	12.521	12.07	0.035	-7.51	0.87
N9	6.6066	15.77	0.0284	-8.20	0.91
N10	20.677	11.10	0.0323	-6.62	0.69
S11	14.607	15.87	0.037	-10.02	0.75

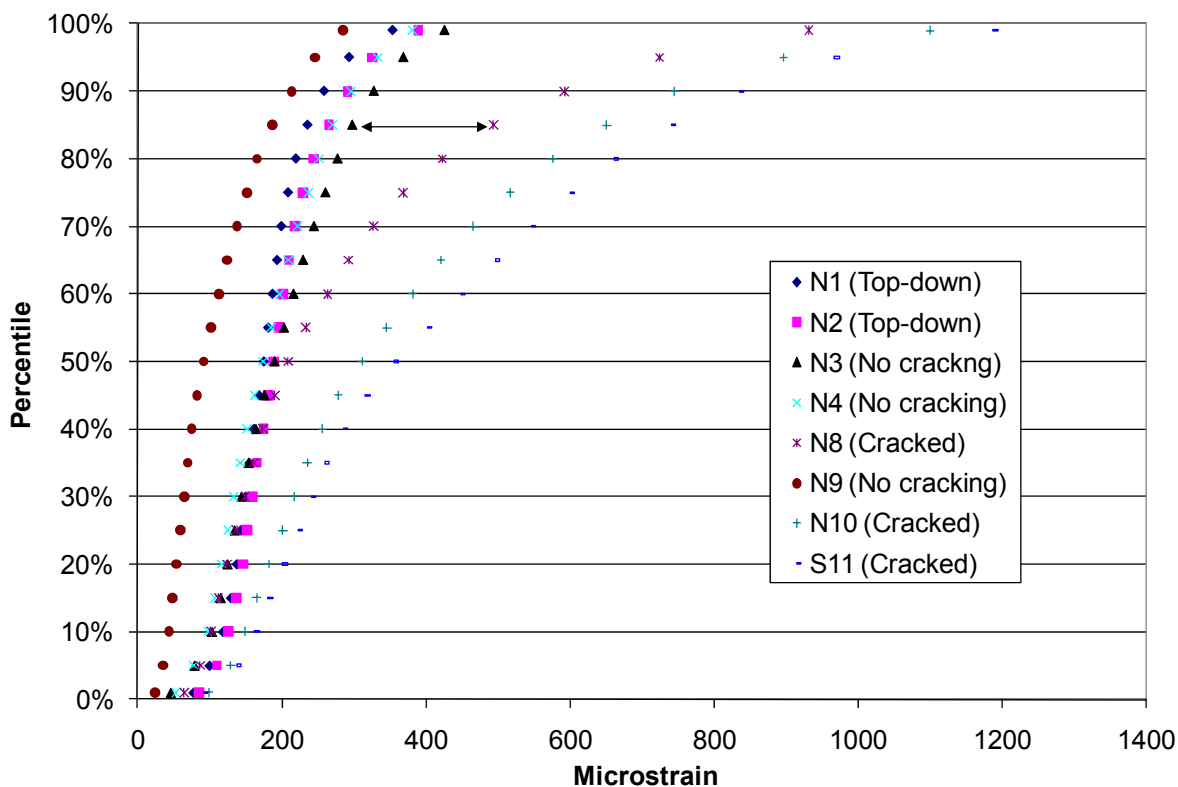


Figure 5.11. Cumulative Distribution of Strains for 2006 Structural Sections (29)

Three of the sections provided in Figure 5.11 experienced fatigue cracking: N8, N10, and S11. Previously-mentioned research showed N1 and N2 also cracked, but the cracking in these sections was top-down and not bottom-up fatigue cracking.

If one were to compare the cracked profiles versus the non-fatigue cracked profiles, a clear breakpoint occurs at the 45th percentile. At this point, the cracked sections begin to diverge

greatly from the non-cracked sections. N3 and N4's strain profiles represent the least conservative strain profiles that were able to withstand trafficking without fatigue cracking. These two sections have also received double the traffic of any other section in the 2006 study. Therefore, these two sections should be considered when determining the uppermost bound for a field-based measured fatigue threshold.

Threshold Development

There are three distinct groups of cumulative strain distributions from the sixteen sections in this investigation (Figure 5.12). The first group is the sections that were overdesigned in 2000. Pavements do not need to be designed at this thickness to prevent fatigue cracking. The second and third groups break apart from each other about the 55th percentile. The group with the smaller magnitude strains includes the sections which did not experience fatigue cracking. The group with the larger strains did experience fatigue cracking. Therefore, a distinction can be made between the cumulative strain distributions of the sections that failed in fatigue to those that did not.

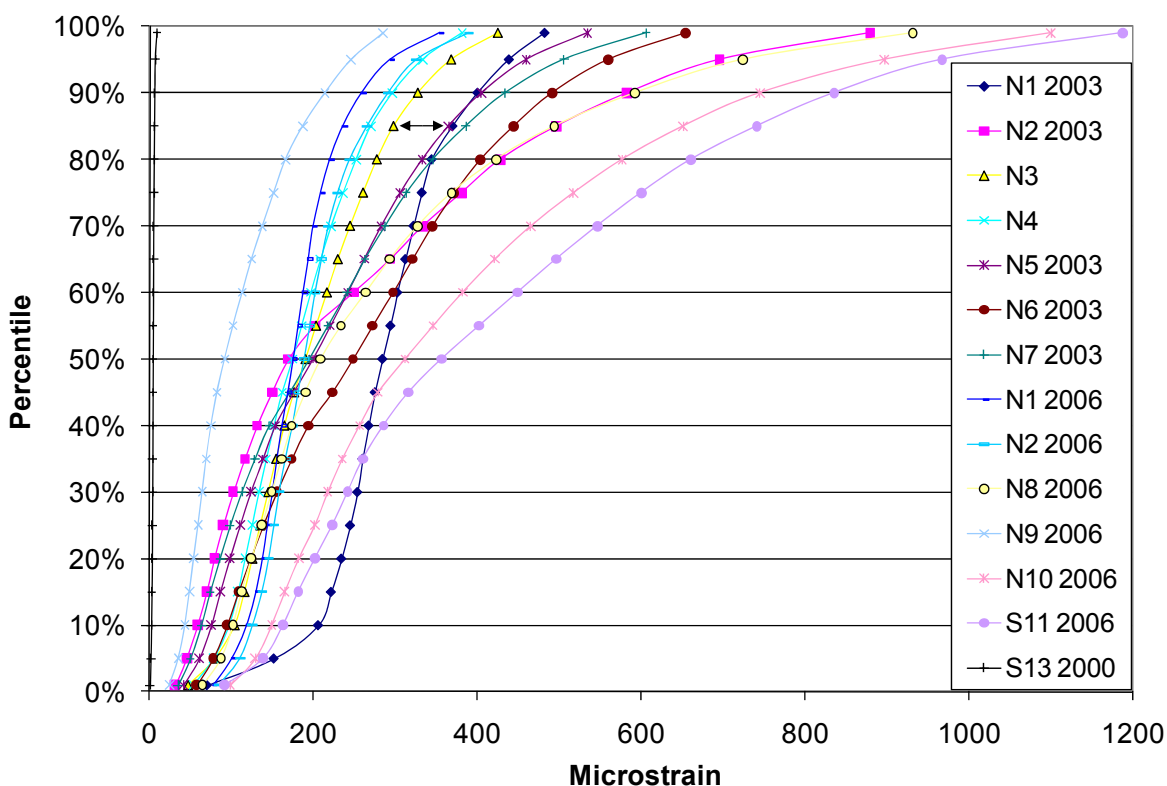


Figure 5.12. Cumulative Distributions from Three Test Cycles (29)

Three criteria were considered to help develop a new strain-criterion for flexible perpetual pavement design: 1) The section could not be overdesigned; 2) The section could not have exhibited any fatigue cracking; 3) They section had to have experienced at least 20 million ESALs. Four analyses met these criteria: N3 by axle, N4 by axle, N3 by truck, and N4 by truck. When these four analyses were carefully analyzed, it was discovered that they were not very different from each other numerically. Previous research conducted at the Test Track found that

duplicate strain gauges should typically be within 30 microstrain ($\pm 15 \mu\epsilon$) of each other. If an average of all four test sections was taken and a $\pm 15 \mu\epsilon$ confidence boundary was put around that average (Figure 5.13), all four cumulative strain distributions would fall within that confidence boundary. Therefore, the average of the aforementioned analyses was determined to be an appropriate field-based strain threshold for flexible perpetual pavement design. These values are given in Table 5.4. If these values are validated for designing perpetual pavements with similar stiffness characteristics and similar loading scenarios, then pavements can be designed thinner without losing performance life.

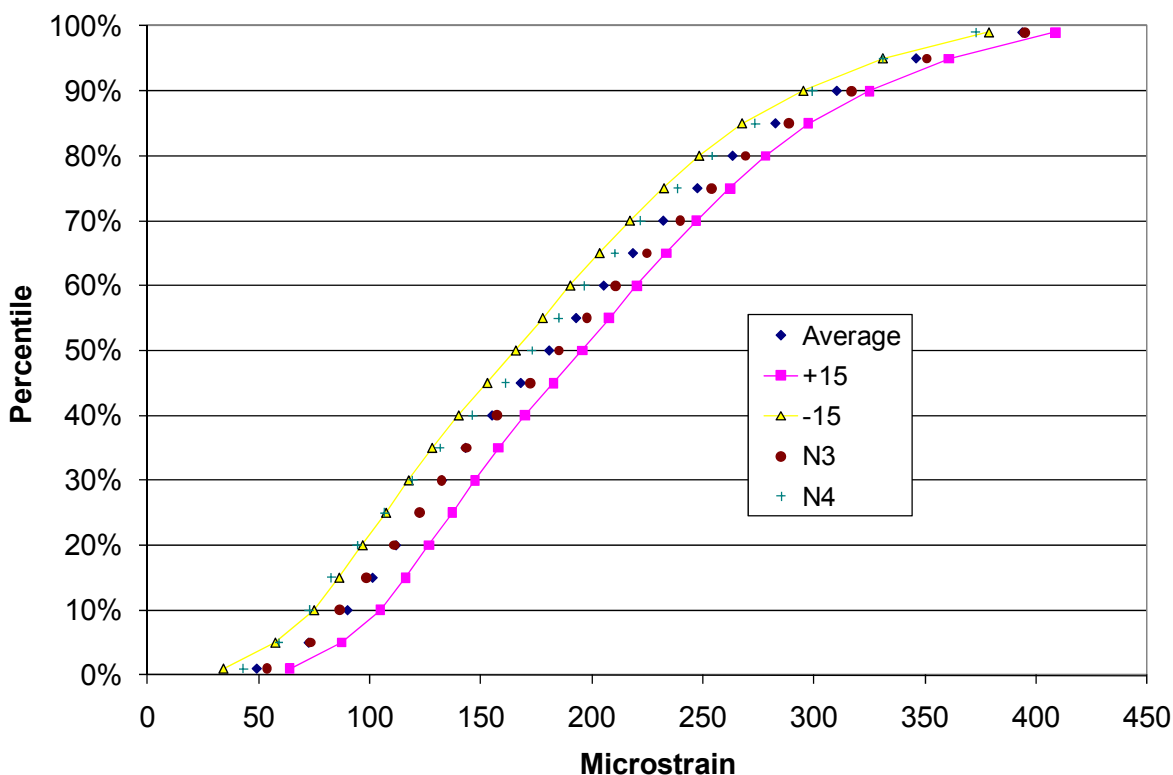


Figure 5.13. Average Strain Distribution with Confidence Bands (29)

Conclusions

The following conclusions were drawn from the previously discussed research:

- Fatigue cracked sections had wider strain profiles when compared to the strain distributions of uncracked sections.
- Higher magnitude strains govern fatigue cracking since many of the cracked and uncracked strain profiles were similar in the lower percentiles.
- Assuming similar traffic and fatigue characteristics, the provided field-based strain profile (Table 5.4) should withstand fatigue cracking. Implementation of these findings beyond the scope of the Test Track requires further validation.

Table 5.4. Field-Based Strain Criteria for Perpetual Pavements (29)

Percentile	Fatigue Limit, $\mu\epsilon$
99%	394
95%	346
90%	310
85%	282
80%	263
75%	247
70%	232
65%	218
60%	205
55%	193
50%	181
45%	168
40%	155
35%	143
30%	132
25%	122
20%	116
15%	101
10%	89
5%	72
1%	49.

CHAPTER 6 - LABORATORY AND FIELD COMPARISONS

One of the most complex and challenging tasks undertaken at the NCAT Test Track is the development of relationships between laboratory test results and field measured data or performance. It is difficult, at best, to capture the complexities that HMA experiences in the field and translate them into a simple laboratory experiment. Three studies were undertaken as a part of the 2006 Test Track to relate laboratory test results to field measured or modeled data. The first experiment characterized the modulus values of the granular materials at the Test Track and compared them to laboratory resilient modulus results. The second study compared the dynamic modulus values from the structural test sections and compared them to models that had been developed by researchers to find a “best fit” model for E^* . The final analysis took the cumulative strain distributions described in the previous chapter and compared them to laboratory determined fatigue thresholds.

GRANULAR MATERIALS LABORATORY AND FIELD COMPARISONS

One of the critical inputs for accurate M-E pavement design is accurate characterization of the stiffness of the unbound pavement material layers. This stiffness is quantified as resilient modulus, and this value can be determined either through laboratory testing with the triaxial apparatus or through non-destructive testing in the field with the FWD. Resilient modulus is typically expressed as a function of unbound material stress-state using a non-linear stress-sensitivity model.

To effectively characterize the stiffness behavior of unbound materials, several factors must be considered. First, does laboratory or field resilient modulus testing provide a better representation of material behavior? Secondly, is the material stress-sensitive and, if so, which stress-sensitivity model best quantifies the behavior of that material? Answering these questions allow for the most accurate quantification of resilient modulus for pavement design and more accurate modeling of pavement design life.

The overall goal of this investigation was to mechanistically characterize the five unbound materials utilized in the eleven structural sections at the NCAT Test Track for effective use in pavement design. Specific objectives included:

- A comparison of laboratory and field derived resilient moduli.
- An evaluation of common non-linear stress-sensitivity models with respect to laboratory and field moduli.
- Developing a recommendation as to the effective use of unbound material moduli in pavement design and analysis.

Unbound Materials Used in the Structural Study

The unbound materials used in this analysis were those incorporated into the design of the 2006 structural study. Table 6.1 shows the material gradations for each of the unbound materials. Note that the three base layer materials (the limerock, granite, and Type 5) have reasonably well-graded particle distributions, with relatively small percentages of material retained above the $\frac{3}{4}$ " sieve. These materials also exhibit lower amounts of material passing the #200 sieve than the two materials that are predominantly used as subgrade materials (the Seale and Track soil). The Seale

material is a very fine-grained soil, with almost 58 percent of the material passing a #200 sieve. The Track soil is more gap-graded, with 17 percent of the material retained on the 1” sieve and 48 percent of the material passing the #200 sieve.

Table 6.1. Unbound Material Gradations (27)

Material	Limerock	Seale	Type 5	Track Soil	Granite
Layers	Base	Subgrade	Base	Subgrade	Base
Sections	N1, N2	N8, N9	N10	All (N8, N9 Base)	S11
Sieve	Percent Passing Control Sieve				
1 1/2"	100	100	100	100	100
1"	100	100	99	83	95
3/4"	100	100	97	81	88
1/2"	88	100	92	78	83
3/8"	81	100	88	75	78
#4	61	100	79	71	57
#8	44	100	71	68	47
#16	32	99	64	66	39
#30	26	98	58	64	31
#50	23	92	49	61	23
#100	21	82	36	56	15
#200	18.8	57.7	25.1	48.0	10.2

Laboratory Testing

For this study, triaxial resilient modulus testing was performed in accordance with NCHRP 1-28A “Laboratory Determination of Resilient Modulus for Flexible Pavement Design.” This testing was performed on each of the five unbound materials present in the eleven structural sections at the Track. This testing was subcontracted to Burns, Cooley, Dennis, Inc. The stresses under which the material was tested is based on material type and whether or not that material is used primarily as a base/subbase or a subgrade material, and three replicates of each material type were tested in accordance with the NCHRP 1-28A procedure.

For each unbound material tested, stress and modulus data generated from testing the three samples were combined into one database for each material. For each testing sequence, the following data were generated: the total axial stress (σ_1), the confining pressure (σ_2 and σ_3), and the calculated resilient modulus. Given these stresses, the bulk stress (θ), deviatoric stress (σ), and octahedral shear stress (τ_{oct}) were calculated for each testing sequence using equations 6-1, 6-2, and 6-3, respectively.

For this study, four common non-linear models relating the material stress-state to the resilient modulus were evaluated for each unbound material. The regression coefficients for these models were generated for each unbound material by entering in the stress-state and resilient modulus data into DATAFIT, a non-linear regression modeling software package developed by Oakdale Engineering. This software is capable of generating multiple non-linear models from a given data

set containing one or more independent variables and one dependent variable. This software also allows the user to define the model for which the software will calculate the regression coefficients (k_1 , k_2 , etc.) as well as pertinent statistics such as those regarding model fit (R^2) and statistical significance of the calculated regression coefficients (p-values).

$$\theta = \sigma_1 + \sigma_2 + \sigma_3 \quad (6-1)$$

$$\sigma_d = \sigma_1 - \sigma_3 \quad (6-2)$$

$$\tau_{oct} = \frac{1}{3} \sqrt{(\sigma_1 - \sigma_2)^2 + (\sigma_2 - \sigma_3)^2 + (\sigma_3 - \sigma_1)^2} \quad (6-3)$$

where:

θ = Bulk Stress, psi

σ_d = Deviatoric Stress, psi

τ_{oct} = Octahedral Shear Stress, psi

σ_1 = Axial Stress, psi

σ_2, σ_3 = Confining Stress, psi

Equations 6-4 and 6-5 are single-variable stress-sensitivity models that relate resilient modulus to bulk stress and deviatoric stress, respectively. These models are commonly specified based on whether the material is a coarse-grained (Equation 6-4) or fine-grained soil (Equation 6-5). Equations 6-6 and 6-7 are multi-variable stress-sensitivity models that model resilient modulus as a function of two stress terms. These models are more universal given they are not constrained for use with a particular soil type. In each model, the first term (the bulk stress) models stress-sensitivity as a function of confining pressure while the second term (either deviatoric or octahedral shear stress) models stress-sensitivity due to shearing stresses. For the purposes of this analysis, equation 6-4 is referred to as the bulk model, equation 6-5 is referred to as the deviatoric model, equation 6-6 is referred to as the MEPDG model, and equation 6-7 is referred to as the universal model.

$$M_r = k_1 * \left(\frac{\theta}{p_a} \right)^{k_2} \quad (6-4)$$

$$M_r = k_1 * \left(\frac{\sigma_d}{p_a} \right)^{k_2} \quad (6-5)$$

$$M_r = k_1 p_a * \left(\frac{\theta}{p_a} \right)^{k_2} * \left[\left(\frac{\tau_{oct}}{p_a} \right) + 1 \right]^{k_3} \quad (6-6)$$

$$M_r = k_1 p_a * \left(\frac{\theta}{p_a} \right)^{k_2} * \left(\frac{\sigma_d}{p_a} \right)^{k_3} \quad (6-7)$$

where:

M_r = Resilient Modulus, psi

P_a = Atmospheric Pressure (14.7 psi)

k_1, k_2, k_3 = Regression Coefficients

Table 6.2 summarizes the laboratory generated stress-sensitivity models that were generated based on the laboratory triaxial data from this project. The multi-variable stress-sensitivity models (the MEPDG and universal models) exhibited much higher model R^2 values (typically above 0.9) than the single-variable stress-sensitivity models (the bulk and deviatoric models) for the different unbound materials. Both the MEPDG and universal constitutive models exhibit a good model fit for each of the unbound materials except for the Track soil material. The Track soil material was clearly the least stress dependent material tested, with none of the four stress-sensitivity models generating an R^2 above 0.7 for this material. For the laboratory data, an average Track soil modulus of 28,335 psi with a standard deviation of 6,650 psi was calculated.

To quantify the relative stiffness of the different unbound materials, three representative stress states for each material were entered into the laboratory generated constitutive equations (for the MEPDG and universal models). These stress-states were generated by analyzing the cumulative distribution functions (CDF) of the stress-states used for testing with each of the different unbound materials. More details regarding the selection of these representative stress-states are documented elsewhere (27). Table 6.3 lists these representative stress-states. Figure 6.1 shows the calculated modulus values for each of the unbound materials at the various stress-states with the laboratory calibrated universal stress-sensitivity models.

The granular base materials from the Test Track (Florida limerock, granite base, Type 5 base) exhibited stress-hardening behavior in the laboratory under increasing load while the Seale subgrade material exhibited stress-softening behavior. The Track soil material showed no significant stress-sensitivity in the laboratory across different stress-states. The MEPDG and universal model R^2 values of 0.42 and 0.66, respectively, confirm this assessment. In comparing the materials at equivalent stress-states, the Track soil material exhibited the highest modulus in the lowest and middle representative stress-states. The limerock base material was the stiffest material at the highest representative stress-states.

Table 6.2. Summary of Laboratory Generated Stress-Sensitivity Models (27)

Model Form	Material	k ₁	p-value (k ₁)	k ₂	p-value (k ₂)	k ₃	p-value (k ₃)	R ²
Bulk	Limerock Base	22966.7	0	0.4773	0.0000	N/A	N/A	0.5618
	Vulcan Granite	10862.1	0	0.6267	0.0000	N/A	N/A	0.886
	Seale Subgrade	6009.8	0	-0.1201	0.0000	N/A	N/A	0.0288
	Type 5 Base	14049.7	0	0.6710	0.0000	N/A	N/A	0.8721
	Track Soil	26833.3	0	0.0447	0.2312	N/A	N/A	0.0179
Deviatoric	Limerock Base	39001.4	0	0.2174	0.0000	N/A	N/A	0.2204
	Vulcan Granite	21350.0	0	0.3866	0.0000	N/A	N/A	0.5765
	Seale Subgrade	4305.8	0	-0.5571	0.0000	N/A	N/A	0.7834
	Type 5 Base	29487.2	0	0.3876	0.0000	N/A	N/A	0.5334
	Track Soil	28878.9	0	-0.0572	0.0465	N/A	N/A	0.0478
MEPDG	Limerock Base	1266.8	0	1.2081	0.0000	-1.2332	0	0.9326
	Vulcan Granite	716.3	0	0.8468	0.0000	-0.4632	0	0.9253
	Seale Subgrade	817.6	0	0.3305	0.0000	-3.3946	0	0.957
	Type 5 Base	883.5	0	1.0050	0.0000	-0.6575	0	0.9478
	Track Soil	1879.0	0	0.4067	0.0000	-0.7897	0	0.4202
Universal	Limerock Base	717.0	0	1.2338	0.0000	-0.5645	0	0.8562
	Vulcan Granite	581.1	0	0.8529	0.0000	-0.1870	0.00001	0.9172
	Seale Subgrade	225.1	0	0.3598	0.0000	-0.7551	0	0.9786
	Type 5 Base	643.7	0	1.0318	0.0000	-0.2833	0	0.9349
	Track Soil	1095.4	0	0.5930	0.0000	-0.4728	0	0.6642

Table 6.3. Representative Stress-States used for Modulus Normalization (27)

	Bulk Stress (psi)	Deviatoric Stress (psi)	Octahedral Shear (psi)
State 1	10	2	1
State 2	25	7	3.5
State 3	50	15	8

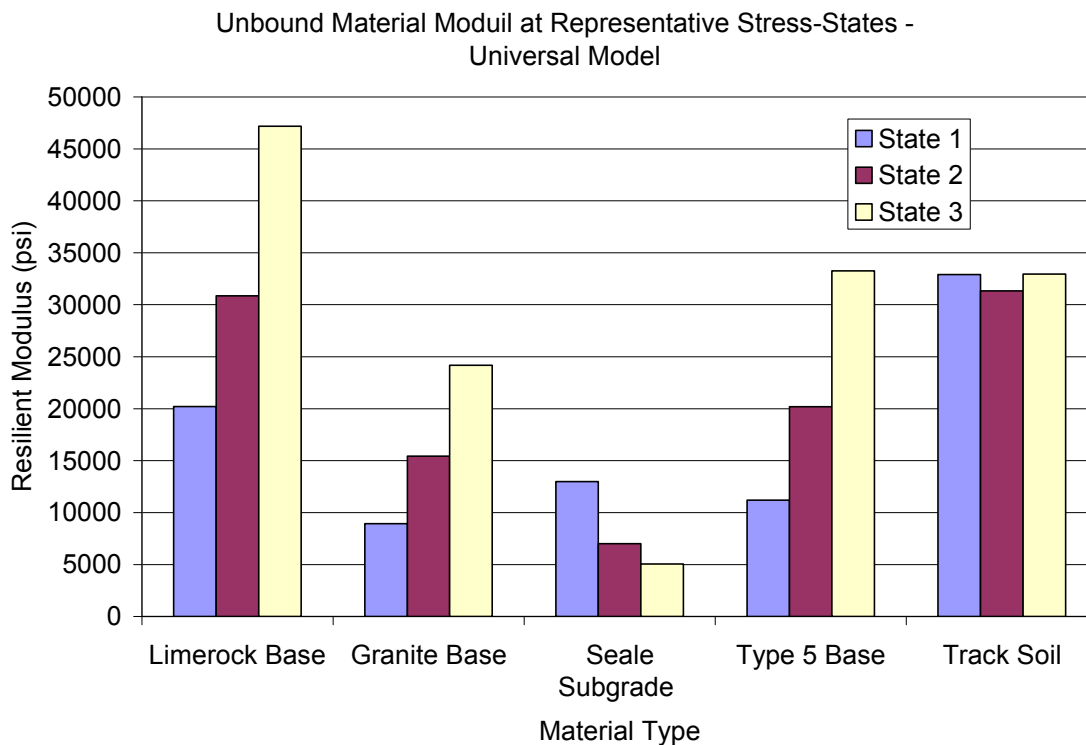


Figure 6.1. Unbound Material Moduli at Representative Stress-States – Universal Model (27)

Backcalculation Cross-Section Investigation

The objective of this portion of the study was to generate the optimal cross-section for backcalculation for each of the eleven structural sections at the Test Track. Optimizing the backcalculation cross-section will allow for the generation of accurate pavement layer moduli for each of the structural sections. Confidence in this data set is necessary for the calibration of viable stress-sensitivity models for the unbound pavement layer materials in the field.

To generate accurate in-situ moduli for each of the structural sections at the NCAT Test Track, an investigation was conducted on each of the structural sections to determine the optimum cross-section for backcalculation. For each structural section, multiple possible backcalculation cross-sections were generated based on how each section was constructed and the composition of the different pavement layers. These cross-sections included a number of 3-layer, 4-layer, and 5-layer pavement systems. Trial cross-sections including a stiff layer were also included to ensure that bedrock or a shallow water table were not influencing the results of the backcalculation. An example of the trial cross-sections utilized for sections N1 and N2 are shown in Figure 6.2. A

similar set of trial cross-sections was developed for each of the eleven structural sections based on the construction information from these sections (27).

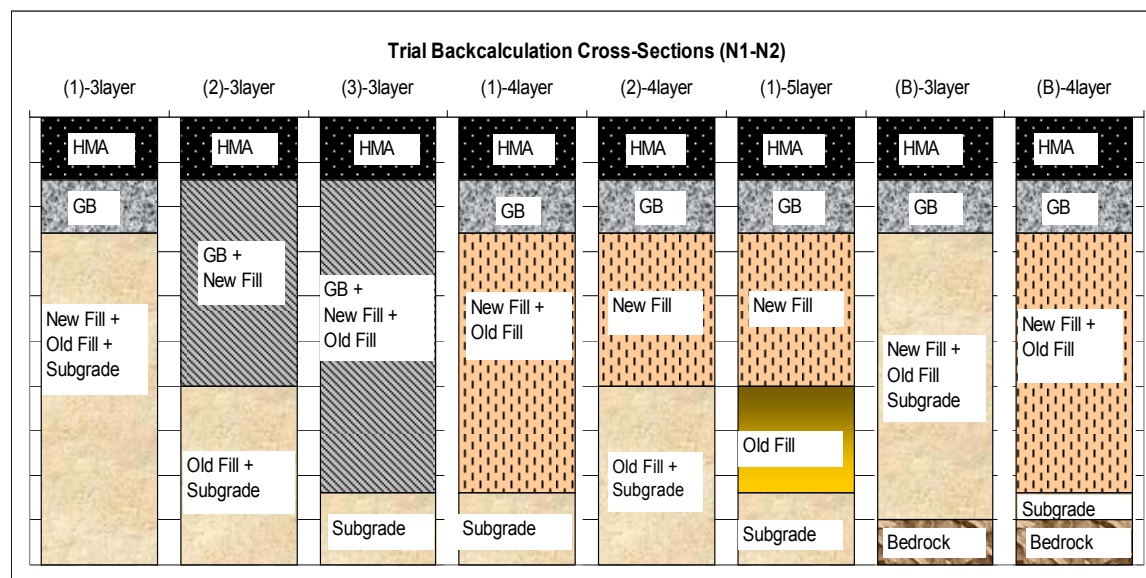


Figure 6.2. Trial Backcalculation Cross-Sections for Sections N1 and N2 (27)

To determine the optimal backcalculation cross-section for each structural section, several sources of information were utilized. First, FWD testing was performed on four different dates for each of the structural sections at the Test Track (these data were collected as part of the regular NCAT FWD testing program). The dates used for this investigation were selected to encompass a wide variety of pavement temperatures. The pavement temperatures on these dates ranged from approximately 45°F to over 130°F. For each structural section, the deflection data from these four dates were backcalculated using each of the trial backcalculation cross-sections. From this, a database of summary files detailing the layer moduli and RMS error for each drop was compiled. These individual databases were then analyzed to determine the quality of the solution.

First, the results from each cross-section were analyzed to determine the percentage of drops exhibiting a reasonable match between measured and calculated deflections (RMS Error). For the purposes of this investigation, the percentage of drops that exhibited an RMS error below 4% was used to determine whether a trial cross-section presented a reasonable solution. The reasoning behind utilizing 4% RMS as a cut-off value is documented elsewhere (27). Secondly, the summary files were analyzed to ensure that the solution for a particular cross-section was stable and presented consistent modulus values between drops at the same load levels. Erratic layer moduli on subsequent drops at identical load levels serve as an excellent indicator of solution instability. Additionally, these files were analyzed to ensure that the modulus values for two adjoining layers were not compensating for one another on consecutive drops. Finally, the individual solutions were analyzed to ensure that the modulus values were reasonable for that particular material. The process outlined above typically eliminated several of the trial cross-sections from consideration, leaving only two or three viable solutions.

The second data set used in determining the optimum backcalculation cross-section was the data from the FWD on gauge testing conducted on 7/17/07. Precise details of this testing procedure are documented by Taylor (27). For each structural section, the deflection files from this testing were backcalculated using the trial cross-sections that were deemed viable after analyzing the data from the multiple FWD testing dates. These files were backcalculated to determine the pavement responses at the locations in which instrumentation was embedded within the pavement structure (e.g. the bottom of the HMA layer, the surface of the base layer, and the surface of the fill layer). These predicted pavement responses generated through backcalculation were then paired with the corresponding measured pavement response from the instrumentation for that particular FWD loading (drop). Comparing the measured versus predicted strain behavior for the remaining trial cross-sections were used as a deciding factor in determining the best cross-section for analysis. Measured versus predicted pressures at the surface of the base and fill layers were also calculated and analyzed to validate the use of the selected backcalculation cross-section.

Figure 6.3 shows a summary diagram of the final backcalculation cross-sections selected for each of the structural sections. Given these cross-sections, backcalculation of the deflection data at the Test Track could then be performed with the aim of characterizing the various unbound material moduli. Through this investigation, it was shown that bedrock or stiff layer effects do not seem to influence the deflection data at the Test Track. It was also shown that 3-layer pavement systems perform much better than 4-layer or 5-layer systems (possibly due to material similarities between base and fill layers). Full details regarding the backcalculation cross-section investigation for each of the eleven structural sections at the 2006 Test Track are documented elsewhere (27).

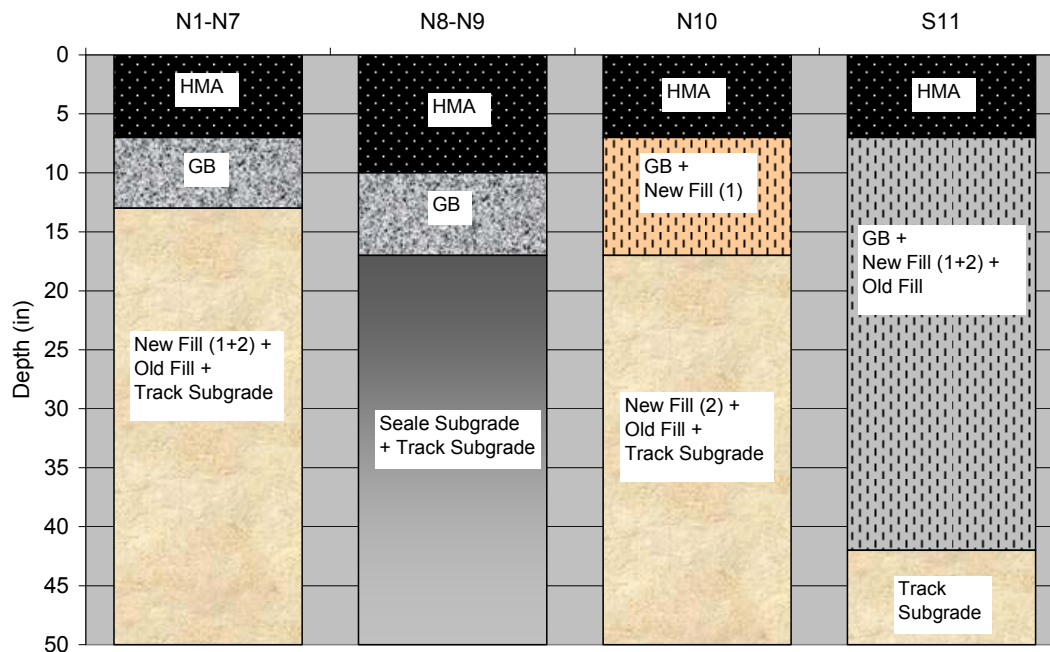


Figure 6.3. Final Selected Backcalculation Cross-Sections (27)

Field Characterization of Unbound Materials

Methodology

For this study, deflection data collected from each of the structural sections at the Test Track were used to evaluate the stress-sensitivity of the unbound materials within those sections. The deflection data used for this study were collected over multiple dates in which a wide range of pavement temperatures was observed to capture the seasonal variability of these materials. Backcalculation was performed on the deflection data for each section using the optimal backcalculation cross-section generated for that section (see previous section). For each FWD test, this process yielded both a backcalculated modulus value for each of the pavement layers as well as a comprehensive stress-state at a pre-defined location within each of the pavement layers. These layered-elastic generated stresses were then adjusted for overburden so that the true stress-state within the pavement cross-section was represented. Given this information, four commonly used stress-sensitivity models (listed above in the laboratory testing section of this report) were generated (using DATAFIT) and evaluated (through a model calibration and validation process) for the various unbound materials.

These stress-sensitivity models were calibrated based on data from four testing dates that encompassed a wide range of pavement temperatures and consequently wide ranging stress-states. These calibrated models were evaluated based on model-fit, the statistical significance of the regression coefficients, and on backcalculated versus predicted modulus behavior. If the selected models for each material were deemed viable, they next underwent the process of validation. This process utilized data from four other FWD testing dates (over a similar wide pavement temperature range) to generate a second database of representative pavement layer

stresses and material moduli. These data were then used to determine how well the calibrated models could predict the unbound material moduli from a different data set. Additionally, the behavior of the HMA layer moduli with changing temperatures was evaluated to ensure that the backcalculated solutions were reasonable for each of the test sections. Full details regarding this investigation are given by Taylor (27).

Model Generation

Figure 6.4 shows the model R^2 summary for the various base material types. This figure shows that the universal model provides the highest model R^2 for the field stress and modulus data. Also, this figure illustrates the superiority of the multiple-variable models versus the single-variable models in terms of model fit for the base layer materials. The universal model seems to provide the best fit for both the limerock and the granite base materials with respect to model R^2 . This model generates R^2 values of 0.83 and 0.67, respectively, for the two material types. These models were deemed high quality considering the vast amount of data generated across four days of testing in addition to the large amount of spatial and seasonal variability generated within the data set. Figure 6.4 also illustrates the poor model fit exhibited by all four models for the Track soil base and combined Type 5 base and Track fill materials. This was expected given the relative stress-insensitivity of the Track soil material in laboratory testing. The combined granite and Track fill in section S11 seems to generate approximately the same model R^2 regardless of model used. Table 6.4 summarizes the field-calibrated universal stress-sensitivity models for each of the materials used at the Test Track. It can be seen from this table that all of the models exhibit statistically significant regression coefficients except for the S11 model, in which no tangible benefit was seen in model R^2 for the multi-variable models over the single-variable models. A separate model for the granite base material that excluded sections N5, N6, and N7 was generated due to there being a large amount of pavement distress in those sections. Validation of this assumption is shown in Taylor (27).

Figure 6.5 shows a model R^2 summary by section and material type for the subgrade layer materials. To generate a material-specific model for the Track soil subgrade material, several combinations of the data sets were utilized to generate the best model fit. This was done because the different cross-sections at the Test Track have this material at various depths with widely varying materials above the subgrade layer. This figure shows that the sections featuring only the Track soil material in the subgrade do not exhibit very strong stress-sensitivity. Many of these sections exhibit model R^2 below 0.5. Additionally, the best R^2 for the material-specific Track soil model (containing the data from sections N1 through N4) is only 0.44. This result was expected given the fact that this material showed the lowest laboratory stress-sensitivity of any of the unbound materials. The most appropriate model for modeling the combined Seale and Track subgrade in terms of model R^2 was the universal stress-sensitivity model based on R^2 data and statistical significance of regression coefficients.

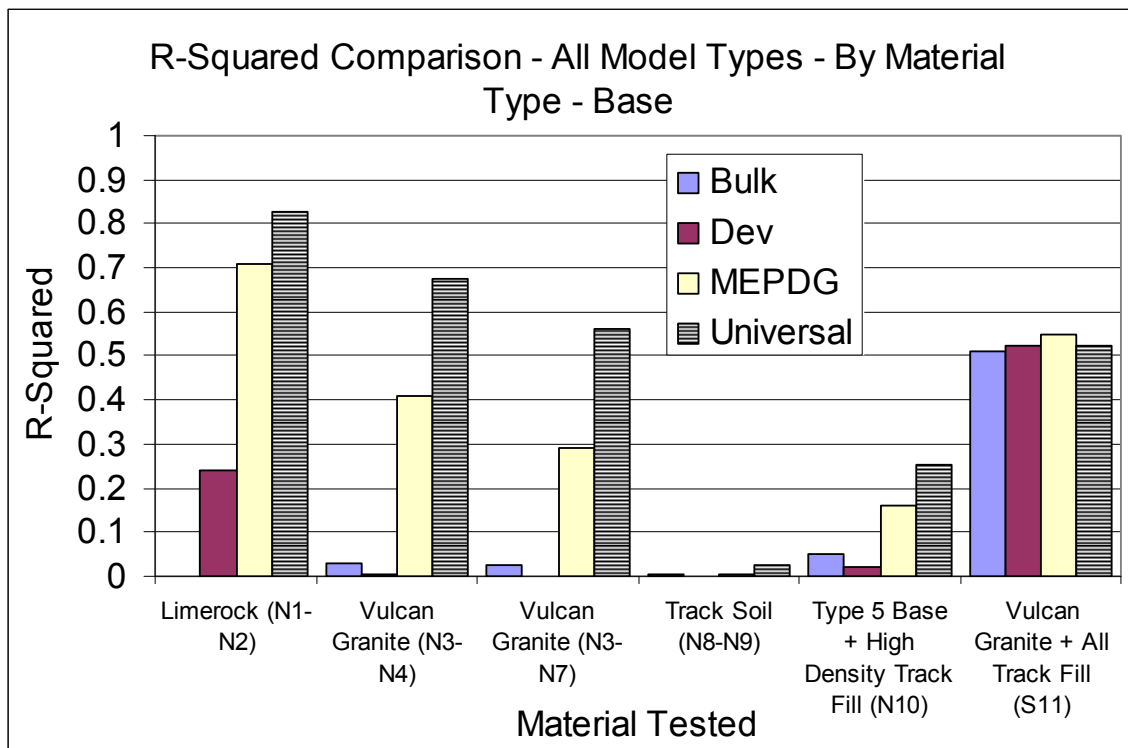


Figure 6.4. Model R-Squared Summary (Base Layer, by Material) (27)

Table 6.4. Field-Calibrated Universal Models (Base Layer, by Material) (27)

Base Material	k1	p-value (k1)	k2	p-value (k2)	k3	p-value (k3)	R2
Limerock (N1-N2)	4621.71	0	-2.0788	0	1.8908	0	0.8266
Granite Base (N3-N4)	10465.42	0	-3.0449	0	2.7613	0	0.6742
Granite Base (N3-N7)	14380.51	0	-3.3340	0	3.0202	0	0.5603
Track Soil (N8-N9)	576.16	0.00001	-0.6687	0.00026	0.6202	0.0004	0.0237
Type 5 Base + High Density Track Fill (N10)	8243.90	0.00251	-3.1639	0	2.8650	0	0.2542
Granite Base + All Track Fill (S11)	769.73	0	-0.1598	0.17916	-0.3246	0.0008	0.5244

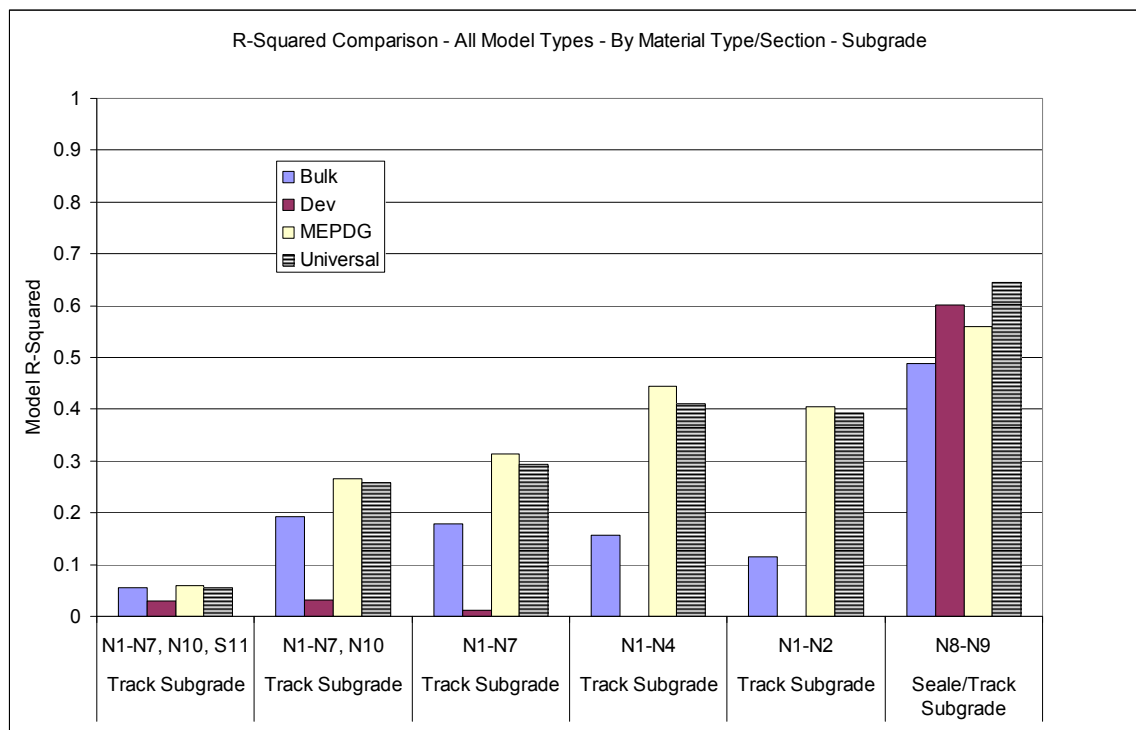


Figure 6.5. Model R-Squared Summary (Subgrade Layer, by Material) (27)

Model Calibration

The next step in the model generation process was to evaluate the measured versus predicted resilient modulus values for each base material type using the most appropriate constitutive model. The models that exhibited reasonable R^2 values, statistically significant regression coefficients, and good agreement between measured and predicted resilient moduli were deemed acceptable. The materials with models that did not meet the criteria of acceptability were deemed non stress-sensitive. An average and standard deviation of the field-calculated moduli for these materials were reported in lieu of a stress-sensitivity model.

For the limerock base material (sections N1 and N2), Figure 6.4 shows that the universal constitutive model provided the highest model R^2 for this data set. Table 6.4 shows that each of the regression coefficients for this model was statistically significant (p-values less than 0.05). Next, the actual backcalculated moduli from this data set were plotted against the modulus values predicted using the field-calibrated model as illustrated in Figure 6.6. This figure shows that the data points for this model seem to track closely to the line of unity (representing the condition where the measured moduli equal the model predicted moduli). As a result, the universal model was deemed suitable for modeling the stress-sensitivity of the limerock base material in the field. A similar procedure was carried out for each of the base and subgrade materials utilized in the structural study at the Test Track.

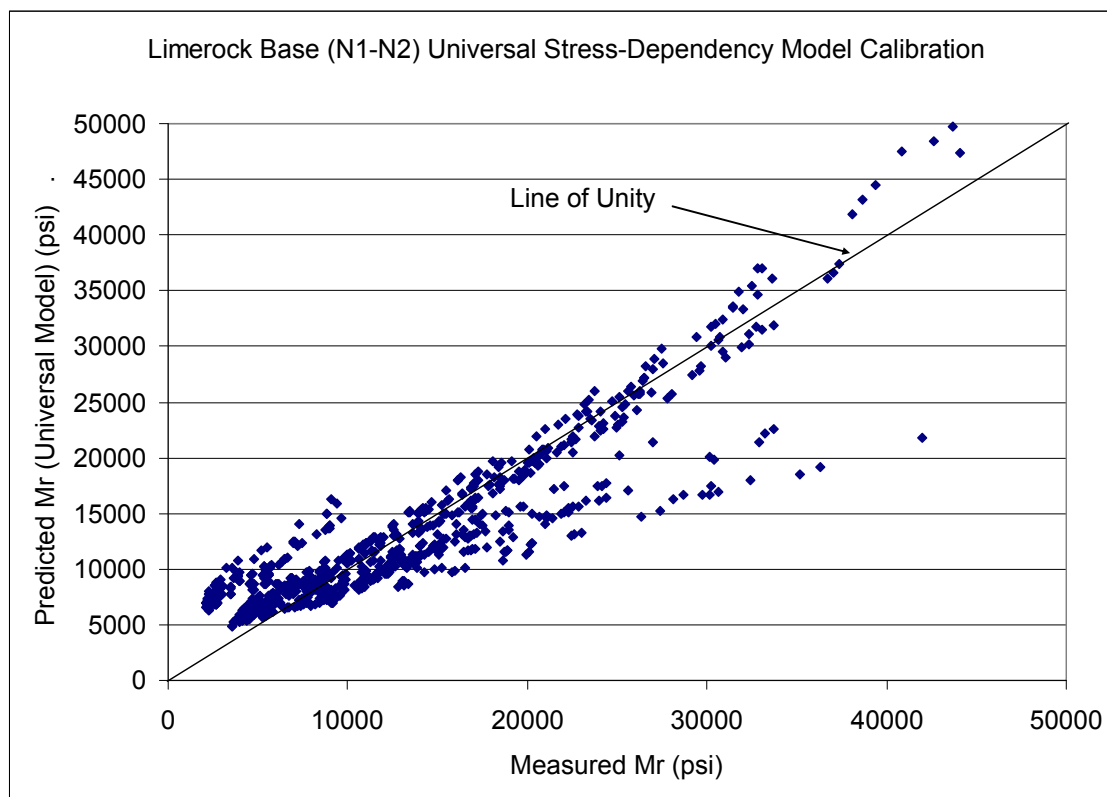


Figure 6.6. Limerock Base Material Universal Model Calibration Data (27)

Model Validation

The next phase in assessing the quality of the field-calibrated stress-sensitivity models was to evaluate the ability of the model at predicting the backcalculated moduli from a different set of deflection data. This process of model validation was performed by first compiling a database containing backcalculated layer moduli and representative stress-states (layered-elastic stresses due to load plus overburden) from four different dates of FWD testing at the Test Track. This testing was performed on all eleven structural sections over a similar wide range of pavement temperatures that were experienced during the dates of calibration testing (45 to 130°F). To validate the generated models, the appropriate stress-states generated within the various unbound materials under a given FWD load were entered into the calibrated constitutive equation for that material to generate a predicted layer modulus under that loading. This predicted modulus was then compared to the measured (or backcalculated) modulus to assess how well the calibrated equation could predict the backcalculated moduli for a different data set.

Figure 6.7 shows the validation data set for the universal stress-sensitivity model calibrated for the limerock base material (shown in Table 6.4). This data set shows a plot of measured versus model predicted backcalculated moduli using a new set of backcalculation data. The figure shows that the equation tends to over-predict modulus values that fall below approximately 5,000 to 7,000 psi. Also, the model tends to under-predict the moduli that fall above approximately 13,000 to 15,000 psi. This trend can also be seen when the residual values (the difference in measured and predicted moduli) are plotted against the measured moduli. This analysis is shown

in Figure 6.8. Even though the equation over-predicts at low modulus values and over-predicts at the higher ones, it appears that the vast majority of the data set fall within 3,000 psi of the measured value. Also, the measured moduli are on the same order of magnitude as the predicted moduli. In summary, the field-calibrated universal model for the limerock material offers reasonable, though not ideal, predicted field modulus values. For future work, perhaps a larger data set for model calibration and validation would yield a more robust model.

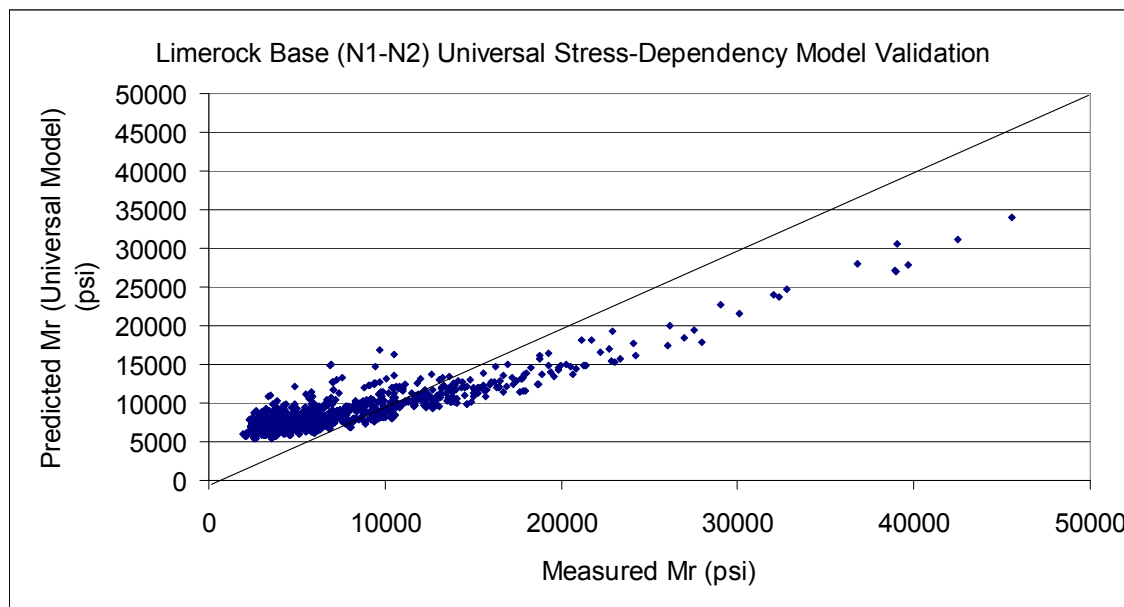


Figure 6.7. Limerock Base Universal Stress-Sensitivity Model Validation (27)

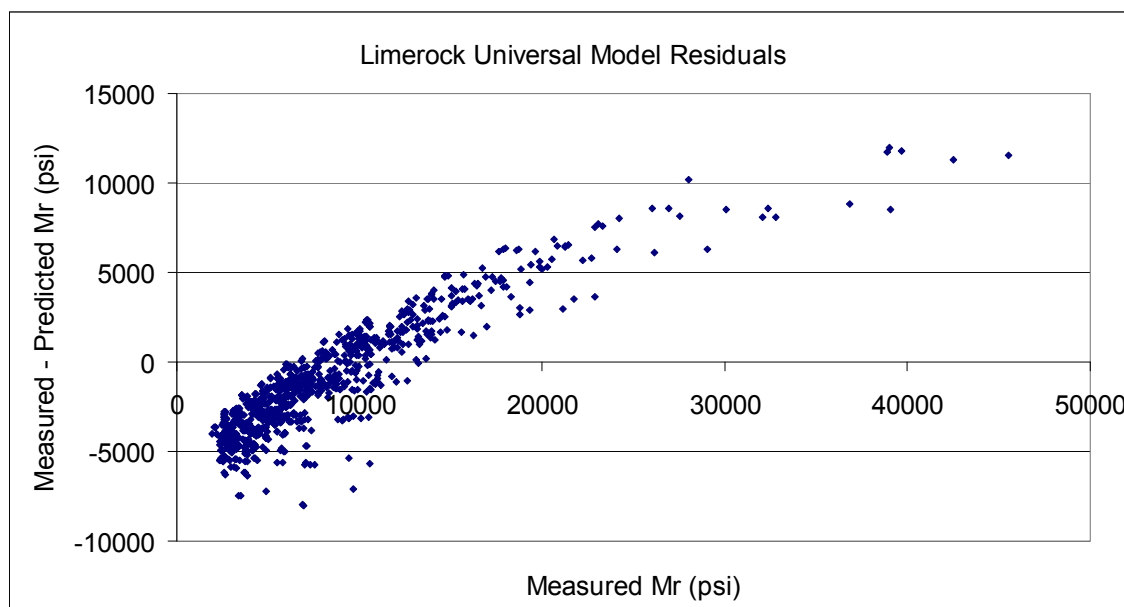


Figure 6.8. Limerock Base Universal Stress-Sensitivity Model Residuals (27)

Summary of Field-Calibrated Stress-Sensitivity Models

For sections N1 and N2, the universal stress-sensitivity model shown as Equation 8 was calibrated to model the resilient modulus behavior of the limerock base material under changing stress-conditions. This model exhibited a very high R^2 (0.83) given its calibration with deflection data taken over a wide range of testing locations and seasonal conditions. The validation of this model with a different data set yielded mixed results. While the model seemed to offer a reasonable modulus prediction for the vast majority of the data set, it would tend to over-predict modulus values below 7,000 psi and over-predict modulus values above 13,000 psi. Therefore, Equation 6-8 is reasonable for moduli in this range, but is not ideal. A more robust model would likely require a larger data set for calibration and validation.

$$M_r = 4621.71 * 14.7 * \left(\frac{\theta}{14.7} \right)^{-2.0788} * \left(\frac{\sigma_d}{14.7} \right)^{1.8908} \quad (6-8)$$

For sections N3 and N4, the universal stress-sensitivity model shown as Equation 9 was calibrated to model the resilient modulus behavior of the granite base under changing stress-conditions. Data from sections N5, N6, and N7 containing this material were not included in the calibration data set given low confidence in these backcalculated data due to large amounts of pavement surface distress in those sections. Equation 6-9 showed a reasonable model fit (R^2 slightly below 0.7) to the calibration data set. This model showed a reasonable ability to predict the backcalculated moduli from a different data set during the model validation process. However, this model exhibited similar behavior to the universal model used for the limerock material in that it tended to over-predict lower modulus values (below 3,000 psi) and under-predict higher modulus values (above 5,000 psi). Despite this, the vast majority of the data set yielded a reasonable predicted resilient modulus for this material. Again, a larger data set for model calibration and validation might generate a more robust model.

$$M_r = 10465.42 * 14.7 * \left(\frac{\theta}{14.7} \right)^{-3.0449} * \left(\frac{\sigma_d}{14.7} \right)^{2.7613} \quad (6-9)$$

The base layers that contained the Track soil material for the purposes of backcalculation did not exhibit strong stress-sensitivity with respect to resilient modulus. As such, no stress-sensitivity model could be calibrated to predict the resilient modulus of these materials in the field. For the Track soil base in sections N8 and N9, the average backcalculated modulus was 3,942 psi with a standard deviation of 1,109 psi. For the combined Type 5 base and Track fill used as the composite base layer in section N10, the average backcalculated modulus was 4,022 psi with a standard deviation of 1,745 psi. For the combined granite base and Track fill in section S11, the average backcalculated modulus was 11,835 psi with a standard deviation of 3,384 psi.

The deep Track subgrade behaved similarly to the Track soil material tested in the laboratory and in the field as a base layer in that it did not exhibit any tangible stress-sensitivity. The average backcalculated modulus for the Track soil material in sections N1 through N4, N10, and S11 was 34,755 psi with a standard deviation of 7,525 psi. This value compared well to the average Track

subgrade modulus of 32,000 generated via FWD testing during the 2003 research cycle at the Test Track (34).

In sections N8 and N9, the combined Seale and Track subgrade material exhibited tangible stress-sensitivity in the field. The universal stress-sensitivity model shown in Equation 6-10 was calibrated to predict the moduli of this layer in the field. This model was validated with another data set and offers a reasonable estimate of backcalculated moduli for this composite subgrade layer. This stress-sensitivity is likely due to this layer containing approximately 40 inches of the Seale material, which was shown to be very stress-sensitive in laboratory testing.

$$M_r = 514.96 * 14.7 * \left(\frac{\theta}{14.7} \right)^{0.7188} * \left(\frac{\sigma_d}{14.7} \right)^{-1.2255} \quad (6-10)$$

Comparison of Laboratory and Field Results

For this project, the five unbound materials were characterized in the laboratory and in the field under various stress-states and load levels. The result of the laboratory resilient modulus testing was a constitutive relationship relating resilient modulus to stress-state for each of the unbound materials. The results of the field resilient modulus testing with the FWD were constitutive equations for stress-sensitive materials and average modulus values for non stress-sensitive materials. To compare the laboratory and field-determined resilient moduli to each other, they must be compared at equivalent stress-states.

First, the stress-states (bulk, deviatoric, octahedral shear) tested in the field at the four FWD drop heights (6k, 9k, 12k, and 16k) were averaged to determine a representative field stress for that particular loading. These representative stresses were entered into both the laboratory-calibrated and field-calibrated constitutive equations to draw comparisons between the two values for a particular material type. For this comparison, the universal stress-sensitivity models were used due to their superior R^2 values generated during field calibration. Additionally, these values were plotted against the average and standard deviation of the backcalculated moduli from the various load levels. This was done to show the range of backcalculated moduli that were generated due to spatial and construction variability in the field. For this analysis, dates of FWD testing were analyzed separately. This was done to eliminate the effects of stress-sensitivity in the modulus variability at the different load levels, since different pavement temperatures will change the modulus of the asphalt and consequently alter the stress-states that are experienced by the unbound layers.

For this analysis, comparisons of the results of the laboratory and field testing were only performed for the materials in which a direct comparison could be made. Several sections required combining materials for the purposes of generating a viable backcalculation cross-section. As a result, no direct comparison could be made between the laboratory and field-determined resilient moduli for those combined layers. This was true for the combined Seale and Track subgrade layer in sections N8 and N9, the combined Type 5 and Track soil base layer for section N10, and the combined granite and Track soil base layer in section S11.

Figure 6.9 shows the laboratory versus field-determined moduli for the FWD testing date on 11/27/06 used to generate the backcalculated data for the limerock base material. Figure 6.9 shows that laboratory and field measured data seem to agree well at the lower levels for the deflection testing on 11/27/06. The laboratory predicted resilient moduli fall within one standard deviation of the average backcalculated moduli at the 6 kip and 9 kip FWD load levels. This also shows that the laboratory and field-measured moduli exhibit different behavior with respect to stress-sensitivity. The laboratory constitutive equation suggests the material to be stress-hardening while the field-calibrated constitutive equation and backcalculated moduli suggest the material is stress-softening. This is opposite of what was expected, since studies have shown unbound materials usually show the same stress-sensitivity behavior in the lab and in the field but with very different resilient moduli. This plot shows reasonable agreement between the field-calibrated constitutive equation and average backcalculated moduli at the different load levels, with the predicted moduli from the field-calibrated equation falling within one standard deviation of the average backcalculated moduli at the various load levels. These results are shown as an example of the process used to compare laboratory and field data for the base layer materials. Complete comparison results for all base layer materials are documented in Taylor (27).

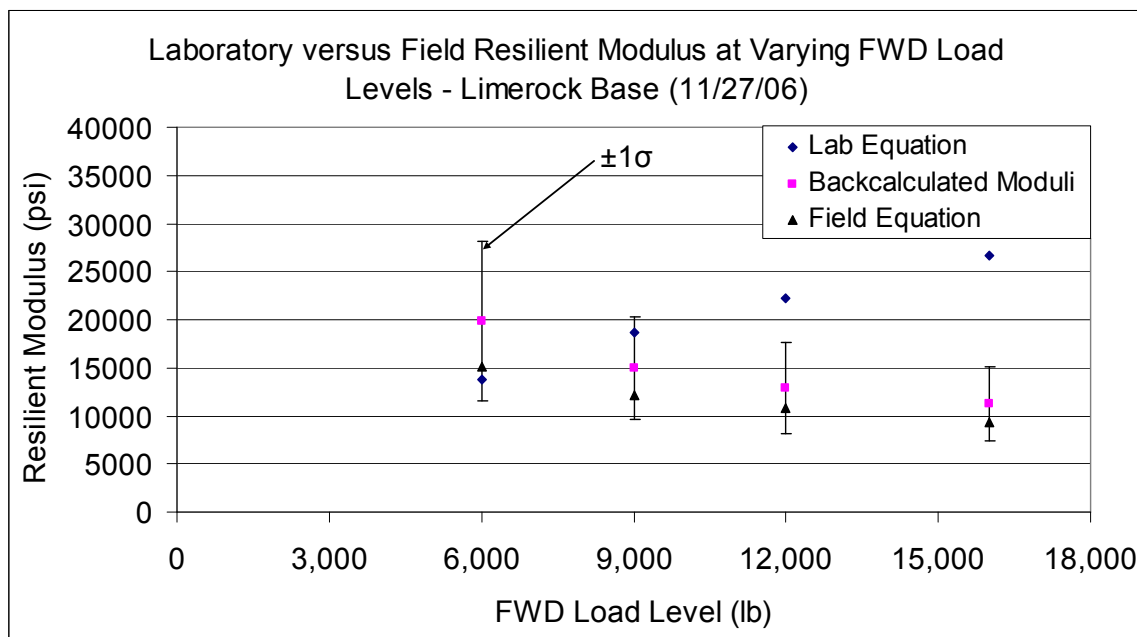


Figure 6.9. Laboratory versus Field Resilient Moduli Comparison (Limerock Base Material, FWD Testing on 11/27/06) (27)

The Track soil material was utilized as the deep subgrade material throughout the structural study at the Test Track. This material was deemed to be non stress-sensitive through both laboratory and field testing. The average laboratory modulus for this material was calculated as 28,335 psi with a standard deviation of 6,650 psi. In the field, the average modulus was calculated as 34,755 psi with a standard deviation of 7,525 psi. The average field modulus was taken from the FWD data calculated in sections N1 through N4, N10, and S11. The data from sections N5, N6, and N7 were excluded from this data given the larger amounts of pavement distress in those sections leading to lower confidence in the accuracy of the deflection data.

Sections N8 and N9 were excluded from this data set because the deep subgrade contained both the Seale and Track soil materials in this section.

A one-way ANOVA test between the two data sets showed that there was a statistical difference between the means of the two data sets (F-statistic = 58.03). Comparing the averages of the means yielded a ratio of field moduli to lab moduli of 1.23. This ratio shows good general agreement between the laboratory and field-measured behavior of the Track soil material when used as a subgrade. This was expected, since literature indicated that agreement between lab and field data tends to improve when unbound materials deeper in the pavement structure are compared (27).

Summary of Findings from Laboratory and Field Modulus Comparisons

For the unbound granular base materials for which comparisons could be drawn (the limerock base and granite base), poor agreement was seen between the moduli backcalculated in the field and a modulus predicted from a laboratory-calibrated constitutive equation over various representative stress-states. For these materials, the laboratory predicted moduli exhibited stress-hardening behavior and the backcalculated moduli exhibited stress-softening behavior. This reversal in stress-sensitivity between the two data sets was opposite of what was seen in literature. Potential reasons for this disagreement include: laboratory samples that were non-representative of the in-situ conditions (compaction, density, moisture content, etc.), inherent disagreement between the nature of the two test methods, and the existence of a very stiff subgrade at the Test Track supporting and altering the stress-sensitivity behavior of these materials in the field.

Despite the opposing trends, generally good agreement was seen between the lab and field data at the stresses representative of the lower FWD loading level (6 kip) on multiple testing dates for both the limerock and the granite base. Given the opposite stress-sensitivity, the laboratory moduli were often larger than the field moduli at the larger FWD load levels (12 kip and 16 kip). Also, the field-calibrated constitutive equation was shown to be a good predictor of the unbound material moduli for these two materials at the Test Track.

For the Track soil material, poor agreement was seen between the moduli of the field-tested base material and the laboratory tested material. The average laboratory modulus was approximately 7.2 times larger than the average backcalculated base modulus for this material. This was expected since the Track soil material for this layer was sandwiched between two much larger layers for the purposes of backcalculation and was supported by the softer Seale subgrade material. The Track subgrade compared well with the laboratory values, however. The average backcalculated Track subgrade modulus was only 23 percent larger than the average laboratory Track soil modulus. This was expected since literature indicates that agreement between laboratory and field-measured resilient moduli show better agreement in the deeper pavement layers (47; 48).

Based on the results of this comparison, it is recommended that the laboratory constitutive equation be utilized to characterize the unbound materials at the Test Track for Level 1 MEPDG design. The poor agreement between the laboratory and field resilient moduli is not necessarily an indicator of low quality lab or field data, but of inherent disagreement between the testing

method and conditions. The field-generated resilient moduli and stress-sensitivity models were shown to accurately characterize the unbound materials in-situ. However, the backcalculation data and field-generated stress-sensitivity models are site-specific to the Test Track. Additional testing at other locations containing the various unbound materials is advised to further validate the field-calibrated stress-sensitivity models.

Recommendations

This research highlighted the effective use of triaxial testing and FWD testing to give a mechanistic characterization of the different unbound pavement materials utilized at the Test Track. The laboratory testing gives a quality representation of the stress-sensitivity of the resilient moduli for each of these materials. Characterization of the materials in this manner is sufficient for obtaining a good representation of the unbound material behavior for Level 1 mechanistic pavement design using the new MEPDG. A quality FWD testing program that encompasses the seasonal and spatial variability of the pavement and tests the pavement at multiple critical load levels can also be used to develop a constitutive relationship for the in-situ unbound material moduli. The equations calibrated for this study are site-specific to the Test Track, and should be validated through comparison of moduli to additional pavement structures that contain the given unbound materials, but have varying structural compositions and thicknesses.

The results of this study showed the following:

- Either the MEPDG model or the universal model provide the best fit to laboratory resilient modulus data, and the universal model provided the best model fit to backcalculated resilient moduli. Therefore, the multi-variable constitutive models are recommended over the single-variable models given the results of this study.
- It is recommended that the laboratory-calibrated multi-variable stress-sensitivity equations provide the best means of characterizing the unbound materials used at the Test Track for Level 1 MEPDG design. However, the FWD testing program at the Test Track provides a good quantification of the seasonal and spatial variability inherent to these materials in the field and should be used to account for field variability in the pavement design process.

E* LABORATORY AND MODEL COMPARISONS

There are three levels of design that engineers can choose from when using the MEPDG for flexible pavement design (49). One significant difference in the three levels of design is how the dynamic modulus, E^* , of HMA is computed and therefore the degree of complexity required for material property inputs. Level one is the most complex degree of design, requiring laboratory test results for both E^* and dynamic shear modulus of the binder, G_b^* . However, dynamic modulus laboratory testing is time consuming and expensive. Therefore, many highway agencies will opt to use levels two and three for most pavement designs since these levels do not require such testing. The required material property inputs for levels two and three are simple parameters typically determined for specification requirements. Level two, the second most complex design, utilizes either the 1-37A or the 1-40D Witczak Predictive E^* equation (at the discretion of the user) as a function of binder information, gradation information, and other volumetric information. Level three, the least complex of the three designs also utilizes either the 1-40D or the 1-37A Witczak Predictive E^* equation, however laboratory binder test results are not required.

Due to the challenges to perform laboratory dynamic modulus tests, there is a need to validate the MEPDG's procedure in calculating E^* at the two lowest levels of design. To evaluate the accuracy of these two designs, three E^* predictive equations were analyzed and compared with E^* laboratory test results. To do so, E^* testing was completed on the materials comprising sections constructed in the 2006 Test Track structural study.

Objectives and Scope

The objectives of this study were to evaluate the three E^* predictive models: the Witczak 1-37A model, the Witczak 1-40D model, and the Hirsch model. Findings from this study should help pavement engineers to accurately estimate E^* .

To meet the objectives of this study, laboratory testing was completed using AASHTO TP 62-07 (49) as a guideline to determine the dynamic modulus of ten different HMA mixtures from the 2006 NCAT Test Track Structural Study. These mixtures represented typical mixtures used on state highways in Alabama, Florida, Missouri and Oklahoma. AASHTO T315-06 (49) was followed to determine the binder complex shear modulus, G_b^* . Also, binder viscosities were obtained following the ASTM D2983-04a (50) for eight binders.

Models to Determine E^*

As part of the NCHRP 1-37A project, a predictive model for E^* was developed utilizing rudimentary mix information including basic binder test results to be included in the MEPDG (51). An initial model was developed in 1996 by Witczak and Fonseca, however it was quickly updated, expanding the dataset and re-calibrating the model. This model, updated by Witczak and Andrei, was implemented for use in the MEPDG levels two and three in 1999 (51). This model will be referred to as the Witczak 1-37A E^* predictive equation. In 2005, another equation was developed by Witczak and others under the NCHRP 1-40D initiative (52). This equation, referred herein as the Witczak 1-40D E^* predictive equation, was implemented into the MEPDG version 1.0 allowing the user to select between the 1-37A and 1-40D equation for use in level

two and three design. However, a note to users explains that the 1-40D equation has not yet been nationally calibrated.

In addition to the Witczak equations, another model recently cited by a number of researchers is the Hirsch E* predictive model (53), developed in 2003. The Witczak 1-37A, the Witczak 1-40D and the Hirsch E* predictive models were analyzed in this research.

The information required for each model is tabulated in Table 6.5. As mentioned previously, the level of complexity of the material property inputs varies among the three models. Two of the three require G_b* testing, while only one requires the phase angle associated with G_b*. It is worthy of noting that the while both Witczak models incorporate the gradation of the mix, the Hirsch model does not. In fact, the Hirsch model relies only on three properties of the mix.

Table 6.5. Material Property Requirements by Model

Parameter	Witczak (1-37A)	Witczak (1-40D)	Hirsch
Gradation:			
P ₂₀₀ Pass.	X	X	
P ₄ retained	X	X	
P ₃₈ retained	X	X	
P ₃₄ retained	X	X	
VMA			X
V _a	X	X	
VFA			X
V _{beff}	X	X	
F	X		
η	X		
G _b *		X	X
δ _b		X	

Witczak 1-37A E* Predictive Equation

The original Witczak model was developed in 1996 by Dr. Witczak and his colleagues using 149 unaged HMA mixtures (51). The binder types utilized in the mixtures were conventional binders only, which severely limits the use of this model. This equation was revised in 1999, by expanding the dataset and deriving an equation that more accurately fit a wider range of gradations, binder stiffness and air voids (53). The revised equation, the Witczak 1-37A E* predictive equation (51), listed in Equation 6-11, and is a function of gradation of the aggregate, air voids, effective binder content, viscosity of the binder, and loading frequency:

$$\log E^* = -1.25 + 0.029\rho_{200} - 0.0018(\rho_{200})^2 - 0.0028\rho_4 - 0.058V_a - 0.0822 \frac{V_{beff}}{V_{beff} + V_a} + \frac{3.872 - 0.0021\rho_4 + 0.004\rho_{38} - 0.000017(\rho_{38})^2 + 0.0055\rho_{34}}{1 + e^{(-0.603313 - 0.313351\log(f) - 0.393532\log(\eta))}} \quad (6-11)$$

where:

- E^* = dynamic modulus of mix, 10^5 psi
- η = viscosity of binder, 10^6 poise
- f = loading frequency, Hz
- ρ_{200} = % passing #200 sieve
- ρ_4 = cumulative % retained on #4 sieve
- ρ_{38} = cumulative % retained on 3/8 in. sieve
- ρ_{34} = cumulative % retained on 3/4 in. sieve
- V_a = air voids, % by volume
- V_{beff} = effective binder content

$$\eta = \frac{|G_b^*|}{10} \left(\frac{1}{\sin \delta_b} \right)^{4.8628} \quad (6-12)$$

where:

- G_b^* = dynamic shear modulus of binder, psi
- δ_b = phase angle of G_b^* , degrees

Equation 6-11 is currently used for a level two design in the MEPDG (49). It is also employed for the level three design with the use of typical viscosity values of the binder based on the binder grading (49). The viscosity can be determined by conventional binder tests or from a dynamic shear modulus (G_b^*) test. When using the G_b^* to determine viscosity, G_b^* and its associated phase angle must be measured at a variety of temperatures for a loading frequency of 1.59 Hz or 10 rad/sec, from which Equation 6-12 is employed to calculate viscosity (49). The loading frequency for G_b^* testing should not be confused with the loading frequencies required for the 1-37A model, as the loading frequencies selected for the model are typical of an E^* laboratory test (0.1, 1, 10, 25Hz, etc.). Viscosity can also be estimated from conventional binder tests. However some methods require a conversion to achieve a viscosity in Poises.

Witczak 1-40D E^* Predictive Equation

The Witczak 1-37A E^* predictive model was revised in 2006, again expanding the dataset used to develop the original model, using a total of 346 HMA mixes to calibrate the model (51). One important difference to note between the 1-37A E^* predictive model and the 1-40D E^* predictive model is the replacement of the viscosity and loading frequency parameters with the complex shear modulus of the binder, G_b^* , and its associated phase angle, δ_b , as shown in Equation 6-13:

$$\log E^* = -0.349 + 0.754 \left(|G_b^*|^{-0.0052} \right) \times \left(\begin{array}{l} 6.65 - 0.032\rho_{200} + 0.0027(\rho_{200})^2 + 0.011\rho_4 \\ - 0.0001(\rho_4)^2 + 0.006\rho_{38} - 0.00014(\rho_{38})^2 \\ - 0.08V_a - 1.06 \left(\frac{V_{beff}}{V_a + V_{beff}} \right) \end{array} \right) + \frac{2.56 + 0.03V_a + 0.71 \left(\frac{V_{beff}}{V_a + V_{beff}} \right) + 0.012\rho_{38} - 0.0001(\rho_{38})^2 - 0.01\rho_{34}}{1 + e^{(-0.7814 - 0.5785 \log |G_b^*| + 0.8834 \log \delta_b)}} \quad (6-13)$$

where:

- E^* = dynamic modulus of mix, psi
- $|G_b^*|$ = complex shear modulus of binder, psi
- ρ_{200} = % passing #200 sieve
- ρ_4 = cumulative % retained on #4 sieve
- ρ_{38} = cumulative % retained on 3/8 in. sieve
- ρ_{34} = cumulative % retained on 3/4 in. sieve
- V_a = air voids, % by volume
- V_{beff} = effective binder content
- δ_b = phase angle of binder associated with $|G_b^*|$, degrees

This equation, referred herein as the Witczak 1-40D E^* predictive equation, was implemented in the MEPDG for use in level two and three design. As mentioned previously, the user as the option of selecting the 1-37A or the 1-40D model for design. At a level three design typical G_b^* and δ_b values are estimated within the program depending on the selected grade of the binder. Although the loading frequency parameter has been omitted in the new model, the time and temperature dependency of dynamic modulus is characterized by G_b^* and δ_b .

Hirsch E^* Predictive Model

The Hirsch E^* predictive equation is similar to the Witczak equations in that it also utilizes volumetric information and G_b^* laboratory test results. However, this model requires only two volumetric properties: voids in mineral aggregate (VMA) and VFA. The Hirsch E^* model was developed based on the law of mixtures, also referred to as the Hirsch model, for composite materials (54). The Hirsch E^* predictive equation for asphalt mixtures, as developed by Christensen and his colleagues is:

$$|E^*|_{mix} = Pc \left[4,200,000 \left(1 - \frac{VMA}{100} \right) + 3|G^*|_b \left(\frac{VFA \times VMA}{10,000} \right) \right] + (1 - Pc) \left[\frac{1 - (VMA/100)}{4,200,000} + \frac{VMA}{3VFA|G^*|_b} \right]^{-1}$$

where:

$$Pc = \frac{\left(20 + \frac{VFA \times 3|G^*|_b}{VMA} \right)^{0.58}}{650 + \left(\frac{VFA \times 3|G^*|_b}{VMA} \right)^{0.58}}$$

(6-14)

where:

- $|E^*|_{mix}$ = dynamic modulus, psi
- VMA = voids in mineral aggregate, %
- VFA = voids in aggregate filled with mastic, %
- VFA = $100 \times (VMA - V_a) / VMA$
- V_a = air voids, %
- $|G^*|_b$ = complex shear modulus of binder, psi

Just as in the 1-40D model, the time and temperature dependency of E^* is characterized in the Hirsch E^* predictive model by G_b^* . According to Christensen, the G_b^* “should be at the same temperature and loading time selected for the mixture modulus, and in consistent units (54).” For this evaluation, it was assumed that the frequency-time relationship is consistent for both G_b^* and E^* tests such that a selected frequency applies the load for the same time in either test. Therefore, the loading frequencies and temperatures selected associated with G_b^* were the same as those from the measured E^* values, which enabled a direct comparison of predicted to measured E^* values.

Testing Protocol

To complete the dynamic modulus testing for each unique mix listed, the testing protocol outlined by AASHTO TP 62-07 was followed (49). An AMPT, shown in Figure 6.11, was utilized to apply haversine compressive loading for a range of frequencies and temperatures. For this investigation E^* results at three temperatures, 40, 70, and 100°F and seven frequencies, 0.5, 1, 2, 5, 10, 20, and 25 Hz were obtained.



Figure 6.11. The AMPT Machine and Close Up of Specimen

Viscosity was obtained for various binders using the Brookfield Viscometer following ASTM D2983-04a (50). The binders were aged in a Rolling Thin-Film Oven (RTFO) and viscosities were obtained at two temperatures, 135 and 165°C. After the test temperatures were converted to °Rankine, Equation 6-15 was utilized to extrapolate viscosity for the temperatures (40, 70, and 100°F) at which E* testing was completed.

$$\log \log \eta = A + VTS \log T_R \quad (6-15)$$

where:

- η = viscosity of binder, centipoise (cP)
- A, VTS = regression parameters
- T_R = temperature, °Rankine

Complex shear modulus, G_b^* , testing, in accordance with AASHTO T 315-06 (49), was also conducted on RTFO aged binders using a Dynamic Shear Rheometer (DSR). Although testing was conducted at four temperatures, 4, 21, 37.8, and 54.4°C (40, 70, 100, and 130°F), results at 40°F were inconsistent and unreliable and thus excluded from the analysis. A frequency sweep, in which thirteen frequencies (0.1, 0.2, 0.3, 0.4, 0.6, 1.0, 1.6, 2.5, 4.0, 6.3, 10.0, 15.9, and 25 Hz) were applied, was completed at each of the four temperatures.

Mixtures Tested

E* laboratory testing was completed for the mixes in each section constructed in 2006 as part of the 2006 Test Track structural study. The mixes investigated are described in Table 6.6, listed by the section and layer in which it was placed. Four different mix types were incorporated in the investigation including Superpave mixes (super), SMA mixes, rich bottom layers (RBL) and a typical mix design used by the Oklahoma E* laboratory testing was completed for the mixes in

each section constructed in 2006 as part of the 2006 Test Track structural study. The mixes investigated are described in Table 6.6, listed by the section and layer in which it was placed. Four different mix types were incorporated in the investigation including Superpave mixes (Super), stone matrix asphalt mixes (SMA), rich bottom layers (RBL) and a typical mix design used by the Oklahoma DOT, designated by “S3.” Each mixture is described by a unique mix number and unique binder number. The gradation information acquired from as-built records, as well as the NMAS and gradation type (coarse/fine) for each mix number is listed in Table 3. As shown in Table 6-6, a total of ten unique mixes were evaluated, however, some unique mixes were used in multiple layers. Associated with a unique binder number is the PG grade, viscosity, and G^* test results (including phase angle values, δ_b). An example is provided in Table 6.7. The other input values are documented elsewhere (55). A total of nine binders were used in the HMA layers investigated, and similar to the unique mix number, some unique binders were used in multiple layers.

Viscosity values were not obtained for unique binder #4, which was used only in mix #7. From these data, the dynamic moduli of the mixes, except mix #7, were predicted for the 1-37A E^* predictive model at three temperatures and seven loading frequencies. G_b^* and δ_b values were obtained at multiple temperatures and frequencies. However, to compare laboratory measured E^* values with E^* predictions from either the Hirsch or 1-40D E^* predictive models, the loading frequencies and test temperatures for G_b^* must equal to those used in the E^* laboratory test. As a result, the 1-40D and Hirsch E^* predictive models were evaluated at two temperatures, 70 and 100°F, and three frequencies, 1, 10, and 25 Hz.

Results and Discussion

In following Equation 6-11 to evaluate the Witczak 1-37A E^* model, 651 data points were produced. The values were plotted against the laboratory measured E^* values (Figure 6.12). For the Witczak 1-40D and Hirsch E^* models, 180 data points were evaluated for each and also plotted against measured E^* values. Ideally, all points would fall along the line of equality, but this clearly is not the case. Upon visual inspection, it can be concluded that overall the 1-40D E^* model consistently lies above this line, indicating a consistent overprediction of the measured values. While there is a large amount of scatter in the data, the 1-37A E^* model generally follows the line of equality, with data points both above and below this line. Similarly, the Hirsch E^* model also generally follows the line of equality, although there is much less scatter in these data.

Fitting a linear regression equation indicates how precisely the modeled values are linearly related to the measured values. Some researchers (51; 53) use the coefficient of determination, R^2 , from as an indication of the quality of the relationship. Inset in Figure 2 are the sample sizes, linear regression equation and associated coefficient of determination in log scale for each model evaluated. All three models produced predictions that were fairly correlated to the measured values by a linear relationship. Overall, these values may be slightly skewed due to the gross overprediction of one mixture. The measured values for this mix are concerning as they are relatively low, on the order of 10,000+ psi, which could be an indication of an error in that particular test. It could also be an indication of bias in all three models. The Hirsch E^* model produced the highest R^2 value, 0.707, while the Witczak 1-40D produced the lowest, 0.573 in log

scale. This is contrary to previous findings in which the 1-40D model was found to be an improvement over both the Hirsch and 1-37A model (51; 53).

Table 6.6. HMA Mixes by Section and Layer

Section	Layer	Sponsor	Mix Type	Binder	Unique Binder #	Unique Mix #
N1	1	FL	Super	67-22	1	1
N1	2	FL	Super	67-22	1	1
N1	3	FL	Super	67-22	14	2
N2	1	FL	Super	76-22	2A	3
N2	2	FL	Super	76-22	2A	3
N2	3	FL	Super	67-22	14	2
N8	1	OK	SMA	76-28	3	4
N8	2	OK	S3	76-28	3	5
N8	3	OK	S3	64-22	4A	6
N8	4	OK	RBL	64-22	4	7
N9	1	OK	SMA	76-28	3	4
N9	2	OK	S3	76-28	3	5
N9	3	OK	S3	64-22	4A	6
N9	4	OK	S3	64-22	4A	6
N9	5	OK	RBL	64-22	4	7
N10	1	MO	Super	70-22	5	8A
N10	3	MO	Super	64-22	6	9
S11	1	AL	Super	76-22	13	28A
S11	3	AL	Super	67-22	14	2
S11	4	AL	Super	67-22	14	2

Table 6.7. Gradation Information by Mix #

Unique Mix #	Unique Binder #	ρ200 % passing	ρ4 % retained	ρ38 % retained	ρ34 % retained	VMA (Avg)	NMAS (mm)	Graded
1	1	8.79	39.61	16.44	0.00	14.17	12.5	Fine
2	14	5.48	45.82	25.19	4.47	15.41	19	Fine
3	2A	8.10	38.61	16.62	0.00	14.22	12.5	Fine
4	3	10.71	68.55	28.62	0.00	15.57	12.5	Coarse
5	3	6.90	34.80	19.53	4.71	10.46	19	Fine
6	4A	6.90	36.31	21.13	5.48	10.69	19	Fine
7	4	10.51	39.93	13.68	0.00	12.44	12.5	Coarse
9	6	6.28	51.79	25.60	1.81	14.17	19	Fine
8A	5	5.40	47.71	16.83	0.79	16.92	12.5	Coarse
28A	13	8.59	13.98	0.10	0.00	18.05	9.5	Fine

However, the coefficient of determination is a measure of how precisely the linear regression equation matches the data. For the model to be accurate, the linear regression equation should be as close to $y = x$ as possible, therefore the slope and intercepts of the regression equations should also be investigated. Table 6.8 lists the linear regression coefficients and goodness of fit in arithmetic scale for each of the models.

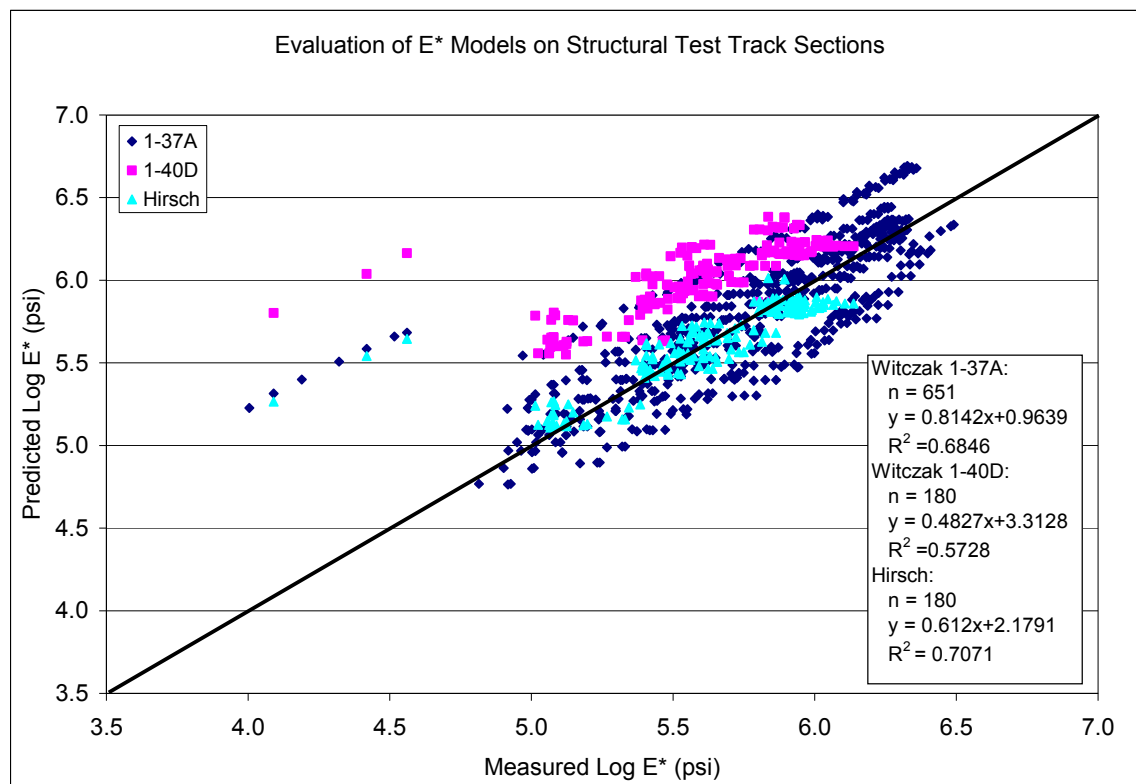


Figure 6.12. Comparison of Predicted E* Values to Measured E* Values by Model

Table 6.8. Linear Regression Coefficients for Each Model

Model	Slope	Intercept (psi)	R ²
Witczak 1-37A	1.1222	56,263	0.5945
Hirsch	0.6354	144,315	0.766
Witczak 1-40D	1.2748	515,267	0.5996

According to these lines of best fit, the Witczak 1-37A has the smallest difference in slopes from the line of equality, deviating above the line by only 12.22%. Additionally, the y-intercept is the smallest of the three models. However, indicated by the R² and Figure 6-12, the 1-37A E* model does not consistently predict the measured values accurately. The Hirsch model is more consistent than the Witczak 1-40D model, however, the slope for the Hirsch model deviates from unity the most. In looking at Figure 6-12, the data for both the Hirsch and 1-40D models appear to flatten out at intermediate measured moduli values (700,000-1,400,000 psi). Given that both of these models follow this trend and utilize G_b^{*}, such inconsistencies could be related to the use of G_b^{*} values, whether it be inherent to the model or G_b^{*} test results. This range of measured E* is consistent with values predicted from G_b^{*} test results at 70°F. This trend is contrary to the time-dependency of HMA, such that increases in the frequency should result in higher E* values. When the data are plotted in arithmetic scale, the flattening out of the data at higher moduli values is more predominant in the Hirsch model than the 1-40D model, which may explain the large deviation in slope from the line of equality. In general, it appears that the Hirsch E* model predicts the measured values most accurately and precisely for low dynamic moduli (100,000-500,000 psi). Consistent with previous research (56), the 1-40D E* model grossly over predicts

dynamic modulus at low values or high temperatures and/or low frequencies. The Witzak 1-40D E* model, is only slightly more precise than the 1-37A E* model.

Summary

Three E* predictive models were evaluated for asphalt mixtures from the southeastern U.S. The dynamic moduli of ten different mixtures from the 2006 Test Track were measured in the laboratory and compared with moduli predicted by the 1-37A, 1-40-D, and Hirsch E* predictive models. Following the Witzak 1-37A E* model, E* was estimated for three temperatures (40, 70, and 100°F) and seven frequencies (0.1, 1, 2, 5, 10, 20, and 25 Hz). E* was also estimated using the Witzak 1-40D and Hirsch E* predictive models for two temperatures (70, and 100°F) and three frequencies (1, 10, 25 Hz). The findings from these comparisons are summarized below:

- The Witzak 1-37A E* model was found to be unreliable with a large amount of scatter.
- The Hirsch E* model was found to be the most precise model, with the highest coefficient of determination, 0.707 in log scale and 0.766 in arithmetic scale.
- The Witzak 1-40D E* model consistently overpredicted E* particularly for low dynamic moduli.
- The Hirsch E* model is most accurate at low dynamic moduli values (100,000-700,000 psi).
- At an intermediate test temperature (70°F), both the Witzak 1-40D E* and Hirsch E* models flatten out, thus misrepresenting the time-dependency of E*.

In the current version of the MEPDG, Witzak E* predictive equations 1-40D and 1-37A, are employed to determine dynamic modulus given volumetric, gradation and binder properties of a mixtures. In applying these models to ten mixtures included in the 2006 Test Track structural study, neither model consistently estimated laboratory dynamic moduli values to a high degree of accuracy. Because both the 1-37A and 1-40D models were found to be unreliable and the 1-40D model largely overpredicts dynamic modulus, it is recommended that the Hirsch E* model be used. It should be used with caution however, as discrepancies at lower temperatures and/or higher frequencies were reported.

LABORATORY FATIGUE THRESHOLDS AND FIELD-MEASURED STRAINS

Laboratory work has been conducted to validate fatigue thresholds for perpetual pavements; however, little has been published to relate these laboratory values to what is experienced in the field. Are there pavement structures that have shown superior performance while undergoing strains greater than the proposed laboratory-based limits? Have field pavements exhibited pavement responses smaller than the proposed strain limit and failed prematurely? Currently, field thresholds for fatigue cracking are only conservative estimates based upon laboratory work. It is possible the field thresholds for fatigue cracking will be higher than those seen in laboratory work. If this is the case, engineers are overdesigning their pavements. This analysis compares the strain distributions developed from the previously mentioned methodologies (Chapter 5) to laboratory fatigue endurance limits tested under the National Cooperative Highway Research Program (NCHRP) Project 9-38.

Laboratory Testing

As part of NCHRP Project 9-38, laboratory fatigue tests were conducted on the base mixes from the structural sections at the 2003 NCAT Test Track. Beam fatigue specimens were fabricated using the average gradation and asphalt contents of the 19.0 mm mixes. As previously seen in Chapter 4, two different mixes were used as the base HMA layers in the first seven sections of the 2003 experiment. Therefore, only two mixes were tested to characterize all seven test sections. The tests used samples compacted to 7% air voids. The detailed methodologies used for the testing are documented elsewhere (57). The fatigue endurance limits and their 95% lower bound confidence limits are presented in Table 6.9. These results were extrapolated from laboratory testing using a Three-Stage Weibull equation (57).

Table 6.9. Fatigue Endurance Limits for 2003 Test Sections (29)

Section	Average Extrapolated Beam Fatigue, $\mu\epsilon$	95% Confidence Lower Bound, $\mu\epsilon$
N1	220	146
N2	172	151
N3	172	151
N4	220	146
N5	220	146
N6	172	151
N7	172	151

Laboratory Testing and Field Data Comparisons

The purpose of this analysis was to determine if a relationship existed between the laboratory fatigue endurance limits determined under NCHRP 9-38 and the cumulative strain distributions developed in the previous chapters. This was accomplished using three phases of data comparisons.

The first phase was conducted by comparing the endurance limit to a strain calculated using the strain-temperature equations developed in Chapters 5. The comparison temperature was the prescribed testing temperature for AASHTO T321.

The second phase compared the magnitude of the laboratory fatigue threshold data to measured field strain distributions. The 95th percentile confidence interval lower bound strain was graphically inserted onto a cumulative distribution plot to determine where this value fell on each section's cumulative strain distribution, and that value was compared to the section's fatigue performance.

The final analysis comparison of the laboratory fatigue thresholds and the developed strain distributions was conducted by comparing the 95th percentile confidence interval lower bound to the entire strain distribution. A fatigue ratio, between the measured strain values and laboratory-established threshold, was developed to make this comparison.

The 95% confidence interval lower bound was chosen to be the basis of comparison between the laboratory fatigue and field strain data. $220 \mu\epsilon$, the predicted beam fatigue value for the PG 76-22 binder mix, was more than double the previously listed fatigue limits in mixes. This value might be due to a high reading or an erroneous test; therefore, it was felt that using the 95% confidence lower bound was more appropriate for comparisons. The 95% confidence interval lower bound also brought the inclusion of mix variability to the analysis; therefore, it proved to be a more conservative estimate of the fatigue threshold.

Phase One – Comparison of Fatigue Threshold to Modeled Strain Levels

The laboratory beam fatigue tests were conducted at 20°C (68°F). Comparative inquiries were conducted to calculate the estimated strains at the test temperature for both the 2003 and 2006 Test Tracks using the strain-temperature relationships previously developed and discussed in Chapter 5. These strains are presented in Table 6.10.

When analyzing the 2003 Test Track estimated strain relationships, one would see that at 20°C , five of the six section's average box trailer produced a microstrain magnitude below its lower confidence limit fatigue threshold. However, when the heavier triple trailers were used, six of the seven test sections were above the 95th percentile threshold strain. While two of the 2003 test sections did not fail in fatigue, one of these two sections had a strain magnitude larger than its fatigue threshold limit at the associated test temperature.

While fatigue testing has not been conducted on the base HMA layers of the 2006 Test Track at this time, if one were to assume similar lower bounds for the fatigue thresholds (i.e. 150 microstrain) for these sections, a similar trend would be seen. Only two sections (N10 and S11) experienced higher strains than the lower bound fatigue limit under the steer axle. The three sections that did not crack were at least 60 microstrain below this value for their steer axles. However, when analyzing the 40 kip tandem axle at the test temperature, the only sections still below the estimated lower bound fatigue endurance limit were the three sections that did not crack.

A final look at the single axles for the 2006 Test Track shows seven of the eight sections measuring strains higher than the lower bound fatigue endurance limit. The only section measuring strain amplitudes below this value is section N9 which was 14 inches thick. To understand this phenomenon, one would only have to look back to the strain-temperature relationships developed for this section. Both the k_1 and k_2 values were small compared to the other sections. This showed that section N9, unlike many of the others, did not experience as much strain variation due to temperature.

Table 6.10. Strains at 20 C Estimated from Field Measurements (29)

	Strain at 20°C		
Section (Year)	Box, $\mu\epsilon$	Triple, $\mu\epsilon$	
N1 (2003)	NA	363	
N2 (2003)	142	231	
N3 (2003)	103	153	
N4 (2003)	87	140	
N5 (2003)	99	172	
N6 (2003)	165	210	
N7 (2003)	111	159	
	Steer, $\mu\epsilon$	Tandem, $\mu\epsilon$	Single, $\mu\epsilon$
N1 (2006)	137	195	221
N2 (2006)	148	203	228
N3 (2006)	90	147	175
N4 (2006)	81	137	163
N8 (2006)	135	173	185
N9 (2006)	46	69	82
N10 (2006)	186	233	279
S11 (2006)	181	265	294

Phase One - Analysis Results

No clear relationship could be developed between the 95th percentile confidence interval lower bound, the computed strain at 20°C, and pavement performance. There was a case where a test section (N3 2003) did not exhibit fatigue cracking; however, its average strain for the triple trailer at laboratory testing temperature was above the designated fatigue threshold. Similar results were seen for the tandem and single axles of N1 and N2 in 2006. Further investigations needed to be conducted to develop the link between laboratory fatigue thresholds, measured field strains, and pavement performance.

Phase Two – Location of Fatigue Thresholds on Cumulative Distribution Plots

Another method for comparing the laboratory fatigue thresholds to the previously developed strain data was to superimpose the 95th percentile confidence interval lower bound strain onto each section’s cumulative strain distribution. The cumulative distributions and fatigue threshold for the PG 67-22 mix are shown in Figure 6.13 while Figure 6.14 shows the data for the PG 76-22 mixes.

When comparing the 2003 strain distributions with their lower bound fatigue limit, it was difficult to find a relationship between the laboratory and field data using this methodology. As can be seen, there is no clear correlation between the lab fatigue threshold, where this threshold occurs on the strain distribution, and the section’s performance.

For example, Section N4 in 2003 had 40% of its strains below the given laboratory fatigue threshold, and it performed well in the field. Conversely, section N2 had 45% of its strains below the laboratory fatigue threshold, but it failed quickly due to fatigue cracking.

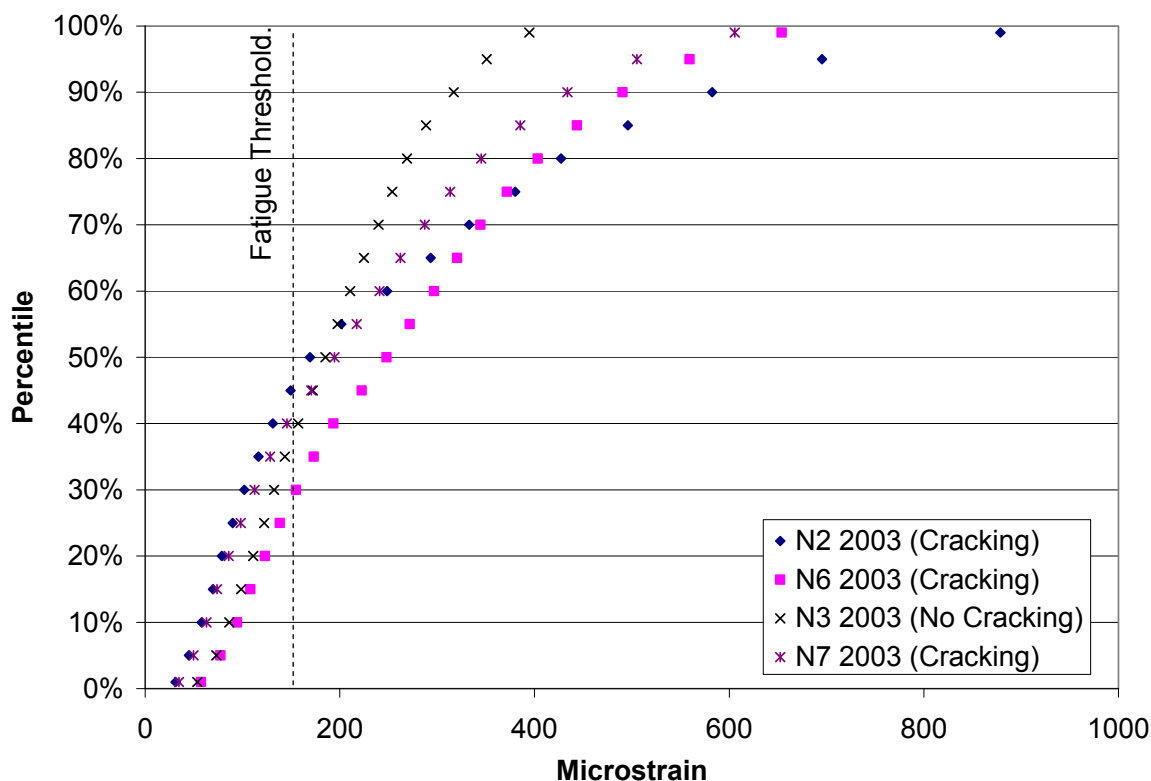


Figure 6.13. Endurance Limits for PG 67-22 Mix (29)

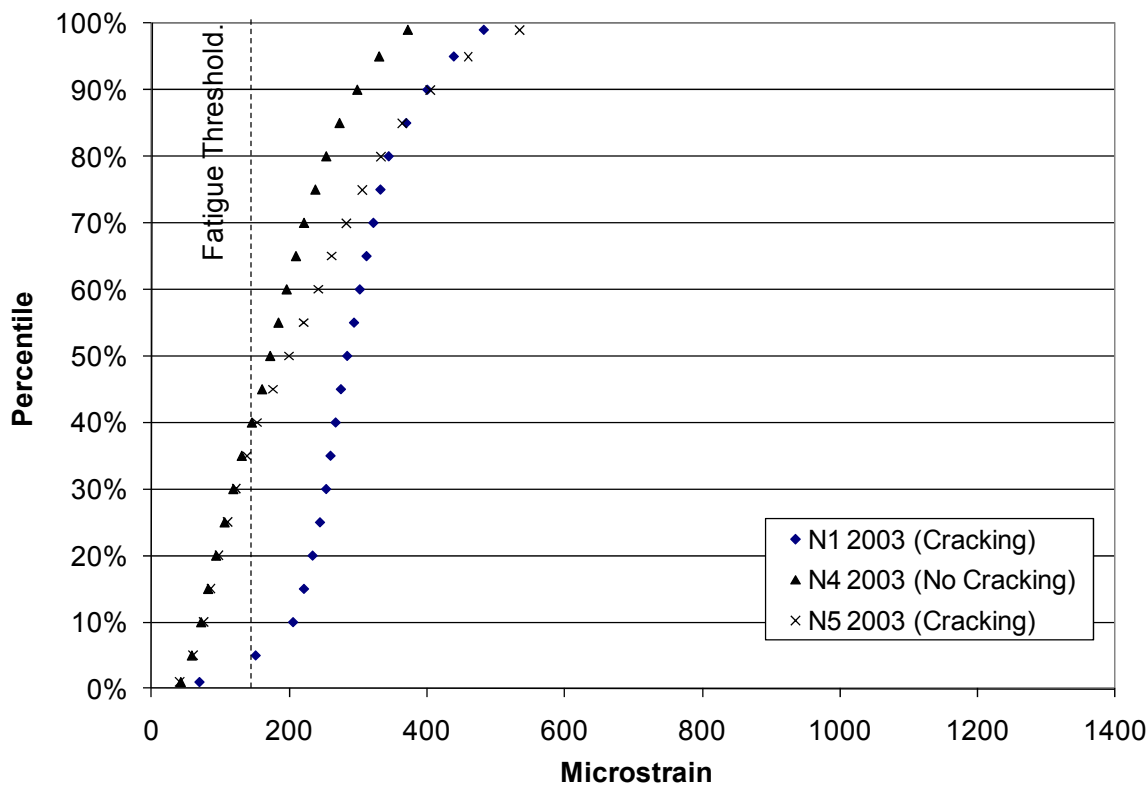


Figure 6.14. Endurance Limits for PG 76-22 Mix (29)

Both base HMA mixes for the 2003 Test Track had similar fatigue properties (i.e. fatigue thresholds near 150 $\mu\epsilon$). Since fatigue data had not been developed from the 2006 Test Track’s base mixes, it was assumed that these mixes had similar fatigue properties for continuation of the analysis. Figure 6.15 displays these data.

The 2006 data finds similar discontinuities between the field and laboratory using this methodology. N2 experienced no fatigue cracking; however, it had fewer strains measured below its fatigue threshold than did section N8 which experienced fatigue distress.

Phase Two – Analysis Results

The goal of this analysis was to determine if a relationship existed between the laboratory fatigue thresholds, the measured strain data, and pavement performance. In order to correlate these three parameters together for comparison across the analyzed test sections, Table 6.11 was developed.

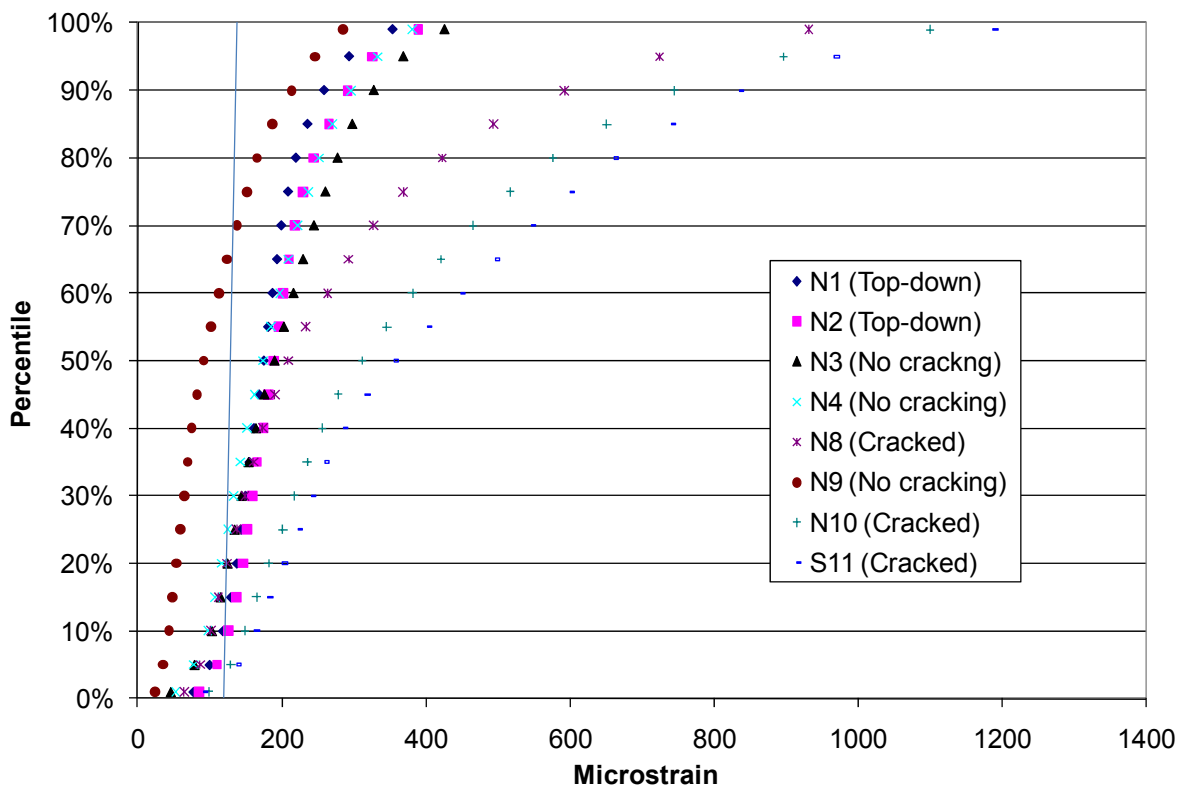


Figure 6.15. Endurance Limits for 2006 Test Sections (29)

Table 6.11. Comparison of Cumulative Strain Distribution and 95% Confidence Interval Lower Bound (29)

Section	Percentile of Fatigue Threshold	Performance
N1 2003	8 th	Cracked
N2 2003	45 th	Cracked
N3 2003	57 th	No cracking
N4 2003	40 th	No cracking
N5 2003	37 th	Cracked
N6 2003	29 th	Cracked
N7 2003	42 nd	Cracked
N1 2006	31 st	Top-down cracking
N2 2006	22 nd	Top-down cracking
N3 2006	33 rd	No cracking
N4 2006	38 th	No cracking
N8 2006	31 st	Cracked
N9 2006	74 th	No cracking
N10 2006	11 th	Cracked
S11 2006	8 th	Cracked

As seen in this table, there is no correlation between the percentile where the fatigue threshold occurred along a section’s cumulative distribution and its fatigue performance; however, a trend was noticed in certain cumulative strain distributions.

If one were to specifically compare N2 and N4 from 2003 again, no correlation between the locations of the fatigue threshold on their cumulative strain distributions and performance could be developed. However, above the fatigue threshold, N2’s strain distribution begins to flatten out while N4’s strain distribution continues on a gradual slope. Since the lower strains were similar between the two sections, it seemed the strains above the fatigue threshold contributed to the deterioration of section N2. This makes sense since one would expect that higher strains contribute more to pavement damage. Therefore, a third analysis phase was developed to try to bridge the laboratory and field data using the entire cumulative distribution rather than just particular points on the distribution.

Phase Three – Ratio Comparison

While the two previous phases this research analysis did not find any relationship between field and laboratory fatigue data, both analysis procedures were limited to one point either on the cumulative strain distribution or on the strain-temperature relationship curves. The third phase of comparisons included comparing the entire cumulative strain distribution of each section to the fatigue threshold by the use of a fatigue ratio (Equation 6-16).

$$R_n = \frac{\epsilon_n}{\epsilon_f} \tag{6-16}$$

where:

- R_n = ratio at the nth percentile
- ε_n = strain at the nth percentile, microstrain
- ε_f = fatigue threshold, microstrain

This ratio was calculated for each test section from the 50th to the 99th percentile on a 5 percent increment. These ratios are tabulated in Tables 6.12 and 6.13.

Table 6.12. Ratio by Percentile for 2003 Test Sections (29)

Percentile	N1 2003	N2 2003	N3 2003	N4 2003	N5 2003	N6 2003	N7 2003
Cracked	Yes	Yes	No	No	Yes	Yes	Yes
99%	3.22	5.86	2.63	2.48	3.56	4.36	4.04
95%	2.93	4.64	2.34	2.21	3.06	3.73	3.37
90%	2.67	3.88	2.11	2.00	2.70	3.27	2.89
85%	2.47	3.31	1.92	1.82	2.43	2.96	2.57
80%	2.30	2.85	1.79	1.70	2.22	2.69	2.30
75%	2.22	2.53	1.69	1.59	2.04	2.48	2.09
70%	2.15	2.22	1.60	1.48	1.88	2.30	1.91
65%	2.08	1.96	1.50	1.40	1.75	2.14	1.75
60%	2.02	1.66	1.40	1.31	1.61	1.98	1.60
55%	1.96	1.34	1.32	1.23	1.47	1.81	1.45
50%	1.90	1.13	1.23	1.15	1.33	1.65	1.30

Table 6.13. Ratio by Percentile for 2006 Test Sections (29)

Percentile	N1 2006	N2 2006	N3 2006	N4 2006	N8 2006	N9 2006	N10 2006	S11 2006
Cracked	Yes*	Yes*	No	No	Yes	No	Yes	Yes
99%	2.36	2.60	2.83	2.54	6.21	1.90	7.33	7.91
95%	1.95	2.17	2.45	2.22	4.83	1.64	5.97	6.45
90%	1.72	1.94	2.18	1.98	3.95	1.42	4.96	5.57
85%	1.57	1.77	1.98	1.80	3.29	1.24	4.34	4.94
80%	1.46	1.63	1.85	1.68	2.82	1.10	3.84	4.40
75%	1.39	1.53	1.74	1.58	2.45	1.01	3.45	4.00
70%	1.33	1.45	1.63	1.48	2.18	0.92	3.10	3.64
65%	1.29	1.40	1.53	1.39	1.95	0.83	2.80	3.30
60%	1.24	1.35	1.44	1.31	1.76	0.75	2.54	2.99
55%	1.21	1.30	1.35	1.23	1.56	0.68	2.30	2.68
50%	1.16	1.26	1.27	1.16	1.39	0.61	2.08	2.37

* top-down cracking only

It was seen that a distinct difference was found between the ratios of the sections that failed and the ratios of those that did not. At the 99th percentile, all the sections exhibiting fatigue cracking had ratios greater than 3.2, and the sections that performed well were all under 2.85. This separation between the ratios of cracked and uncracked sections continues until the 55th percentile.

Phase Three – Analysis Results

Based upon these limited data, it is proposed that control points could potentially be set along strain distributions using the fatigue ratio to help eliminate fatigue cracking for perpetual pavement designs. These control points (Table 6.14) were based upon the section that remained in-tact while returning the highest fatigue ratio during the 2003 and 2006 Test Track analyses (i.e., N3 using the by axle analysis).

Table 6.14. Fatigue Control Points for Fatigue Crack Prevention (29)

Percentile	Maximum Fatigue Ratio
99%	2.83
95%	2.45
90%	2.18
85%	1.98
80%	1.85
75%	1.74
70%	1.63
65%	1.53
60%	1.44
55%	1.35
50%	1.27

Fatigue Threshold Summary

While it was difficult to determine a relationship between the laboratory fatigue threshold, field pavement responses, and pavement performance using just one location on either a strain distribution or strain-temperature model, it was possible to propose a new perpetual pavement design concept using the entire strain distribution as a basis for comparison. The following results were established in this research.

- A relationship could not be developed between the field-measured strain at the laboratory testing temperature (20°C) and field performance.
- The laboratory fatigue threshold did not consistently occur on a pavement's cumulative strain distribution in similar locations for cracked or uncracked pavements.
- While more data are needed from differing mix designs to validate the concept of a fatigue ratio, data from the 2003 and 2006 Test Tracks support the concept of using control points set by multiples of the laboratory fatigue 95th percentile confidence interval lower bound to govern fatigue design.

CHAPTER 7 – FINDINGS AND STATE DOT IMPLEMENTATIONS

The Test Track operates as a facility where highway owners and the private industry sector can test new pavement design concepts and technology in a controlled and monitored environment. For the test track to be beneficial to its sponsors, the research findings need to be implemented by the sponsoring agencies. The following paragraphs describe how sponsors have used past Track research findings and implemented the results into their practices and plan to make use of the current Track research as well.

Mechanistic-Empirical Pavement Design

Through sponsorship of instrumented structural experiment sections, ALDOT, FDOT, MODOT, ODOT, and FHWA are helping refine the M-E pavement design approach and facilitate implementation of the MEPDG. Detailed laboratory testing in conjunction with surface performance measurements are essential in the calibration of the MEPDG using local materials and methods. Pavement response measurements in these instrumented test sections provide refinements or validation of the response models in the MEPDG as well as a calibration mechanism for other M-E design methodologies that output pavement response (e.g., PerRoad). Each sponsor's individual study provides the necessary connection to local materials, and data from the entire group of experiments provides an opportunity to test M-E pavement analysis and design using a broad range of materials and structural buildups. Agencies can have confidence in the utility of M-E pavement design as a result of the highly controlled experiment at the Test Track.

Alabama

The Alabama DOT has proactively used the Track in all three completed research cycles to refine specifications and introduce new methodologies aimed at reducing the life cycle cost of pavements. When Superpave was introduced, its requirements encouraged coarser-graded mixes. However, these mixes were susceptible to permeability problems. Multiple experiments on the 2000 Track proved that fine gradations could perform as well as coarse gradations in the field. These experiments encouraged Alabama and other agencies to change their specifications allowing requiring fine-graded mixes to be placed on their high-volume roadways. In Alabama, upper binder and wearing courses (within 4" {100 mm} of the surface, not counting OGFC) are no longer allowed to be designed on the course side of the restricted zone.

Florida

Prior to the 2000 Track research results, the Florida DOT also required mixes to be designed on the coarse side of the maximum density line (MDL) for all heavy traffic applications. When fine mixes were found to exhibit comparable performance, FDOT specifications were revised to allow their use. Now, over 90 percent of mixes in the FDOT QC database are fine-graded mixes, which is an indication of the popularity of fine blends within the contracting community.

The 2003 research cycle was used to validate results from FDOT's heavy vehicle simulator (HVS). This research found that mixes produced with polymer-modified PG 76 binder rutted at half the rate of the same mix produced with unmodified PG 67 binder. This finding was significant for several reasons. The validation of results from the HVS research program made it

possible to apply other polymer versus non-polymer findings. The outcome of this effort was a specification for the use of polymer modified binders in various layer combinations as a function of traffic in order to optimize the cost of construction.

In 2006, FDOT sponsored research that had two objectives. The first objective was to help advance understanding of mechanistic pavement designs by building two instrumented structural sections using a pavement thickness and materials commonly used in Florida. The other objective was to validate the energy ratio method developed at the University of Florida to predict mixes prone to top-down cracking. Prior to construction, laboratory testing and analysis following the energy ration concept indicated that by changing surface mix from a PG 67 to a polymer modified PG 76 binder would yield a substantial improvement in cracking resistance. As predicted, it took the application of approximately 50 percent more ESALs (2.9 million in N2 versus 1.9 million in N1) in order to induce surface cracking throughout the length of the PG 76 section. In conjunction with the Track study, FDOT also sponsored a project at the University of Florida to refine the laboratory procedure for their mix design evaluation process. When the simplified equipment is made available, FDOT plans to use the validated approach to either approve mixes on a case by case basis or to establish guidelines that can be used to ensure new mix designs will be resistant to surface cracking.

Another outcome of the FDOT experiment was that strains measured at the bottom of the two pavement structures were essentially identical until the surface layer cracked in the unmodified section. Based on these results, it can be inferred that surface mixes with modified binders does not affect strain performance at the bottom of the HMA layers.

Georgia

In past research cycles, GDOT sponsored research on the Test Track to compare rutting and durability performance of more expensive SMA surfaces to dense-graded Superpave mixes. Although the dense-graded mix exhibited excellent rutting performance that was statistically equivalent to the SMA mix, the SMA surface proved to be more resistant to raveling and general degradation associated with surface aging. As a result of these findings, GDOT implemented a policy whereby lower volume roadway surfaces that would otherwise have been resurfaced using a drainable surface mix (to optimize safety) over an SMA (to optimize performance) were instead resurfaced using a drainable surface over a less costly dense-graded Superpave mix (to reduce the cost of construction). This change in practice was expected to offer the same rutting performance as SMA, while at the same time eliminating the durability shortcoming of the dense mix by protecting it with a permeable surface. A significant cost savings resulted from the substitution of dense mix for SMA without compromising performance.

In order to ensure a stable aggregate structure in permeable surface mixes, GDOT specifies a 5:1 flat and elongated limit of 10 percent on the coarse aggregate fraction of the mix. GDOT sponsored test sections on the 2006 Test Track to investigate the possibility of changing the flat and elongated specification to 3:1 in order to improve drainage properties. It was observed that the porous surface mix containing an aggregate having more flat and elongated particles actually improved the drainability of the pavement surface, an effect that was measured both in the laboratory and on the surface of the Track. The performance of the comparative drainable surfaces was equal in every other way.

Another GDOT test section was also built with a double-layer porous surface course. The lower layer contained the coarse aggregate with more flat and elongated particles, and the upper layer used a smaller NMA open-graded mix. The two porous mixes were laid simultaneously using a European twin layer paver. In many urban areas, such as Atlanta, Georgia, federal policy requires the installation of sound barriers in order to minimize the effect of traffic noise on nearby communities. It has been observed in Europe that smaller NMA porous mixes placed simultaneously on larger NMA porous mixes creates an acoustic condition that is favorable to noise reduction. Additionally, the smaller NMA surface mix may provide a filtering mechanism that would promote the long-term drainability of the larger NMA mix. Since tack coat and construction traffic could hinder the permeability of the porous mixes, the European paver was developed to place both layers in a single process without the use of tack. GDOT's twin layer section on the NCAT Pavement Test Track proved to be the most drainable and quietest surface from start to finish over the entire 2-year (10 million ESAL) research cycle. Ideally, this section will remain in place for the 2009 research cycle in order to document the long term (drainability and noise-reducing) performance of twin layer pavements.

Indiana

INDOT has reported unexpectedly high variability for air voids of plant produced HMA. Some QC data has shown air voids $\pm 4\%$ from the job mix formula compared to the specified $\pm 1\%$. Indiana developed an experimental program which would allow it to quantify the performance of low air void pavements in the field in order to validate new acceptance criteria for pavements. Pavements were built with air voids ranging from 0 to 4% air voids and rutting was measured weekly. The data suggest that for surface mixes containing an unmodified asphalt binder, rutting rates increase dramatically when the QC air voids fall below 2.75%. At this point, removal and replacement of the HMA layer may be appropriate for pavements expected to experience heavy traffic.

Mississippi

Mississippi's original dense gravel mix placed in section S2 on the 2000 Track was designed with 100 gyrations. Although rutting performance was exceptional, the section exhibited extensive top-down cracking (Figure 7.1). Cracking was first noticed in this section after approximately 12.5 million ESALs. Some of this cracking was not load related, as it was observed in both the outside (research) and inside (non-trafficked) lane. A crack map for the original section S2 near the end of the 2003 research cycle is shown in Figure 7.2. The original 1.5 inch thick section S2 surface mix was milled to facilitate reconstruction for the 2006 Track. The milled material was stockpiled onsite and used as RAP in the replacement mix, which was a similar dense-graded gravel mix designed using 85 gyrations. The reduced gyration design mix in section S2 again exhibited very good rutting performance (3.0 mm); however, at the very end of the 10 million ESAL traffic cycle extensive surface cracking was noted. The final crack map for section S2 is shown in Figure 7.3



Figure 7.1. Cracking Severity in Section S2 after 30 Million ESALs

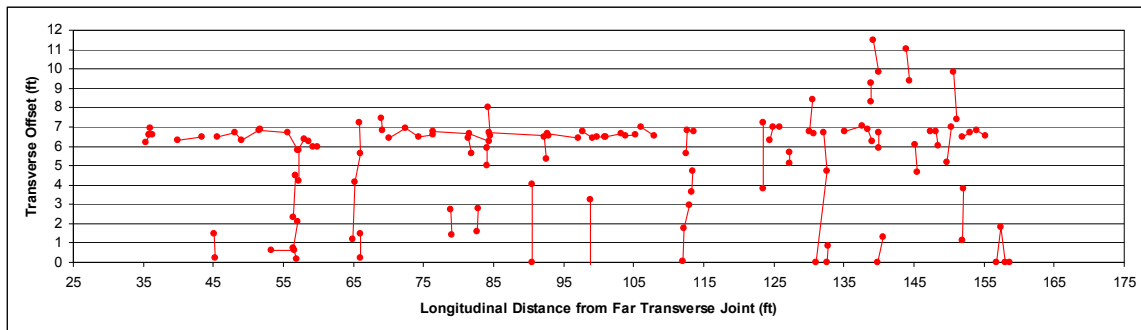


Figure 7.2. Crack Map for Original Section S2 Near End of the 2003 Research Cycle

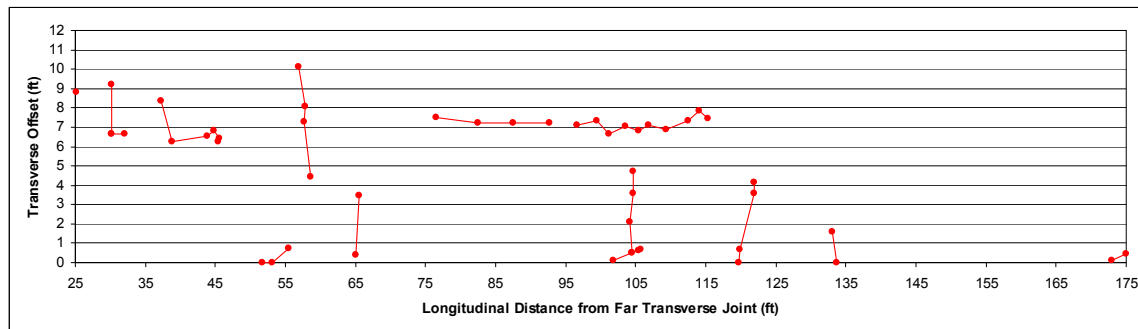


Figure 7.3. Cracking Exhibited after 10 million ESALs in Section S2

Following the successful performance of a 100 percent gravel SMA on the 2000 Track, the Mississippi DOT chose to take gravel use one step further and evaluate a 100 percent gravel OGFC on the 2006 Track. The new mix was placed at a target thickness of 1 inch. The new performed well in terms of rutting (7.0 mm) and drainability. As seen in Figure 7.4, the coefficient of permeability in section S3 was second only to section N13.

Missouri

Missouri DOT's "traditional" SMA specification required that 50 percent, by volume, of the plus #8 material be a hard, durable aggregate. There is basically one source of material that meets this requirement and it is located in Southeast Missouri. The limited availability of the hard, durable aggregate resulted in a substantially higher cost for SMA. Therefore, SMA was limited to MODOT's highest traffic roadways. These are known as commercial zones and encompass the cities of Kansas City, St. Louis, Springfield and St. Joseph. Missouri's objective on the 2003 Track was to determine if a 100 percent limestone SMA mix would perform similar to the "traditional" SMA with the restrictive aggregate specification. Based upon the findings from the 2003 cycle, Missouri now has a specification for 100 percent limestone mixes and has expanded its use to all interstate and high volume routes. The "traditional" SMA continues to be used inside the commercial zones, and the 100 percent limestone mixes are used everywhere else. By the end of the 2009 construction season, Missouri estimates it will have placed 176,000 tons of SMA using the revised aggregate specification. Although the savings varies across the state, evidence suggests that on average they are saving approximately \$3.75 per ton. The revised specification has only been used on 5 projects over two paving seasons, but Missouri estimates a total savings to date of approximately \$646,000. It is expected the revised specification will be used more in coming paving seasons, leading to more savings for Missouri taxpayers (*Dale Williams, unpublished data*).

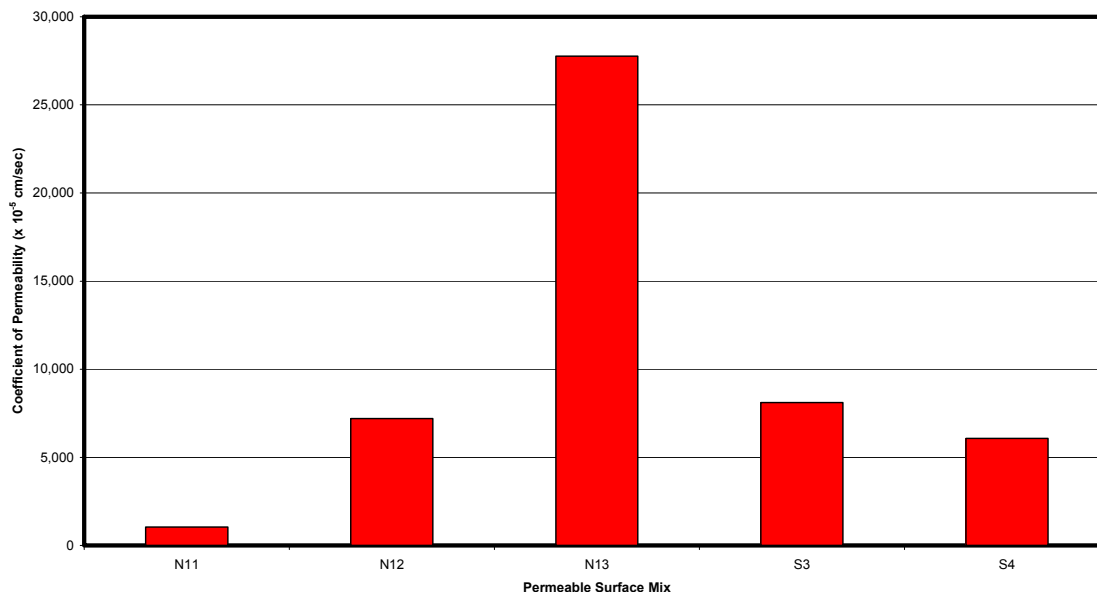


Figure 7.4. Coefficient of Permeability in Drainable Surfaces Using Field Permeameter.

North Carolina

As noted above, past Track research cycles have shown that fine mixes can provide rutting performance that is comparable to coarse mixes. This finding was significant and led to many states changing mix specification requirements to favor fine mixes in order to prevent construction problems common with coarse mixes such as low mat densities and segregation. The North Carolina DOT adjusted their Superpave specifications by relaxing their specifications for $N_{initial}$ which opened the door to finer mixes (58). North Carolina has continued traffic on two of its original coarse vs. fine comparison sections: S9 (coarse) and S10 (fine). Now after 30 million ESALs and nine years, there is evidence from these sections that fine-graded mixes are more resistant to top-down cracking than coarse mixes. Section S10 shows less centerline cracking and less cracking from road scars (e.g., flat tires, axle failures, etc.). Other comparison sections in the curves which remain from the 2000 research cycle, also support this observation.

Oklahoma

Previous Test Track experiments showed SMA mixtures performed well under accelerated loading conditions. This knowledge was used by Oklahoma to gain confidence in specifying and constructing SMA pavements. Oklahoma also used correlations between rutting measured at the Track and APA test results to gain confidence in their new APA specification (58).

The relationship between strain, temperature and speed was successfully quantified in Oklahoma's sections N8 (with a total asphalt thickness of 10 inches) and N9 (with a total asphalt thickness of 14 inches). This outcome can be considered a successful validation of M-E pavement analysis and design. Cracking was first noted in section N8 after approximately 6.8 million ESALs. In consideration of beam fatigue performance in the laboratory, strain measurements at the bottom of the pavement and cracking measurements on the surface, it appears that section N9 can be considered a perpetual pavement. A methodology is under

development based on the results from these two sections, as well as other results from all 3 research cycles, to relate laboratory beam fatigue results to multi-temperature strains in the field.

South Carolina

At the end of the 2003 research cycle, absolute rut depths were measured at 4.1 mm in South Carolina’s section N13 (a 30% LA abrasion loss, granite SMA control mix) and 4.9 mm in S1 (a 54% LA abrasion loss, SMA experimental mix). Although production problems with the soft material in section S1 made it difficult to control gradations (resulting in a blend that was slightly finer than desired), both sections had exhibited favorable rutting performance for 10 million ESALs. South Carolina decided to continue traffic on section S1 to quantify long-term performance of the mix with the softer aggregate while opting to discontinue research on the N13 control mix. At the end of the 2006 research cycle (after the application of 20 million ESALs), absolute wire line rut depths in S1 averaged 7.7 mm (an additional 2.8 mm of rutting over the second 10 million ESALs). In consideration of the extremely hot summer of 2007 (average 7-day maximum air temperature = 100.5°C), this mix performed well. It was also observed that macrotexture increased in section S1 by approximately 0.15 mm between 8 million ESALs (near the end of the 2003 Track) and 20 million ESALs (at the end of the 2006 Track). In comparison, the 35% LA abrasion loss granite SMA placed by Alabama in section W1 on the 2000 Track did not show any increase in macrotexture until about 25 million ESALs (increasing by about 0.1 mm to 30 million ESALs). Macrotexture measurements on both sections are shown in Figure 7.5 with no data shown for W1 before the beginning of the 2003 research cycle in order to keep the sections on the same ESAL scale. The difference in macrotexture performance between the two sections is presumably due to the softer aggregate in section S1, and may be indicative of a difference in long term durability.

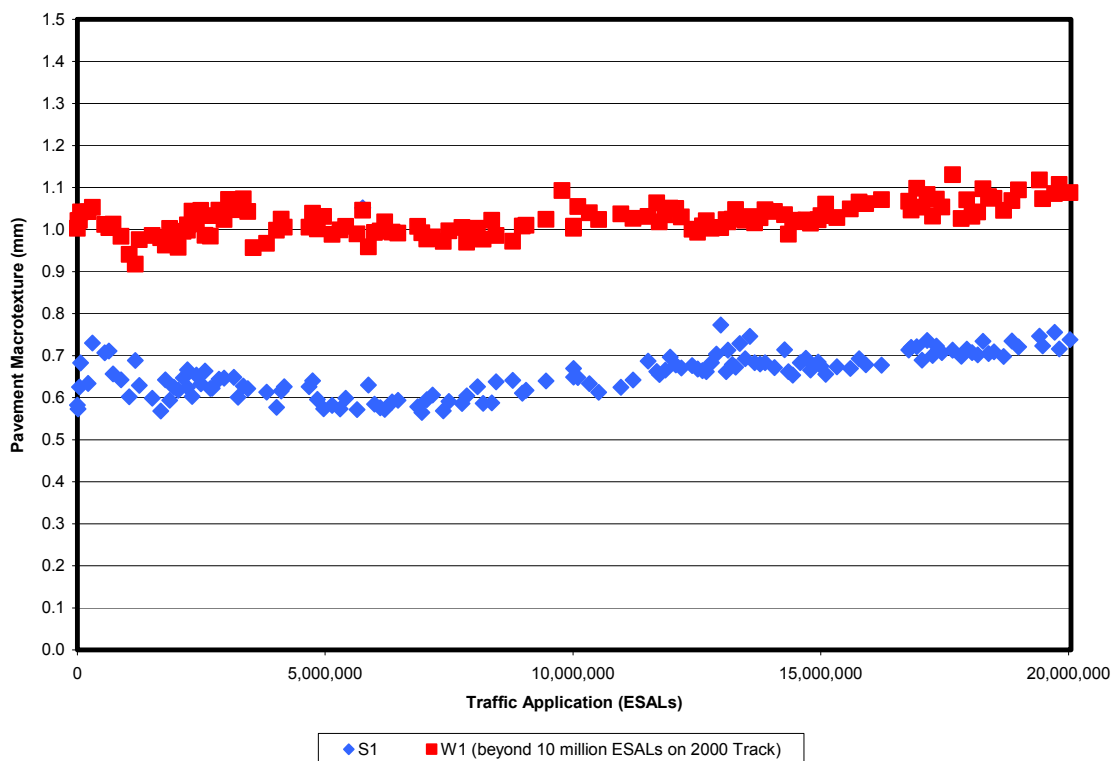


Figure 7.5. Increase in Macrotexture of High LA Abrasion Loss SMA Surface

Tennessee

Tennessee and Mississippi have designed test sections which relate aggregate selection to pavement performance. Prior to the Test Track research, both states required blends of limestone and crushed gravel for asphalt mixes. With their respective test sections, both states have verified that 100% crushed gravel mixes can perform well in the field if proper construction and design techniques are used (58).

Traffic continuation on Tennessee's sections S4, S5 and E1 continued to yield valuable performance information for experimental mixes. As seen previously in Figure 7.3, field permeability measurements and observations indicated the OGFC in section S4 remained drainable after 20 million ESALs with an average rut depth of only 6.5 mm. Likewise, the 75 gyration dense-graded gravel mix in section S5 exhibited only 3.4 mm of rutting; the limestone SMA in section E1 exhibited 4.6 mm. Both of these measurements were taken after the application of 20 million ESALs. The average rut depth of the new 65 gyration mix in section S6 containing a blend similar to the older mix in S5 was only 1.5 mm. These results have provided Tennessee with confidence in the lower gyration level design.

Texas

2006 was the first cycle that TXDOT participated in the NCAT Test Track. For this cycle TXDOT was interested in evaluating a one inch rich bottom layer known as a CAM (crack arresting mix). This mix was placed on section S12 after the Track foundation had been carefully separated into slabs using a large diameter concrete masonry saw. A fine-graded sand was used to fill the saw cuts to keep the slabs from healing back together during hot weather. The CAM mix was a fine-graded 9.5 mm NMAS mix containing a PG70-22 binder designed with 75 gyrations. A two inch lift of TXDOT Dense-Asphalt mix was placed over the CAM mix. The Dense-Asphalt mix was designed with 50 gyrations and contained a PG76-22. At the end of the cycle, no cracks were evident at the surface of the Texas test section. However, the joints are perceptible at night under headlights. Additional coring is being conducted to determine if any cracks currently exist in the CAM layer. 26.0 mm of rutting was measured on the surface of the pavement by the end of the cycle. A coring investigation revealed that all of the deformation was confined to the upper layer of dense-graded mix. Very little deformation had occurred in the CAM lift.

CHAPTER 8 – 2009 TEST TRACK PLANS

Planning is currently underway for the 2009 NCAT Pavement Test Track (Phase IV). This cycle of the Track is expected to consist of an even larger structural experiment as well as more mill/inlay surface mixes, with research sponsorship expanded to include private sector partners.

While individual test sections will still be optional on the 2009 Track, NCAT is also developing a pre-designed six section “Group Experiment” that is intended to encompass multiple timely issues that are important to the entire pavement community. All sections in the “Group Experiment” will be supported by the same subgrade and base, and the total thickness of all bituminous lifts will be 7 inches. This thickness was chosen because in past studies, 7-inch sections exhibited significant performance differences within the planned traffic cycle.

In addition to a control section that will be built with conventional HMA, two sections will be built using different WMA technologies in every lift. Although the two WMA technologies will be selected by the sponsors who choose to financially support the experiment, it is envisioned that one of the sections will use a foaming process and the other will be produced using an additive. These sections are proposed because reduced energy demand, lower emissions, and enhanced workability make WMA technology a very attractive alternative for the construction industry if it can be proven that early rutting, moisture damage and structural performance are not compromised.

As a result of the rising cost of virgin materials, pavement engineers are also very interested in high recycled content mixes. There are some concerns that the use of high percentages of RAP in surface mixes may compromise durability. Likewise, there is concern that high RAP content base and binder mixes may compromise fatigue resistance. It is critical that decision makers determine whether high RAP content mixes are suitable for these applications so that specification limits can be set at the highest level that exhibits performance characteristics comparable to virgin mixes. In order to address this issue, one section will be built with a high RAP content in lower lift(s) and low RAP contents in upper lift(s). Another section will be built with high RAP contents in both lower and upper lifts.

Many state DOTs are using drainable surface mixes in order to improve wet weather driving visibility, reduce accident/fatality rates, and reduce noise created by pavement tire interaction. Although drainable surface mixes have aggregate structures that are very similar to rut resistant SMA mixes, it is typically assumed they do not contribute to the load carrying potential of the pavement structure. The sixth section in the “Group Experiment” will be built identical to the control section, except that the conventional surface mix will be replaced with a drainable surface mix.

By monitoring response instrumentation (i.e., pressure plates and strain gauges) installed in each of these sections at the time they are constructed and by documenting changing surface conditions (rutting, roughness, cracking, etc.) under heavy truck traffic, it will be possible to compare both surface and structural performance. It is expected that this information will provide

for the optimization of specifications regarding the deployment of these modern technologies on the pavement infrastructure with a high level of confidence.

Utilization of as many sections as possible for structural purposes would facilitate the implementation of M-E methods for structural pavement design. For example, the development of the new MEPDG represents a significant change and advancement over existing design methodologies. Historically, the structural design of asphalt pavements has been largely empirical based upon vehicle designs, axle loads, and material properties. The new design guide, however, relies heavily on principles of engineering mechanics to produce thickness designs that control specific modes of pavement distress. Before this new methodology gains wide acceptance or use, it must be validated and calibrated to ensure that it provides adequate design guidance using modern methods and materials under traffic by actual design vehicles. Calibration of the conservative distress models that could eliminate only a 10 percent margin of error in excess design thickness would generate an annual taxpayer savings nationwide of as much as one billion dollars. To this end, there is a need for a full-scale structural experiment to validate the methodology.

REFERENCES

1. Brown, E.R., L.A. Cooley, D. Hanson, C. Lynn, B. Powell, B. Prowell, and D. Watson, "NCAT Test Track Design, Construction, and Performance", NCAT 02-12, National Center for Asphalt Technology, Auburn University, 2002.
2. Timm, D.H. "Design, Construction, and Instrumentation of the 2006 Test Track Structural Study", NCAT Draft Report, Auburn University, 2008.
3. Wang, J. et al, "Windows-Based Top-Down Cracking Design Tool for Florida: Using Energy Ratio Concept", In *Transportation Research Record: Journal of the Transportation Research Board, No. 2037*, Transportation Research Board of the National Academies, Washington, D.C., 2007, pp 86-96.
4. Roque, R. et al, "Development and Field Evaluation of Energy-Based Criteria for Top-Down Cracking Performance of Hot Mix Asphalt", *Journal of the Association of Asphalt Paving Technologists*, Vol. 73, 2004, pp. 229-260.
5. Zhang, Z. et al, "Evaluation of Laboratory-Measured Crack Growth Rate for Asphalt Mixtures", In *Transportation Research Record: Journal of the Transportation Research Board, No. 1767*, Transportation Research Board of the National Academies, Washington, D.C., 2001a, pp. 67-75.
6. Zhang, Z. et al, "Identification and Verification of a Suitable Crack Growth Law" *Journal of the Association of Asphalt Paving Technologists*, Vol. 70, 2001b, pp. 816-827.
7. Birgisson, B. et al, "Hot Mix Asphalt Fracture Mechanics: A Fundamental Crack Growth Law for Asphalt Mixtures", *Journal of the Association of Asphalt Paving Technologists*, Vol. 71, 2002, pp. 816-827.
8. Roque, R. et al, *Implementation of SHRP Indirect Tension Tester to Mitigate Cracking in Asphalt Pavements and Overlays*. Final Report for FDOT BA-546 Contract, University of Florida, Gainesville, FL, 2002.
9. Timm, D.H. et al, "Forensic Investigation and Validation of Energy Ratio Concept", Submitted to the 88th Annual Meeting of the Transportation Research Board. *Transportation Research Record* (in press), 2008.
10. Willis, J.R. and D.H. Timm. *Forensic Investigation of a Rich-Bottom Pavement*. Report No. 06-04, National Center for Asphalt Technology, Auburn University, 2006.
11. Willis, J.R. and D.H. Timm. "A Forensic Investigation of Debonding in a Rich-Bottom Pavement, In *Transportation Research Record: Journal of the Transportation Research Board, No. 2040*, Transportation Research Board of the National Academies, Washington, D.C., 2007, pp. 107-114.
12. Federal Highway Administration RAP Expert Task Group, "10 Obstacles for Increased RAP Use", HMA Recycling Expert Task Group website: <http://www.ncat.us/RAP/Past%20RAP%20ETGs/05-07.html> , accessed November 14, 2008.
13. West, R. et al, "Laboratory and Accelerated Field Performance Testing of Moderate and High RAP Content Mixes at the NCAT Test Track", Submitted to the 88th Annual Meeting of the Transportation Research Board, (in review), 2009.
14. Smit, A.d.F and B. Waller, "Sound Pressure And Intensity Evaluations Of Low Noise Pavement Structures With Open Graded Asphalt Mixtures", NCAT Report 07-02, National Center for Asphalt Technology at Auburn University, Auburn, AL, 2007.

15. Smit, A.d.F and B. Waller, “Sound Pressure and Intensity Evaluations of Low Noise Pavement Structures with Dense-Graded and Stone Matrix Asphalt Mixtures”, Draft NCAT Report 07-03, National Center for Asphalt Technology at Auburn University, Auburn, AL, 2007.
16. Smit, A.d.F and B. Waller, “Evaluation Of The Ultra-Light Inertial Profiler (ULIP) For Measuring Surface Texture Of Pavements”, NCAT Report 07-01, National Center for Asphalt Technology at Auburn University, Auburn, AL, 2007.
17. Powell, B. “Construction and Performance of Georgia’s Permeable Surface Mixes on the 2006 NCAT Pavement Test Track,” Submitted to the 88th Annual Meeting of the Transportation Research Board. Transportation Research Record (in press), 2009.
18. Beuving, E. European Asphalt Pavement Association, Presentation made at the National Center for Asphalt Technology, March 2006.
19. Ingram, L. S., Herbold, K. D., Baker, T. E., Brumfield, J. W., Felag, M. E., Ferragut, T. R., Grogg, M. G., Lineman, L. R., and R. O. Rasmussen, “Superior Materials, Advanced Test Methods, and Specifications in Europe,” FHWA/PL-04-007, Federal Highway Administration International Technology Exchange Program, April 2004.
20. Asphalt Institute. *Superpave Mix Design (SP-2)*. Lexington, KY, 1996.
21. National Asphalt Pavement Association. *An Industry Discussion on Superpave Implementation*. Lanham, MD.
22. Kandhal, P. and Cooley L.A., Jr. *Accelerated Laboratory Rutting Tests: Evaluation of the Asphalt Pavement Analyzer*. NCHRP report 508, Transportation Research Board, Washington, D.C., 2008.
23. Witczak, M. *Simple Performance Tests: Summary of Recommended Methods and Database*. NCHRP Report 547, NCHRP, TRB, National Research Council, Washington D.C., 2005.
24. Eres Consultants Division (2004), *Guide For Mechanistic-Empirical Pavement Design of New and Rehabilitated Pavement Structures*, Final Report, NCHRP 1-37A.
25. Bonaquist, R., D. Christensen, and W. Stump. *Simple Performance Tester for Superpave Mix Design: First Article Development and Evaluation*. NCHRP report 513, NCHRP, TRB, National Research Council, Washington D.C., 2003.
26. NCAT Pavement Test Track. www.pavetrack.com, accessed July 27, 2008.
27. Taylor, A.J. *Mechanistic Characterization of Resilient Moduli for Unbound Pavement Layer Materials*. M.S. Thesis. Auburn University. Auburn, AL. August 2008.
28. Robbins, M.M. and D.H. Timm, “Temperature and Velocity Effects on a Flexible Perpetual Pavement” Transportation Research Record Preprint, 2009.
29. Willis, J.R., “Field-Based Strain Thresholds for Flexible Perpetual Pavement Design,” PhD Dissertation, Auburn University, 2009.
30. Eres Consultants Division, *Guide For Mechanistic-Empirical Pavement Design of New and Rehabilitated Pavement Structures; Appendix CC-3, Updated Traffic Frequency Calculation for Asphalt Layers*, Final Document, NCHRP 1-37A, 2003.
31. Newcomb, D.E., M. Buncher, and I.J. Huddleston. Concepts of Perpetual Pavements. In *Transportation Research Circular: Journal of the Transportation Research Board, No. 503*, TRB, National Research Council, Washington, D.C., 2001, pp 4-11.
32. Newcomb, D.E. and H. Von Quintus. Wanted: Transfer Functions – Experience Needed. *Hot Mix Asphalt Technology*, Vol. 7, No. 8, 2002, pp 22-25.

33. Priest, A.L. and D.H. Timm. *Methodology and Calibration of Fatigue Transfer Functions for Mechanistic-Empirical Flexible Pavement Design*, Report No. 06-03, National Center for Asphalt Technology, Auburn University, 2006.
34. Timm, D.H. and A.L. Priest, "Material Properties of the 2003 NCAT Test Track Structural Study," Report No. 06-01, National Center for Asphalt Technology, Auburn University, 2006.
35. Miner, M.A. Estimation of Fatigue Life with Emphasis on Cumulative Damage. *Metal Fatigue*, edited by Sines and Wiseman, McGraw Hill, 1959, pp 278-89.
36. St. Martin, J., J.T. Harvey, F. Long, E. Lee, C.L. Monismith, and K. Herritt. "Long-Life Rehabilitation Design and Construction," Transportation Research Circular, Number 503, 2001, pp 50-65.
37. Walubita, L.F., W. Liu, T. Scullion, and J. Leidy. "Modeling Perpetual Pavements Using the Flexible Pavement System (FPS) Software," Transportation Research Board 2008 Annual Meeting, CD-ROM.
38. Al-Qadi, I.L., H. Wang, P.J. Yoo, and S. H. Dessouky. "Dynamic Analysis and In-situ Validation of Perpetual Pavement Response to Vehicular Loading," Transportation Research Board 2008 Annual Meeting, CD-ROM.
39. Willis, J.R. "A Synthesis of Practical and Appropriate Instrumentation Use for Accelerated Pavement Testing," International Conference on Accelerated Pavement Testing, Madrid, Spain, 2008.
40. Hornyak, N.J., J.A. Crovetti, D.E. Newman, and J.P. Schabelski. "Perpetual Pavement Instrumentation for the Marquette Interchange Project – Phase 1," SPR #0092-06-01, Wisconsin Highway Research Program, August 2007.
41. Romanoschi, S.A., A.J. Gisi, M. Portillo, and C. Dumitru. "The first findings from the Kansas Perpetual Pavements experiment" Transportation Research Board 2008 Annual Meeting, CD-ROM.
42. Yang, Y. et al, "Perpetual Pavement Design in China," International Conference on Perpetual Pavement, Ohio Research Institute for Transportation and the Environment, 2005.
43. American Association of State Highway and Transportation Officials. *AASHTO Guide for Design of Pavement Structures*. Washington, D.C., 1993.
44. Willis, J.R. and D.H. Timm, "Repeatability of Asphalt Strain Measurements under Full Scale Dynamic Loading," Transportation Research Board Preprint, 2008.
45. Selvaraj, S.I., "Development of Flexible Pavement Rut Prediction Models from the NCAT Test Track Structural Study Section's Data," PhD Dissertation, Auburn University, 2007.
46. Priest, A.L. and D.H. Timm, "Mechanistic Comparison of Wide-Base Single Versus Standard Dual Tire Configurations," Transportation Research Record No. 1949, Transportation Research Board, 2006b, pp. 155-163
47. Seeds, S.B., S.H. Alavi, W.C. Ott, M. Mikhail, and J.A. Mactutis. "Evaluation of Laboratory Determined and Nondestructive Test Based Resilient Modulus Values from the WesTrack Experiment." *Nondestructive Testing and Backcalculation of Moduli: Third Volume*. ASTM STP 1375. S.D. Tayabji and E.O. Lukanen, Eds., American Society of Testing and Materials, West Conshohocken, PA, 2000.
48. Parker, F. and D.J. Elton. *Methods for Evaluating Resilient Moduli of Paving Materials*. Auburn University Highway Research Center: Auburn, AL. 1990.

49. American Association of State Highway and Transportation Officials T 315-06. Standard Test Method for Determining the Rheological Properties of Asphalt Binder Using Dynamic Shear Rheometer (DSR). AASHTO, 2008.
50. ASTM D2983-04a(2004). Standard Test Method for Low-Temperature Viscosity of Lubricants Measured by Brookfield Viscometer. *ASTM International*, West Conshohocken, Pa., 2004. www.astm.org.
51. ARA Inc., Eres Division. Part 2 Design Inputs: Chapter 2 Material Characterization. *Guide For Mechanistic-Empirical Pavement Design of New and Rehabilitated Pavement Structures*, Final Document, NCHRP 1-37A, 2004.
52. Bari, J. and M.W. Witzak. Development of a New Revised Version of the Witzak E* Predictive Model for Hot Mix Asphalt Mixtures. *Proceedings of the Association of Asphalt Paving Technologists*, Vol. 75, 2006, pp381-423.
53. Andrei, D., M.W. Witzak, and W. Mirza. Appendix CC-4: Development of a Revised Predictive Model for the Dynamic (Complex) Modulus of Asphalt Mixtures. *Development of the 2002 Guide for the Design of New and Rehabilitated Pavement Structures*, Final Document, NCHRP 1-37A, 1999.
54. Christensen, Jr., D.W., T. Pellinen, and R.F. Bonaquist. Hirsch Model for Estimating the Modulus of Asphalt Concrete. *Proceedings of the Association of Asphalt Paving Technologists*, Vol. 72, 2003, pp97-121.
55. Robbins, M.M. Master's Thesis. Auburn University. Draft Copy, 2009.
56. Azari, H., G. Al-Khateeb, A. Shenoy, and N. Gibson. Comparison of Measured SPT E* of ALF Mixtures with Predicted E* Using NCHRP 1-37A and Witzak's New Equations. In *Proceedings of the 86th Annual Transportation Research Board*, TRB, National Research Council, Washington, D.C., 2007.
57. Prowell, B., E.R. Brown, J. Daniel, S. Bhattacharjee, H. Von Quintus, S. Carpenter, S. Shen, M. Anderson, A.K. Swamy, and S. Maghsoodloo. "Endurance Limits of Hot Mix Asphalt Mixtures to Prevent Fatigue Cracking in Flexible Pavements." NCHRP Report 9-38, Updated Final Draft Report, National Center for Asphalt Technology, Auburn, AL. May 2008.
58. Brown, E.R., B. Powell, R. West, and D. Timm. *NCAT Test Track Findings*, NCAT Report, National Center for Asphalt Technology, Auburn University, 2005.